NE

REPORT DOCUMENTATION PAGE

Form Approved
OMB No. 074-0188

1. AGENCY USE ONLY (Leave blank)	2. REPORT DATE	3. REPORT TYPE AND DATES COVERED
	April 10/2006	Final report, 06/15/2002 – 1/14/2006

4. TITLE AND SUBTITLE
Bragg Multiple Quantum Wells: Tunable Cavities for optoelectronics applications

5. FUNDING NUMBERS
F49620-02-1-0305

6. AUTHOR(S)
Lev Deych
Alexander Lisyansky

7. PERFORMING ORGANIZATION NAME(S) AND ADDRESS(ES)
Research Foundation CUNY
655 West 57th Street, 11th floor
New York, NY 10019

8. PERFORMING ORGANIZATION REPORT NUMBER

9. SPONSORING / MONITORING AGENCY NAME(S) AND ADDRESS(ES)
AF Office of Scientific Research
875 N Randolph St
Arlington VA 22203
Dr. Silversmith/NE

10. SPONSORING / MONITORING AGENCY REPORT NUMBER
AFRL-SR-AR-TR-06-0313

11. SUPPLEMENTARY NOTES

12a. DISTRIBUTION / AVAILABILITY STATEMENT
Distribution Statement A: unlimited

12b. DISTRIBUTION CODE

13. ABSTRACT *(Maximum 200 Words)*
The main objective of the proposal was to conduct feasibility studies of Bragg Multiple Quantum Well (BMQW) structures from the point of view of their applications as tunable logical elements (switches, modulators, filters, etc) for optical and optoelectronic circuits and identify structures most suitable for such applications. As a result of this research the authors developed new approaches to computations of excitonic characteristics of quantum well structures and their response to static electric field, analyzed the effects of the interface disorder on optical and electro-optical properties of these structures, suggested a concrete design of a defect BMQW structure with optimal for switching applications characteristics, and demonstrated theoretically its reversible tunability. Authors also developed a comprehensive theoretical approach to describing reflection, transmission, absorption, and luminescent spectra of generic resonant photonic structures, and designed computer codes for efficient computation of these spectra. An important outcome of the work was demonstration of the possibility to significantly affect the performance characteristics of the systems under consideration through a smart structural design. Two graduate students and two post-docs actively participated in the work on this project. One of those students has successfully defended his Ph.D. thesis, and the second student is completing his dissertation.

14. SUBJECT TERMS			15. NUMBER OF PAGES
			16. PRICE CODE
17. SECURITY CLASSIFICATION OF REPORT	18. SECURITY CLASSIFICATION OF THIS PAGE	19. SECURITY CLASSIFICATION OF ABSTRACT	20. LIMITATION OF ABSTRACT

I. INTRODUCTION

The main objective of our proposal was to demonstrate possibilities of using Bragg multiple-quantum-well (BMQW) structures as tunable optical elements of optoelectronic and all optical circuits, and to suggest possible structural designs ready for experimental implementation. To achieve this objective several tasks have been identified in the proposal. These tasks included theoretical modeling of exciton characteristics in quantum wells (QW), developing efficient theoretical tools for studying optical spectra of BMQWs and identifying structures with the most promising optical characteristics. While some of the initially proposed directions and approaches had to be modified in the course of the research, all the main objectives of the project were successfully accomplished. We can identify several tangible outcomes of the project:

1. A novel, more accurate and universal, approach to calculating exciton energies and oscillator strengths in QWs was developed and a computer code implementing this approach was designed.

2. A method of all optical switching and modulation in defect BMQW structures based on screening of the external electric field by photo-excited carriers was suggested and analyzed theoretically.

3. Parameters of several structures with optimal for tunable optical switching applications characteristics were identified and recommendations for their experimental realization were formulated.

4. A non-trivial effect of the electric field and interface correlations on inhomogeneous broadening of excitons in QWs was discovered.

5. A new approach allowing for analytical analysis of optical spectra of generic one-dimensional resonant photonic crystals (of which BMQWs are an example) was developed.

6. A method to increase the width of the polariton bandgap by at least 40% by designing periodic structures with complex elementary cells was demonstrated.

Results obtained within this project made a significant contribution in understanding of optical processes in semiconductor based photonic crystals and a synergy between microscopic characteristics of semiconductor heterostructures and their macroscopic (at the scale of the wavelength) arrangement. This contribution is documented in 14 papers published in leading journals and 2 papers submitted for publication, as well as in 21 presentations at scientific conferences and colloquia. In the subsequent sections of the Report we present our main scientific results in more details.

Work on the project also contributed significantly to developing human resources: two graduate students and two post-docs took part in this project. One of the students has graduated with the bulk of his dissertation based on the results obtained within this project, another student is near completion of his thesis. One of the post-docs is working currently at the Naval Research Lab.

II. EXCITONS IN SINGLE QUANTUM WELLS

A. Novel approach to calculations of exciton binding energies

In this part of the project we suggested a novel approach to calculating exciton energies in semiconductor QW, which is based on application of the ideas of the self-consistent Hartree method to the excitons in QWs. The idea of this approach is that instead of imposing a particular functional dependence on the envelope wave function, as is done in the previous approaches,[1–14] we present it as a special combination of some unknown functions, which depend on fewer than the total number variables. Applying the variational principle to this combination we derive a system of equations describing both the motion of electrons and holes in the direction of confinement, and the relative two-dimensional in-plane motion of the exciton. Effective potentials entering these equations have to be found self-consistently along with the wave functions. Unlike the perturbative methods,[15–18] our approach takes into account the Coulomb mixing of the electron and hole sub-bands in a non-perturbative way, and is expected to give more accurate results even for the cases when such mixing is important.

This approach has a number of advantages compared to the previous methods. First of all, in its most general statement it must give better results for the exciton energy because

we span a much larger functional space in the search for the minimum. Second, as it is discussed below, this approach automatically gives a self-consistent description. Third, the approach can be naturally expanded to more complicated systems such as asymmetric QWs, and also allows for incorporating external electric and magnetic fields, stress, and disordered potential acting on electrons and holes in the QW because of inherent inhomogeneities of the structure. All these effects, which modify the single particle part of the Hamiltonian, appear automatically in self-consistent equations for the variational functions.

Applying variational approach to a function of the following form

$$\Psi_{self}(r, z_e, z_h) = \psi(r)\chi_e(z_e)\chi_h(z_h), \tag{1}$$

where the first term corresponds to exciton center-of-mass motion, while two other terms describe "single-particle" motion of electrons and holes, respectively, in the confinement direction. Such a separation, however, is only possible in the zero order approximation, and in the final self-consistent solution each of these functions are influenced by all other functions. Main equations of our method, which take into account the discontinuity of electron and hole masses across interfaces between wells and barriers have the following form:

$$\left[H_e + \overline{V}_e(z_e)\right] \chi_e(z_e) = E_e\chi_e(z_e), \tag{2}$$

$$\left[H_h + \overline{V}_h(z_h)\right] \chi_h(z_h) = E_h\chi_h(z_h), \tag{3}$$

$$\left[\alpha K_r + \overline{V}_r(r)\right] \psi(r) = E_X\psi(r), \tag{4}$$

where $H_{e,h}$ is the single-particle electron (hole) Hamiltonian describing their motion in the confinement direction, K_r is the exciton kinetic energy, $\alpha = \langle\chi_e\chi_h|\frac{\mu_\perp}{\mu_\perp(z_e, z_h)}|\chi_e\chi_h\rangle$ is a coefficient appearing as a manifestation of the mass mismatch effect ($\mu_\perp$ is an reduced mass of the electron-hole pair for the in-plane motion), and the effective potentials are defined as:

$$\overline{V}_r(r) = \langle\chi_e\chi_h|V_{reh}|\chi_e\chi_h\rangle, \tag{5}$$

$$\overline{V}_{e,h}(z_{e,h}) = \langle\psi\chi_{h,e}|V_{reh}|\psi\chi_{h,e}\rangle. \tag{6}$$

The angle brackets indicate the integration over two of three independent variables. As it can be seen, α is identically equal to unity in case of absence of the mass mismatch effect and approaches $\mu_\perp^w/\mu_\perp^b$ with increasing width of the QW. The initial form of the electron-hole interaction potential V_r takes into account dielectric discontinuity and is obtained by solving

a Poisson equation for a layered system.[19] The total energy of the electron-hole pair is given by the expression:

$$E = \langle\Psi|\hat{H}|\Psi\rangle = E_e + E_h + E_X - \langle\chi_e|\overline{V}_e|\chi_e\rangle - \langle\chi_h|\overline{V}_h|\chi_h\rangle. \tag{7}$$

In order to obtain solution for Eqs. (2)-(4) we apply the method of successive iterations. Expecting that the renormalization of the confining potentials is not very strong, we obtain the zero-order approximation by setting $\overline{V}^{(0)}_{e,h} = 0$ and solving equations

$$H_{e,h}\chi^{(0)}_{e,h}(z) = E^{(0)}_{e,h}\chi^{(0)}_{e,h}. \tag{8}$$

The calculated eigenfunctions $\chi^{(0)}_{e,h}(z_{e,h})$ are then substituted into integral (5) in order to find $\overline{V}^{(0)}_r(r)$, a zero approximation for $\overline{V}_r(r)$:

$$\overline{V}^{(0)}_r(r) = \langle\chi^{(0)}_e\chi^{(0)}_h|V_{reh}|\chi^{(0)}_e\chi^{(0)}_h\rangle \tag{9}$$

The next step is to substitute the obtained effective potential into Eq. (4):

$$\left[\alpha K_r + \overline{V}^{(0)}_r(r)\right]\psi^{(0)}(r) = E^{(0)}_X\psi^{(0)}(r) \tag{10}$$

which describes properties of a two-dimensional electron-hole pair interacting via the effective potential $\overline{V}^{(0)}_r(r)$. This potential is the result of quantum-mechanical averaging of the Coulomb potential with zero-order wave functions $\chi^{(0)}_e$, $\chi^{(0)}_h$.

Substituting calculated zero-order wave functions $\psi^{(0)}(r)$, $\chi^{(0)}_{e,h}(z_{e,h})$ in Eq. (6) we can compute a correction to the QW electron and hole confined potentials $\overline{V}^{(1)}_{e,h}(z_{e,h})$ due to electron-hole interaction:

$$\overline{V}^{(1)}_{e,h}(z_{e,h}) = \langle\psi^{(0)}\chi^{(0)}_{h,e}|V_{reh}|\psi^{(0)}\chi^{(0)}_{h,e}\rangle. \tag{11}$$

This process is continued until potentials are self-consistent with a desired degree of accuracy. The condition of self-consistence can be presented in the following form

$$\langle\psi^{(n)}|\overline{V}^{(n)}_r|\psi^{(n)}\rangle \approx \langle\chi^{(n)}_e|\overline{V}^{(n)}_e|\chi^{(n)}_e\rangle \approx \langle\chi^{(n)}_h|\overline{V}^{(n)}_h|\chi^{(n)}_h\rangle. \tag{12}$$

The system of equations (2)-(11), including the self-consistency condition (12), represents the complete set of equations required to find the minimum value of the ground state energy of the exciton described by the factorized form (1) of the trial function Ψ. The details of

TABLE I: Parameters of the materials used in the calculations: gap energy (E_{gap}), conduction band offset ($\Delta E_c/\Delta E_g$), Luttinger parameters (γ_1 and γ_2), effective mass of the electron in conduction band (m_e^*), dielectric constant (ϵ), units of length (a_B) and energy (E_B). a_B and E_B are given only for the well materials. Luttinger parameters correspond to the heavy-hole effective mass.

Material	E_{gap} (eV)	$\Delta E_c/\Delta E_g$	γ_1	γ_2	$m_e^*(m_0)$	ϵ	q	a_B (Å)	E_B (meV)
GaAs	1.518	60%	6.85	2.1	0.0665	12.53	0.043	159	7.23
$Al_{0.4}Ga_{0.6}As$	2.163		4.67	1.17	0.0895	11.5			
$In_{0.53}Ga_{0.47}As$	0.813	40%	11.0	4.18	0.041	13.9	0.049	291	3.56
InP	1.423		5.15	0.94	0.0803	12.6			

calculations of the effective potentials (5) and (6) as well as the respective computer code are given in Appendixes A and B, respectively.

The calculations were performed for two different material systems: $GaAs/Al_{0.4}Ga_{0.6}As$ and $In_{0.53}Ga_{0.47}As/InP$, which have been extensively studied in the past so that our calculations can be compared with previous results. The concrete parameters of these structures used in our calculations are listed in Table I. In order to compare our method with the standard variational approach we calculated the dependence of the binding energy of the heavy-hole exciton in $GaAs/Al_{0.4}Ga_{0.6}As$ and $In_{0.53}Ga_{0.47}As/InP$ structures on the width of the quantum well. These calculations are compared with the results obtained by a standard variational method in Ref. 19. The authors of that work calculated binding energy using a trial function with two variational parameters:

$$\phi(\rho, z_e, z_h) = \exp\left(-\frac{1}{a}\sqrt{\rho^2 + \lambda^2(z_e - z_h)^2}\right) u_e(z_e)u_h(z_h), \tag{13}$$

where $u_{e,h}(z_{e,h})$ are single-particle one-dimensional wave functions describing confinement of the electrons and holes in the well.

The results of our calculations are presented in Figs. 1 and 2, where we plotted the dependence of the binding energy of a heavy-hole exciton in a $GaAs/Al_{0.4}Ga_{0.6}As$ and $In_{0.53}Ga_{0.47}As/InP$ structures as a function of well width for several different approximations: without any mismatches, with mass or dielectric mismatch only, and with both mismatches taken into account simultaneously. Comparing the results of our calculations with those of the standard variational approach one can see that our method gives better (meaning lower) values for the exciton energy for entire considered range of QW thicknesses and for both

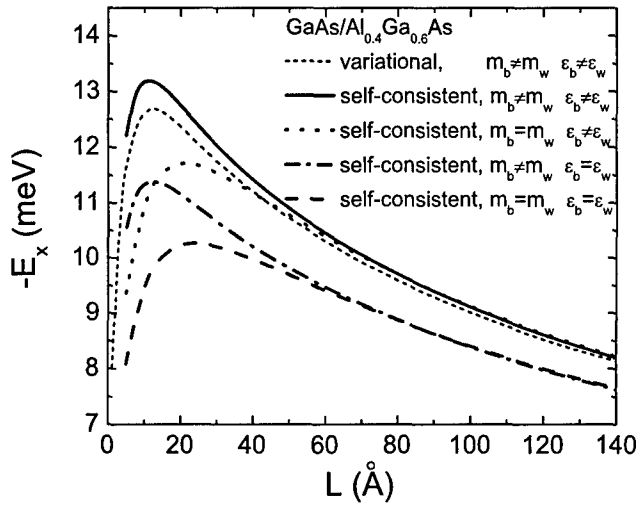

FIG. 1: Dependence of the binding energy of a HH exciton in a $GaAs/Al_{0.4}Ga_{0.6}As$ single QW on the width of the well. Curves represent different parameters of the well and barrier materials with and without mass mismatch (*mm*) and dielectric mistmatch (*dm*): *mm* and *dm* (solid line), only *dm* (dotted line), only *mm* (dashed dotted line) and dashed line doesn't have any mismatch. Comparison with the results of the standard variational approach (short dashed line) is based on data taken from Ref. 19 and includes both mismatches.

considered material systems.

B. New variational approach to quantum confined Stark effect

Since we intended to use an electric field as a switching and/or tuning mechanism in the suggested MQW structures, it was necessary for us to have an effective method for calculating electric field induced changes in exciton frequencies and oscillator strengths. While these effects have been rather well studied previously, the existing methods were insufficient for our objectives because, first, most of them used a mode of infinite potential well,[20–23] which was not applicable to our situation, and, second, they were not able to deal with the electric field induced broadening of exciton levels. To address these issues we adopted a method of complex scaling, widely used in atomic physics to deal with atomic resonances, to the

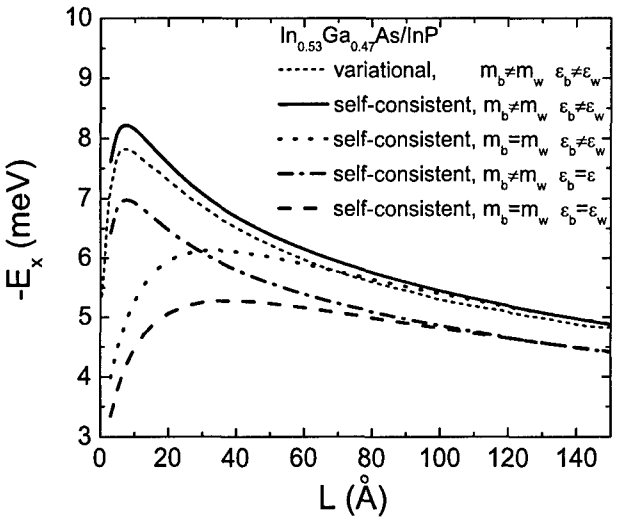

FIG. 2: Dependence of the binding energy of a HH exciton in a $In_{0.53}Ga_{0.47}As/InP$ single QW on the width of the well. Curves represent different parameters of the well and barrier materials with and without mass mismatch (*mm*) and dielectric mistmatch (*dm*): *mm* and *dm* (solid line), only *dm* (dotted line), only *mm* (dashed dotted line) and dashed line doesn't have any mismatch. Comparison with the results of the standard variational approach (short dashed line) is based on data taken from Ref. 19 and includes both mismatches.

exciton problem. As far as we know, that was the first such attempt that proved to be rather successful.

The complex scaling (also known as complex coordinates, coordinate rotation) approach was developed in the 1970s to deal with resonances in atomic and molecular physics and chemistry.[24,25] This approach addressed the main conceptual problem in dealing with the resonances: because of the inherent finite life-time, they cannot be described as stationary states of a system with the Hermitian Hamiltonian. As a result, an arsenal of powerful methods for calculating eigenvalues and eigenfunctions of "normal" bound states becomes useless in the case of resonances. The main idea of the method is to introduce such a transformation of an original Hamiltonian that would produce a non-Hermitian Hamiltonian, whose complex eigenvalues would give the positions and the widths of the resonances.

One of the simplest realizations of this idea is to introduce a complex scaling of coordi-

nates in an original Hamiltonian, $\hat{H}$, $r \rightarrow r\exp(i\theta)$, which can be described as a similarity transformation of the Hamiltonian

$$\hat{\tilde{H}}(\theta) = \hat{S}(\theta)\hat{H}\hat{S}^{-1}(\theta), \tag{14}$$

where the complex scaling operator $\hat{S}$ is defined as

$$\hat{S}f(r) = f(re^{i\theta}). \tag{15}$$

The physical meaning of this transformation can be illustrated by applying it to a typical asymptotic form of a scattering wave function for a potential vanishing at infinity

$$\psi(r \rightarrow \infty) \propto \exp(ikr), \tag{16}$$

where r is a radial coordinate and k is a wave number. If one tries to describe a resonance as an eigenvalue problem with a boundary condition given by Eq. (16), the value of k will come out complex, $k = \mid k \mid e^{-i\phi}$, and the respective wave function will exponentially diverge at infinity. If however, we apply transformation (15) to this wave function, it will become

$$\hat{S}\psi(r \rightarrow \infty) \propto e^{i|k|\exp[i(\theta-\phi)]},$$

which with the proper choice of θ can be made square integrable. This example illustrates the main idea of the complex scaling: with an appropriate choice of the transformation parameter θ, the transformed Hamiltonian, $\hat{\tilde{H}}(\theta)$ can be made to have square integrable eigenfunctions with complex eigenvalues. Their real and imaginary parts are interpreted as the energies and widths of the resonance respectively.

The independence of resonant eigenvalues on θ lies at the foundation of various variational schemes to calculating resonances within the complex scaling method. Since the transformed eigenfunctions belong to L^2 Hilbert space, one can calculate the value of the energy following the standard expression

$$E = \frac{\langle\psi(r)|\hat{\tilde{H}}(\theta)|\psi(r)\rangle}{\langle\psi(r)|\psi(r)\rangle}, \tag{17}$$

where, however, the traditional definition of the scalar product must be modified because of the non-Hermitian nature of the Hamiltonian. While the standard definition requires complex conjugation of the function appearing at the left side of the product, the new rule requires one to conjugate only those parts of the wave-function that would have been complex

without the scaling transformation. Since exact eigenfunctions of the transformed Hamiltonian are usually not known, any kind of an approximate representation of these functions would result in a θ-dependence of the resulting resonance energies. It was suggested, therefore, that the approximate values must be stabilized with respect to the changes of θ. Thus θ plays a role here as an additional variational parameter. It should be understood, however, that applying the variational principle to Eq. (17) one does not obtain an upper limit for the energy as in the case of regular variational calculations. Nevertheless, it was found in numerous calculations of resonances in molecular and atomic physics that stabilization with respect to θ is key to successful application of complex scaling.[24]

In order to realize complex scaling in the exciton problem, we choose the trial exciton function in the following form:

$$\Psi_{\text{trial}}(r, z_e, z_h) = \chi_e(z_e e^{-i\theta_e})\chi_h(z_h e^{-i\theta_h})\psi(re^{-i\theta_r}). \tag{18}$$

where the first two functions obey single particle equations for electrons and holes respectively. These equations solved with rotated Siegert boundary conditions yield complex energy values, $W_{e,h}$, but because of the dilatation transformation the respective wave functions are square integrable despite the presence of an electric field. This fact makes these functions suitable for calculating an effective potential, $\overline{V}_r(r)$, that enters an equation determining the last of the functions in Eq. (18):

$$\left[K_r(r) + \overline{V}_r(r)\right]\psi(re^{-i\theta_r}) = W_X\psi(re^{-i\theta_r}) \tag{19}$$

where $\overline{V}_r(r)$ is defined according to

$$\overline{V}_r(r) = \langle\chi_e\chi_h|V_{reh}(R)|\chi_e\chi_h\rangle. \tag{20}$$

The inner product, designated in Eq. (20) as $\langle\cdots\rangle$ is understood as a bi-orthogonal product and implies, as usual, integration of the Coulomb potential with corresponding wave functions over electron and hole z-coordinates, but unlike regular normal product in problems with Hermitian hamiltonians, it does not involve complex conjugation. The corresponding value of the total quasi-bound energy $W = E - i\Gamma/2$ can be found as

$$W = \langle\Psi|\hat{H}|\Psi\rangle = W_e + W_h + W_X \tag{21}$$

The main advantage of the approach described above is that it allows one to calculate, in principle, not only field-induced single-particle widths $\Gamma_{e,h}$ but the *exciton width* Γ_X as

well, which describes a renormalization of the electron-hole pair lifetime by the effective interaction. In this project we limited our attention to a particular case of shallow QWs, for which electric field induced broadening is of a greater importance than for deeper wells. We showed that in this case single-particle energies and life-times can be with a good accuracy described by an approximate wave functions of the following form

$$\chi_{tr}(ze^{-i\theta};\beta,\theta) \equiv \chi_{tr}(\tilde{z};\beta,\theta) = \sqrt{\kappa_0(1-\beta^2)e^{-i\theta}}\exp\left[\kappa_0\left(-|\tilde{z}|+\beta\tilde{z}\right)\right], \tag{22}$$

where variational parameters β and θ are allowed to be complex with the only restriction $\mathrm{Re}(\beta) < 1$, which is dictated by the square integrability of the biorthogonal scalar product of this function. Applying the complex variational principle we obtain the following equations for the energy

$$\kappa^2(\beta,\theta) = \left(1-\beta^2\right)\left(2e^{-i\theta}-e^{-i2\theta}\right) + \frac{f\beta e^{i\theta}}{1-\beta^2}. \tag{23}$$

After performing a variation of independent variational parameters β, θ and simple algebraic manipulations we obtain the following equations for their optimal values:

$$e^{-i\theta} = 1-\beta^2, \tag{24}$$

$$-f+2\beta-3f\beta^2-2\beta^3-12\beta^5+28\beta^7-22\beta^9+6\beta^{11} = 0. \tag{25}$$

For small fields, all but the first two terms on the left hand side of Eq. (25) can be omitted, and we obtain $\beta \approx f/2$. The corresponding value for energy shift $\varepsilon_R - 1 \approx f^2/4$, which differs from a result obtained by a usual perturbation treatment of the Airy equation only by a factor of 1.25. For moderate values of the electric field this variational energy is even closer to the exact value than the perturbative result. Including in the approximate solution of Eq. (25) the third quadratic term of its l.h.s we obtain a modified solution

$$\beta = \frac{1-\sqrt{1-3f^2}}{3f}, \tag{26}$$

from which it is seen that when the electric field exceeds a critical value $f = f_{cr} = 1/\sqrt{3} \approx 0.58$, a square-root singularity appears, and the corresponding energy acquires an imaginary part. The exact solution of Eq. (25) moves this critical value to lower fields:

$$f_{cr} \approx 0.416, \quad \beta_{cr} = 1/3. \tag{27}$$

Thus, the combination of the complex scaling and variational approaches allows us to find not only the real part of the electric field induced shift of the single-particle energy, but

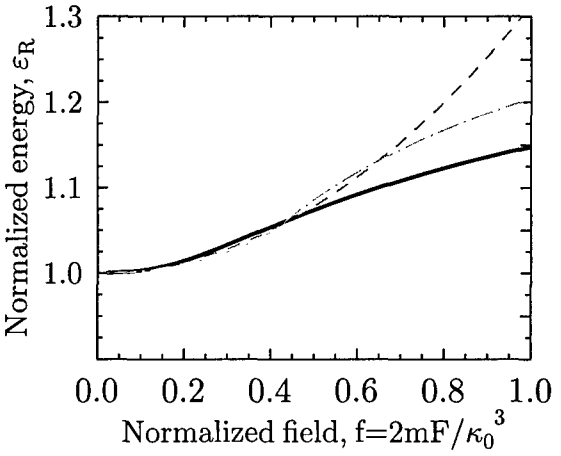

FIG. 3: The real part ε_R of the normalized energy κ^2 as a function of normalized electric field $f = 2mF/\kappa_0^3$. The solid line represents the exact solution in terms of Airy functions. The dashed line shows the quadratic behavior of perturbative solution for small f. The dot-dashed line is the real part for the energy, Eq. (23), obtained with the help of a variational method with a trial function (22).

also its imaginary part. Of course, the presence of the ionization threshold at f_{cr} predicted by the variational calculations does not correctly reproduce the type of the singularity in the field dependence of the resonance width (this hardly can be expected from any variational approach), it gives a remarkably good description of both the real and imaginary parts of the energy at values of electric field exceeding f_{cr}. At smaller fields the difference between exact zero given by our approach for the imaginary part and exponentially small value obtained from the exact solution is also negligible. In order to illustrate this point we plot the dependencies of the real and imaginary parts of variational energy, Eq. (23), on the normalized electric field, obtained from the solutions of Eqs. (24) and (25) in Figs. 3 and 7. One can see that the variational results for the real and imaginary parts of the energy are in very good agreement (especially in the case of small and moderate fields) with the results of the exact solution of the single particle equation obtained with the help of Airy functions. Using these results we were able to calculate the effective electron-hole potential modified by electric field, and, respectively, corrections to electron-hole energy due to Coulomb interaction. We showed that these corrections had real and imaginary parts,

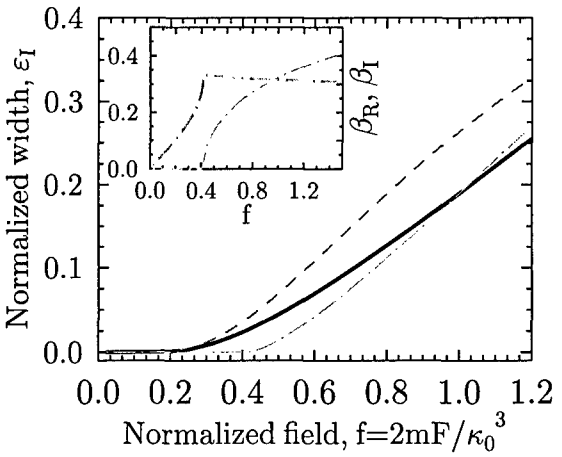

FIG. 4: The imaginary part ε_I of the normalized energy κ^2 as a function of normalized electric field $f = 2mF/\kappa_0^3$. The solid line represents the exact solution of in terms of Airy functions. The dashed line shows the exponential non-analytical growth of the perturbative solution. The dot-dashed line is the imaginary part for the energy, Eqs. (23, obtained with the help of a variational method with a trial function (22). The insert shows the behavior of the real and the imaginary parts of the variational parameter β for the trial function (22).

which corresponded to exciton binding energy and Coulomb corrections to exciton field ionization rates. Results for the real and imaginary parts of the exciton binding energy are presented in Figs. 5,6, where we also plot single-particle electron hole contributions, and the total exciton energy and its width, defined by Eq. (21).

C. Effects of electric field on inhomogeneous broadening of quantum well excitons

An important part of this project was concerned with understanding of broadening mechanisms for QW excitons, especially in the presence of the external electric field. While the inhomogeneous broadening of excitons in QWs was studied extensively,[26–31] the effects due to the electric field have been given very little attention so far. At the same time, for this project these effects are very important, and thus it is only natural that we carried out the first study of electric field effects on the inhomogeneous broadening of QW excitons.

We demonstrated in this project that the main effect of the electric field is due to modi-

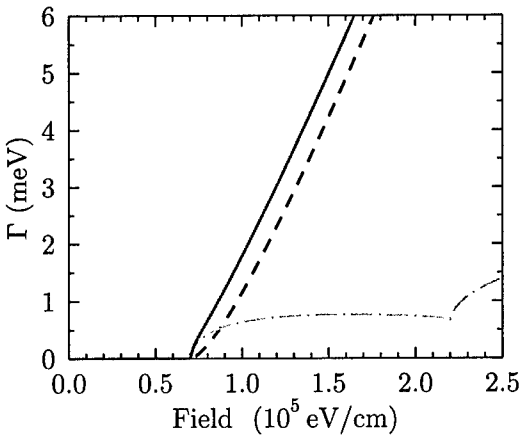

FIG. 5: The dependence on the electric field for the total (solid line), the exciton (dotted-dashed line), and the net hole-electron (dashed line) imaginary parts of complex energies (widths). Data are for $L = 20\mathring{A}$ AlGaAs/GaAs SQW.

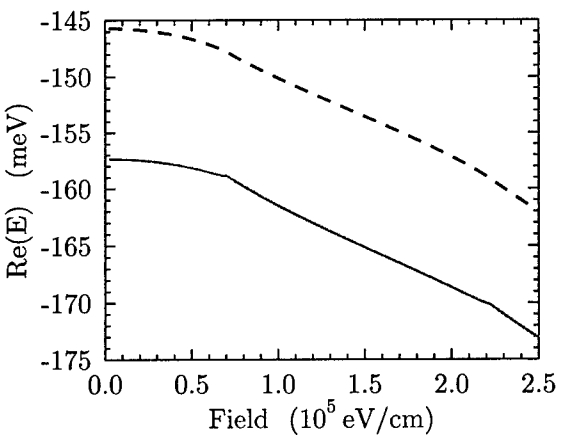

FIG. 6: The dependence on the electric field for the total (solid line), and the net hole-electron (dashed line) real parts of complex energies. Energy is counted from the barrier band gap.

fication of the random potential caused by the field induced reconstruction of electron-hole wave functions, while broadening due to Stark effect in moderate electric fields remains rather small. We found that for QWs whose thickness, L, is smaller than some critical value, L_{cr}, an electric field reduces fluctuations of this potential resulting in a counterintu-

itive *narrowing* of the exciton line width with the electric field. When $L > L_{cr}$, the sign of the electric field contribution to the line width changes and exciton lines becomes broader with an increase of the field.

Our primary goal in this part of the project was to calculate the variance of the effective random exciton potential, V_{eff}, defined as $W = \sqrt{\langle V_{eff}(\mathbf{R})^2 \rangle}$, which is the main quantity responsible for manifestations of the inhomogeneous broadening. Usually, the effective random potential acting on the exciton's center-of-mass, for each type of disorder, is dominated by heavy-hole contribution, and can be presented in the form

$$V_{eff} = \int U(\mathbf{R} \pm m_h \boldsymbol{\rho}/M; z) \psi^2(\boldsymbol{\rho}) \chi_h^2(z) \, d^2\rho dz. \tag{28}$$

where $U(\mathbf{R} \pm m_h \boldsymbol{\rho}/M; z)$ is a microscopic random potential acting on the hole due to surface roughness or alloy fluctuations, and functions $\psi(\boldsymbol{\rho})$ and $\chi_h(z)$ represents wave functions characterizing motion of the excitons in the plane of the QW, and the hole motion in the growth direction respectively. The microscopic potential describing the alloy disorder can be presented as[31]

$$U_{alloy}(\mathbf{r}) = \alpha \xi(\mathbf{r}) \theta \left(L^2/4 - z^2 \right) / N, \tag{29}$$

where $\theta(z)$ is a step-function, N is the concentration of lattice sites ($N = 4/a_{lat}^3$ for zincblende materials, a_{lat} is a lattice constant), $\xi(\mathbf{r})$ is the random fluctuation of the local concentration of atoms in the alloy from the average value xN, and $\alpha = dE_v/dx$ characterizes the rate of shift of the valence bands with composition x. The interface roughness potential can be presented in the following form[32]

$$U_{int}(\mathbf{r}) = V_0 \left[\eta_1(\boldsymbol{\rho}) \delta(z + L/2) - \eta_2(\boldsymbol{\rho}) \delta(z - L/2) \right], \tag{30}$$

where $\delta(z)$ is a δ-function, V_0 is a hole off-set band energy. Random functions $\eta_{1,2}(\boldsymbol{\rho})$ with zero mean characterize a deviation of the ith interface from its average position.

The statistical properties of alloy and interfacial roughness are characterized by the correlators:[29,32,33]

$$\langle \xi(\boldsymbol{r}_1) \xi(\boldsymbol{r}_2) \rangle = x(1-x) N \delta(|\boldsymbol{r}_1 - \boldsymbol{r}_2|), \tag{31}$$

$$\langle \eta_i(\boldsymbol{\rho}_1) \eta_j(\boldsymbol{\rho}_2) \rangle = h^2 f_{ij} \zeta(|\boldsymbol{\rho}_1 - \boldsymbol{\rho}_2|), \tag{32}$$

where h is an average height of interface inhomogeneity, and $\langle \cdots \rangle$ denotes an ensemble average. For the interface height-height correlator we assumed that the dependence of

both diagonal and non-diagonal correlations on the lateral coordinates $\boldsymbol{\rho}$ is described by the same function $\zeta(\boldsymbol{\rho})$. The diagonal elements f_{ii} are different if two interfaces are grown under different conditions, which happens naturally for $GaAs$ based structures. (Growth of a ternary alloy on $GaAs$ occurs differently from growth of $GaAs$ on the alloy; besides using techniques of growth interruption one can significantly modify statistical properties of the grown interfaces.) The non-diagonal element $f_{12}(L/\sigma_{\|})$ introduces correlations between different interfaces. The respective quantity, which can be called the *cross-* or *vertical-correlation function*,[33] is a function of the average width of the well and is characterized by the vertical correlation length $\sigma_{\|}$. We showed that cross-correlations play a very important role in QWs, and has to be taken into account in order to explain experimentally observed exciton broadening.

We calculated the effective potential using exciton wave functions found with the help of variational approach described in the previous section of this report. The results of these calculations are summarized in the following expressions.

$$W^2_{all}(F) \qquad \propto \left[\gamma_0^{(all)} + \gamma_2^{(all)} F^2\right], \tag{33}$$

$$W^2_{int}(F) \propto \left[\gamma_0^{(int)} + \gamma_1^{(int)} F + \gamma_2^{(int)} F^2\right], \tag{34}$$

where F represents the strength of the electric field and parameters γ_i are monotonic functions of the QW width. These expressions show that in the range of parameters where the Stark broadening is exponentially small, there exists a strong *power law* field dependence of inhomogeneous exciton broadening caused by the field induced changes in the variance of the effective exciton potential.

A remarkable feature of Eqs. (33) and (34) is the presence of a linear-in-field term in the interface roughness contribution with factor $\gamma_1^{(int)}(L) \propto (f_{11} - f_{22})$. One can see that this term results from asymmetry between two interfaces of the well, which manifests itself through different roughnesses, $f_{11} \neq f_{22}$. The presence of the linear term gives rise to an interesting effect: one can switch between field induced narrowing or broadening of the exciton line by simply changing the polarity of the applied field. In $GaAs$ based heterostructures the interface asymmetry appears naturally because of the polar nature of $GaAs$, and thus, this effect should play an important role in electric field dependence of the exciton broadening in GaAs quantum wells. Quadratic in the field terms in Eqs. (33) and (34) also possess nontrivial properties . We showed that the respective coefficient γ_2 changes sign as

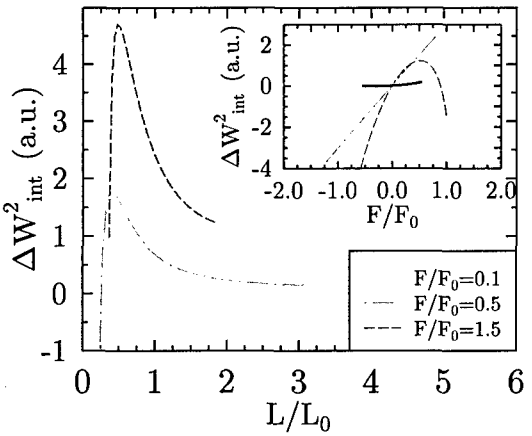

FIG. 7: The field dependent part of the variance, $\Delta W^2_{int} = \Omega\left[\gamma_1 F + \gamma_2 F^2\right]$, as a function of QW widths for interface roughness contribution with different corrugation at interfaces ($f_{11} = 4, f_{22} = 1$) for three fixed electric fields: $F/F_0 = 0.1, 0.5, 1.5$. Inset: ΔW^2_{int} as a function of electric field for three QW widths: $L/L_0 = 0.3$ (dashed), $L/L_0 = 0.55$ (dotted-dashed), and $L/L_0 = 3$ (solid). Note that $L/L_0 = 0.55$ corresponds to the case, when second order term in the field dependence changes sign. (see text).

a function of the thickness of the well: its negative for narrower well and positive for wider ones. This intriguing behavior is illustrated in Fig. 7.

III. OPTICAL PROPERTIES OF BRAGG MULTIPLE-QUANTUM-WELL STRUCTURES

A. Spectral engineering with MQW structures

Preliminary studies of the optical spectra of BMQW structures, carried out by us before the start of the work on the current project,[34–36] showed that the transmission and reflection spectra of BMQW structures can be significantly modified by deliberately introducing defects into the structures. Those findings laid the foundation for the current project, but they were conducted for ideal structures. Therefore, our first task was to incorporate into consideration homogeneous and inhomogeneous broadenings of the excitons. We carried out first studies

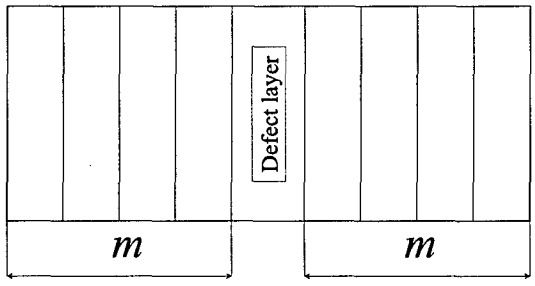

FIG. 8: A MQW structure with a defect.

of the effects of the inhomogeneous broadening on the BMQW structures with defects, and as a by-product we developed a solid theoretical foundation for the effective medium approximation, which has been used previously for calculation of optical properties of ideal BMQW structures on a heuristic basis. We proved that the reflection coefficient of a QW with an in-plane disorder with a good accuracy is determined by an average value of the exciton susceptibility (neglecting exciton spatial dispersion). Thus, the optical properties of inhomogeneously broadened QW excitons can be described by replacing a susceptibility of an ideal system

$$\chi(\omega) = \frac{\Gamma_0}{\omega_0 - \omega - i\gamma}, \tag{35}$$

where ω_0 is the exciton resonance frequency, γ is the exciton relaxation rate due to inelastic processes, Γ_0 inverse radiative life-time of excitons with an effective susceptibility

$$\tilde{\chi} = \int d\omega_0 f(\omega_0) \frac{\alpha}{\omega_0 - \omega - i\gamma}. \tag{36}$$

where $f(\omega_0)$ is the distribution function of the exciton frequencies. The inhomogeneous broadening is characterized, in this approach, by the variance of $f(\omega_0)$. Using this approach we analyzed reflection and transmission spectra of a BMQW structure with so called Ω-defect, which consists of $N = 2m + 1$ quantum well-barrier layers which are all identical except for one, at the center, where the QW has a different frequency of the exciton resonance (Fig. 8). Such a defect in $GaAlAs/GaAs$ system can be produced either by changing the concentration of Al in the barriers surrounding the central well,[37,38] or the width of the well itself[39] during growth. To describe spectral properties of such a structure we needed to calculate total transfer matrix through the MQW structure:

$$M = T_h \dots T_h T_d T_h \dots T_h, \tag{37}$$

where T_h and T_d are the transfer matrices through the host and defect layers, respectively, described by the reflection and transmission coefficients $r_{h,d}$ and $t_{h,d}$. The possibility of an analytical analysis of the spectral properties is based on a convenient representation of matrix M in the basis of eigenvectors of the host transfer matrix T_h

$$M = \begin{pmatrix} e^{-\Lambda} M_- & a_+ A \\ -a_- A & e^{\Lambda} M_+ \end{pmatrix}, \tag{38}$$

where $\Lambda = N\lambda_h$,

$$M_\pm = e^{\pm(\lambda_d - \lambda_h)} \pm \frac{2e^{\mp\lambda_h}}{\sinh\lambda_h} \sinh^2 \frac{1}{2}(\lambda_d - \lambda_h), \tag{39}$$

and

$$A = \frac{\sin\phi}{\sinh\lambda_h} (\chi_d - \chi_h). \tag{40}$$

Here we introduced $a_\pm$, non-unit components of the eigenvectors of T_h,

$$a_\pm = \frac{1 - e^{\pm\lambda_h} t_h}{r_h}, \tag{41}$$

and $\lambda_{h,d}$ are the eigenvalues of the host and defect QW's transfer matrices obeying the dispersion law in a periodic quantum well superlattice:[40–42]

$$\cosh\lambda_{h,d} = \frac{1}{2}\mathrm{Tr}\, T_{h,d} = \cos\phi - \chi_{h,d}\sin\phi. \tag{42}$$

A defect inserted into the structure leads to a modification of the reflection spectrum of the MQW in the vicinity of the exciton frequency, ω_d, of the defect well. As it was expected, we confirmed that the most prominent changes occur when ω_d falls into the polariton band-gap of the host structure. A typical form of such a modification in broadened systems is shown in Fig. (9), and is characterized by the presence of a closely positioned minimum and maximum. We found it convenient to present the reflection coefficient in the form

$$r_{MQW} = \frac{r_0}{1 - r_{add}}, \tag{43}$$

where

$$r_0 = \frac{2\sinh(\Lambda)}{a_- e^{\Lambda} - a_+ e^{-\Lambda}} = -\frac{\chi_h}{\alpha + i\coth(\Lambda)\sinh\lambda_h} \tag{44}$$

is the reflection coefficient of a pure MQW structure (without a defect) with the length N, $\alpha = \sin\phi + \chi_h\cos\phi$, and r_{add} introduces the modification of the reflection caused by the

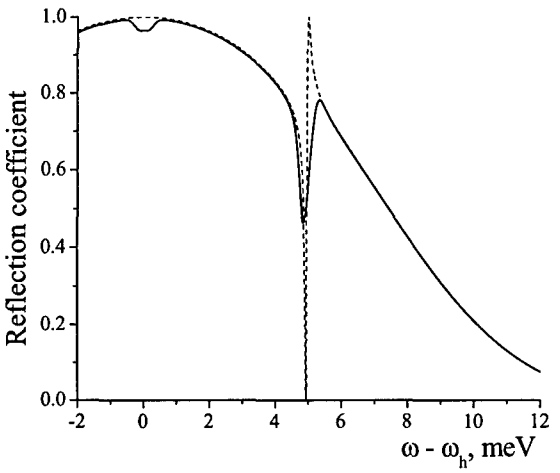

FIG. 9: A typical dependence of the reflection coefficient of a MQW structure with an embedded defect well in a neighborhood of the exciton frequency of the defect well. The dotted line shows the reflection for a lossless system, and the solid line corresponds to a broadened system (parameters are taken for GaAs/AlGaAs).

defect

$$r_{add} = (\chi_d - \chi_h)\sin\phi\,\frac{\sinh\lambda_h + i\chi_h\sinh\Lambda}{\chi_h\cosh\Lambda - \alpha} \times\frac{1}{A(\alpha+\chi_h\cosh\Lambda) - \chi_h\sinh\Lambda}. \tag{45}$$

This expression demonstrated that regardless of the value of the defect frequency ω_d, r_{add} vanishes at frequencies $\omega = \omega_h$ because of the phase factor $\sin\phi \approx -\pi q$, where q is the detuning from the Bragg resonance

$$q = \frac{\omega - \omega_h}{\omega_h}, \tag{46}$$

This is a significant for applications observation because it tells that in order to achieve a substantial modification of the spectrum, it is necessary to choose ω_d as far away from ω_h as possible. In this case, however, we showed that the broadening of the host wells did not affect the defect-induced features of the reflection spectrum.

We carried out a more detailed analysis of the reflection spectrum in the case of relatively short structures, $\Lambda \ll 1$, which presents the most immediate interest for possible applications. In this case we found following approximate expression for the reflection coefficient,

which is very convenient for qualitative analysis.

$$r = \frac{i\bar{\Gamma}}{\omega_h - \omega + i(\gamma + \bar{\Gamma})} \frac{\Omega_s - \Gamma_0 D_d}{i\Gamma_0 - \Gamma_0 D_d}, \tag{47}$$

where $D_{d,h} = 1/\chi_{d,h}$, and $\bar{\Gamma}$ is the radiative width of the pure Bragg MQW structure, which is N-fold enhanced because of the formation of a superradiant mode[43]

$$\bar{\Gamma} = \frac{\Gamma_0 N}{1 - i\pi q N}. \tag{48}$$

Reflection spectrum in this case is characterized by the Fano-like behavior with reflection minimum at ω_- and a subsequent maximum at ω_+. It is significant that the Fano-like form of the reflection survives even in structures as short as less than 10 periods. In this case we derived following approximate expressions for frequencies ω_- and ω_+

$$\omega_- = \omega_d - \Omega_s - \frac{\gamma^2}{\Omega_s}, \tag{49}$$

where Ω_s is defined as

$$\Omega_s = \frac{\omega_d - \omega_h}{N}. \tag{50}$$

and

$$\omega_+ = \omega_d + \frac{1}{\pi}\left(\tilde{\Omega}_s - \Omega_s\right) + \frac{\Gamma_0 \tilde{\gamma}}{\tilde{\Omega}_s \Omega_s}\left(\tilde{\Omega}_s + \Omega_s\right) \tag{51}$$

where $\tilde{\Omega}_s = \sqrt{\Omega_s^2 + 4\tilde{\gamma}^2}$ and $\tilde{\gamma}$ is the effective broadening defined by $\tilde{\gamma} = \gamma + \frac{\sqrt{\pi}}{2}\Delta$. The values of the reflection at these points are

$$\begin{aligned} R_{min} &= \frac{|\bar{\Gamma}|^2 \gamma^2 N^4}{(\omega_d - \omega_h)^4 (N-1)^2}, \\ R_{max} &= \frac{|\bar{\Gamma}|^2 (\tilde{\Omega}_s + \Omega_s)^2}{(\omega_+ - \omega_h)^2 (2\Gamma_0 + \pi\tilde{\gamma})^2}. \end{aligned} \tag{52}$$

Fig. 10 illustrates the Fano-like form of the reflection coefficient and also demonstrates that our analytical formulas give a satisfactory description of the reflectivity in the vicinities of the extrema for such short systems. An important technological characteristics relevant for switching/modulating applications is the reflection contrast defined as defined as the ratio of the maximum and minimum reflections $\eta = R_{max}/R_{min}$,

$$\eta \approx \left[(\omega_d - \omega_h)/N\sqrt{\gamma\tilde{\gamma}}\right]^4. \tag{53}$$

The highest values of the contrast in the structure under consideration are obtained when the number of periods in the structure is small. For low temperature values of γ, the contrast

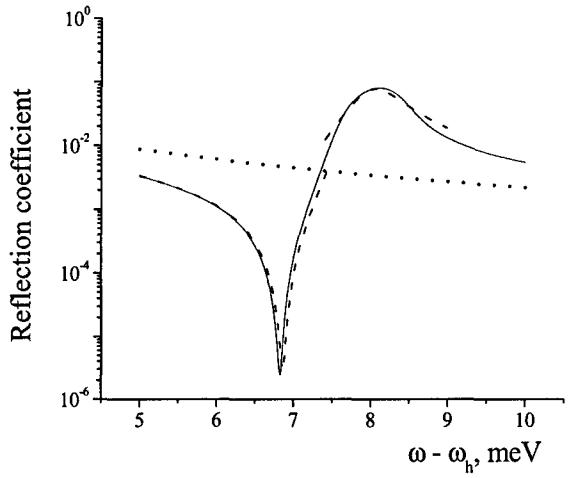

FIG. 10: Reflection coefficient near the exciton frequency of the shallow defect (solid line) for $N = 7$. The dashed lines depict approximation using different expressions for the defect QW susceptibility at the vicinities of the extrema. For reference, the reflection coefficient of a pure MQW structure without a defect is also shown (dotted line).

can be as large as 10^4. However, these large values of the contrast are accompanied by rather small values of R_{max}. For switching or modulating applications, it would be useful to have large contrast, and a large maximum reflection. We demonstrated that this can be achieved in structures with multiple defect wells. Fig. 11 shows the results of numerical computations of the dependence of R_{max} and the contrast upon the number of defects. The structures were constructed of several blocks, each of which is a 9-period long BMQW with a single defect well in the middle.

One can see that, indeed, the spectrum of such multi-defect structures exhibits large R_{max} (up to 0.8 for structures no longer than 80 periods), while preserving high values of the contrast (of the order of 10^4). We demonstrated, therefore, that the most promising for switching applications is a BMQW structure with multiple defects, and that the good values of the contrast can be achieved with experimentally readily available structures of no more than 100 periods with about 10 defects per structure.

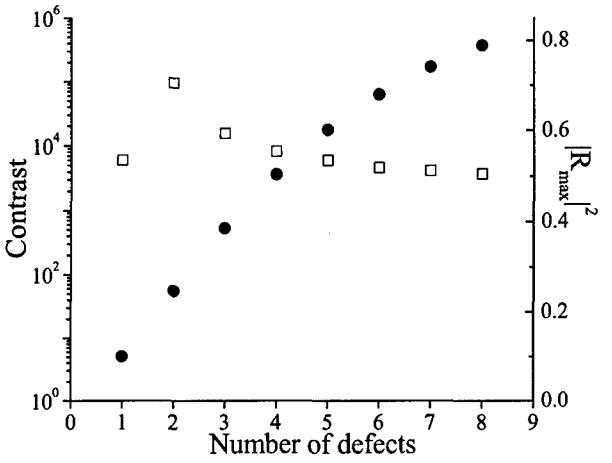

FIG. 11: Dependencies of the maximal reflection (filled circles, right scale) and the contrast (empty squares, left scale) upon the number of the defects in BMQW structures.

B. Tuning and all optical manipulation of the optical spectra of defect BMQW structures

1. Tuning

In this project we studied possibility to tune optical spectra of MQW structures using electric field induced shift of exciton frequencies (quantum confined Stark effect) and also realize an all-optical switching scheme. We suggested using QCSE to shift exciton frequencies by about 10 meV and using angular dependence of the band structure to compensate the ensuing de-tuning of the structure away from the Bragg resonance. We demonstrated that it takes only small adjustment in the direction of propagation of light to compensate for the shift of the exciton frequency, and that the structure of the spectrum does not suffer from any serious distortions. To obtain this result we had to develop a general theory of optical spectra of multiple-quantum-well structures for an arbitrary angle of incidence, polarization state, and taking into account the contrast in the refractive indexes between wells and barriers. One of the main achievements of our group in the course of working on this project was developing highly effective analytical approach allowing analytical qualitative and quantitative analysis of optical spectra of resonant photonic crystals.

A transfer-matrix describing propagation of light across well-barrier interfaces and a QW

involves the product of three matrices $\widetilde{T}_w = T_{bw}T_wT_{wb}$, where

$$T_w = \begin{pmatrix} e^{i\phi_w}(1-i\tilde{\chi}) & -i\tilde{\chi} \\ i\tilde{\chi} & e^{-i\phi_w}(1+i\tilde{\chi}) \end{pmatrix} \tag{54}$$

is the transfer matrix through the QW, where $\phi_w = \omega n_w d_w \cos\theta_w/c$, where d_w is the width of the QW, n_w is the refractive index of the well, and θ_w is the angle between wave vector $\mathbf{k}$ inside the QW, and the growth direction of the structure, $\hat{\mathbf{e}}_z$. Effective susceptibility $\tilde{\chi}$ takes into account the presence of excitons, which can be inhomogeneously and homogeneously broadened, as it was explained in the previous Section of the report. Interfaces matrices T_{bw},T_{wb} are expressed in terms of Fresnel coefficients,

$$T_{bw} = T_{wb}^{-1} = T_\rho(\rho) \equiv \frac{1}{1+\rho}\begin{pmatrix} 1 & \rho \\ \rho & 1 \end{pmatrix}, \tag{55}$$

which contain all information regarding propagation direction and polarization of the incident radiation:

$$\begin{aligned} \rho_s &= \frac{n_w\cos\theta_w - n_b\cos\theta_b}{n_w\cos\theta_w + n_b\cos\theta_b}, \\ \rho_p &= \frac{n_w\cos\theta_b - n_b\cos\theta_w}{n_w\cos\theta_b + n_b\cos\theta_w} \end{aligned} \tag{56}$$

for s ($\mathbf{E} \perp (\mathbf{k}, \hat{\mathbf{e}}_z)$) and p ($\mathbf{E} \parallel (\mathbf{k}, \hat{\mathbf{e}}_z)$) polarizations respectively.

We discovered that the product of the transfer matrices $T_{bw}T_wT_{wb}$ can be presented in the form of the pure quantum well matrix, Eq. (54), but with renormalized parameters:

$$\widetilde{T}_w = T_{bw}T_wT_{wb} = \begin{pmatrix} e^{i\tilde{\phi}_w}(1-i\tilde{S}) & -i\tilde{S} \\ i\tilde{S} & e^{-i\tilde{\phi}_w}(1+i\tilde{S}) \end{pmatrix}, \tag{57}$$

where the effective excitonic susceptibility, $\tilde{S}$, and the phase shift, $\tilde{\phi}_w$, are defined as

$$\begin{aligned} \tilde{S} &= \tilde{\chi}\frac{1+\rho^2-2\rho\cos\phi_w}{1-\rho^2} + 2\rho\frac{\sin\phi_w}{1-\rho^2}, \\ e^{i(\tilde{\phi}_w-\phi_w)} &= \frac{1-\rho e^{-i\phi_w}}{1-\rho e^{i\phi_w}}. \end{aligned} \tag{58}$$

Taking into account the diagonal form of the transfer matrix through the barrier T_b we showed that the total transfer matrix through the period of the structure again has the form of a single quantum well transfer matrix and is determined by Eq. (54) where the phase $\tilde{\phi}_w$

is replaced by a total phase $\phi = \phi_b + \tilde{\phi}_w$. This representation of the transfer matrix allowed us to us all results obtained previously with the refractive index contrast neglected to this most general case.

Next important innovation introduced by us in the course of working on this problem, which enabled us to consider propagation of light through defect structures at an arbitrary angle consisted in rewriting the transfer matrix (57) in the following form

$$T(\theta,\beta) = \begin{pmatrix} \cos\theta - i\sin\theta\cosh\beta & -i\sin\theta\sinh\beta \\ i\sin\theta\sinh\beta & \cos\theta + i\sin\theta\cosh\beta \end{pmatrix}, \tag{59}$$

where the parameters of the representation, θ and β, are related to the "material" parameters S and ϕ_w entering the transfer matrix by

$$\begin{aligned} \cos\theta = \mathrm{Tr}\, T/2 = \cos\phi + S\sin\phi, \\ \coth\beta = \cos\phi - S^{-1}\sin\phi. \end{aligned} \tag{60}$$

Due to the general character of the representations (59), the material parameters entering Eq. (60) can be either the parameters of a single QW, Eq. (54) or the effective parameters $\tilde{S}$ and $\tilde{\phi}$, Eqs. (57) and (58), of a barrier-well sandwich, or even parameters characterizing the entire MQW structure as long as the latter possess the mirror symmetry.

Using this representation we showed that an expression for the transfer matrix T_N of any sequence of identical blocks, including multiple-quantum-well structure, is described by $T(\theta,\beta)$:

$$T_N = T(\theta,\beta)^N = T(N\theta,\beta). \tag{61}$$

This expression immediately allowed us obtaining the general formula for the reflection coefficient of such a structure

$$r_N = -\frac{i\sinh\beta}{\cot N\theta + i\cosh\beta}. \tag{62}$$

This reflection coefficient written in terms of the parameters θ and β does not depend upon the specific form of the transfer matrix and therefore Eq. (62) can be applied to a variety of different structures. In particularly, this formalism allowed us to demonstrate the possibility to compensate the shift of the exciton frequency by the change in the angle of propagation, and confirm, therefore, our assertion that BMQW structures can be tuned with the help of the electric field. This result is illustrated in the figure below, which demonstrates that the

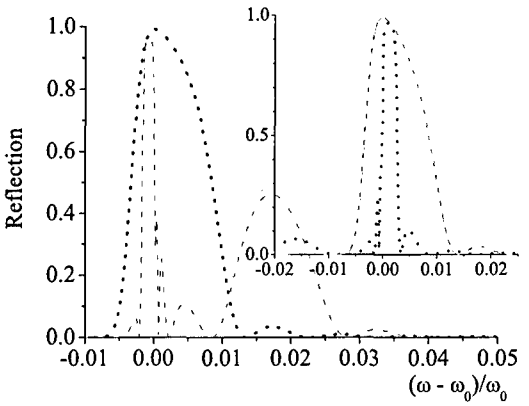

FIG. 12: The change of the reflection spectrum with the angle of incidence. The dotted line shows the reflection at normal incidence. The solid and dashed lines show the reflection at $\theta_b = \pi/18$ of s- and p-polarized waves, respectively. The main plot corresponds to the structure that is tuned to the Bragg resonance at normal incidence. The inset shows the reflection of a structure which is tuned to the Bragg resonance at $\theta_b = \pi/18$.

reflection spectrum of the structure detuned from the Bragg-resonance at normal incidence can be restored to the regular Bragg form for an incident angle equal to $\pi/18$.

2. All optical switching in BMQW structures

We demonstrated in this work that the Fano-like shape of reflection spectrum of BMQW structures with multiple defects can be used for all optical switching between states with low and high reflection. The contrast ratio for such a switch depends on the temperature and at cryogenic temperatures can reach values as large as 10^4. In this subsection we describe our work on design of such a version of defect BMQW structures that would allow for all-optical control of light reflection. The idea of our design is to use a combination of the quantum confined Stark effect due to external electric field and non-coherent photo-excitation of carriers in the barrier materials to control the strength of this field. A structure, in which this idea can be realized is shown in Fig. 13. The "defect" QW differs from other QWs by its exciton frequency and is separated from the rest of the structure by greater hight of its barriers, $E_{g3} > E_{g1}$. Thus, the whole structure can be treated as a defect region of length d sandwiched between two MQWs (MQW1 and MQW2) which are mirror images of each

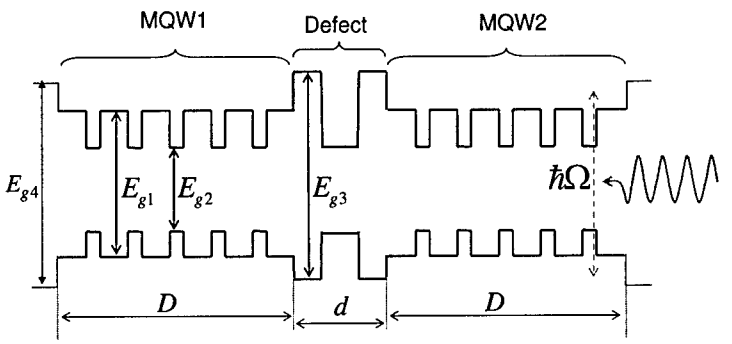

FIG. 13: Band diagram of the analyzed device.

other. The whole structure is assumed to be electrically isolated from the external circuit by the large band offset at the ends of the structure, $E_{g4} > E_{g1}$. During the full cycle of the switch/modulator operation the structure is biased, and the total potential V falls across the device.

The switching is achieved by illuminating structure by a laser pulse with frequency above the band gap of the BMQW barrier but below the band gap of the barriers defining the "defect" and those separating the structure from the external circuit, $E_{g1} < \hbar\Omega < E_{g3}, E_{g4}$. Electrons and holes excited by the laser pulse quickly redistribute inside the structure and screen the electric field inside MQW1 and MQW2. While the fraction of the applied bias that drops across the MQW parts of the device is significantly reduced by screening, the electric field at the ends of the structure and in the regions adjacent to the defect significantly increases, as well as the fraction of the applied bias that falls across the defect region. This results in increase of the QCSE shifts in the defect, while in the rest of the structure the QCSE shifts are reduced. As a result positions of the frequencies corresponding to maximum/minimum reflection shifts, and by selecting bias and the concentration of photo-excited carriers one can switch between low and higher reflection states.

We studied the effectiveness of screening in BMQW structures assuming that the carrier distributions in QWs and in three-dimensional spectrum have come to equilibrium with each other but recombination processes have not yet occurred and using Thomas-Fermi approximation. Within this approximation the quasi-equilibrium distribution of carriers, mentioned above, means the constant value of electrochemical potentials throughout the structure:

$$\zeta_e = E_F^e - e\varphi(z) = const_e, \ \zeta_h = E_F^h - e\varphi(z) = const_h \tag{63}$$

where $\zeta_{e,h}$ are the electrochemical potentials for electrons and holes, $E_F^{e,h}$ are the corresponding Fermi energies, and $e\varphi(z)$ is the potential energy of carriers in the self-consistent potential $\varphi(z)$, which varies only in the direction perpendicular to the QWs. The densities of mobile (i.e. those that belong to three-dimensional spectrum) electrons and holes are given by

$$n_m(z) = 2\left(\frac{m_e k_B T}{2\pi\hbar^2}\right)^{3/2} F_{1/2}\left[\left(\zeta_e - E_c + e\varphi(z)\right)/k_B T\right], \tag{64}$$

$$p_m(z) = 2\left(\frac{m_h k_B T}{2\pi\hbar^2}\right)^{3/2} F_{1/2}\left[\left(E_v - \zeta_h - e\varphi(z)\right)/k_B T\right]. \tag{65}$$

In these equations $m_{e,h}$ are electron and heavy hole effective masses, k_B is the Boltzmann constant, T is the temperature, $\hbar$ is the Plank constant, whereas $E_{c,v}$ denote the conduction and valence band edges of the barrier material. $F_{1/2}(\eta)$ is the Fermi integral-1/2: $F_{1/2}(\eta) = (2/\sqrt{\pi})\int_0^\infty dx\sqrt{x}/\left(\exp\left(x-\eta\right)+1\right)$. The concentrations for the carriers bound in the QWs are given by

$$\begin{aligned} n_{qw}(z) &= \frac{m_e k_B T}{\pi\hbar^2}\sum_{j=1}^{N}\left|\psi_0^e(z-z_j)\right|^2 \times \\ &\quad \ln\left[1+exp(\left(\zeta_e - E_0^e + e\varphi(z)\right)/k_B T)\right] \end{aligned} \tag{66}$$

$$\begin{aligned} p_{qw}(z) &= \frac{m_h k_B T}{\pi\hbar^2}\sum_{j=1}^{N}\left|\psi_0^h(z-z_j)\right|^2 \times \\ &\quad \ln\left[1+exp\big(\left(E_0^h - \zeta_h - e\varphi(z)\right)/k_B T\big)\right] \end{aligned} \tag{67}$$

where $\psi_0^{e,h}(z-z_j)$ is the z-dependent part of the wave function for electrons/holes localized in j-th QW, whereas $E_0^{e,h}$ is the corresponding confinement energy (we assume that each QW has only one subband). When applying Thomas-Fermi approximation to the carrier confined in QWs, we neglected a quantum mechanical shift of electron and hole levels due to Stark effect, but took into account that different wells feel different electrostatic potentials. Since we were not interested in the details of the charge distribution inside the wells, and since the width of the wells is much smaller than the inter-well spacing, we approximated the density of charges bound to a QW as in infinitely thin charged plane, i.e. $\left|\psi_0^{e,h}(z-z_j)\right|^2 = \delta(z-z_j)$. The potential $\varphi(z)$ involved in the expressions for the charge densities was calculated self-consistently by solving the Poisson equation,

$$\frac{d^2\varphi(z)}{dz^2} = -\frac{4\pi e}{\varepsilon}\left[p_m(z) - n_m(z) + p_{qw}(z) - n_{qw}(z)\right] \tag{68}$$

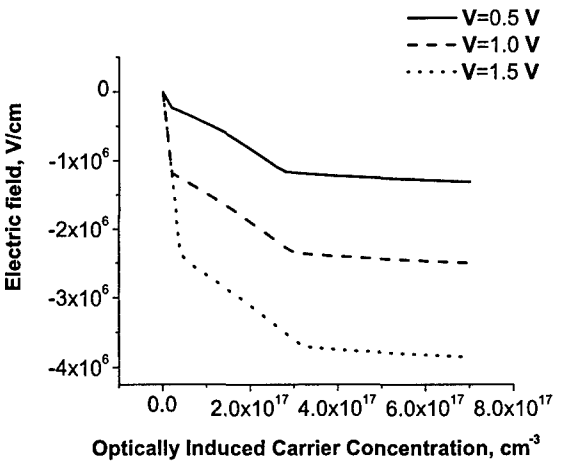

FIG. 14: Electric field at the end of the structure vs. optically induced carrier concentration for different applied bias, $N = 10$.

with the boundary conditions $\varphi(0) = -V/2$, $\varphi(D) = V/2$, where $z = 0$ and $z = D$ are the end points of the MQW structure, whereas V is the applied bias. Eqs. (64), (65), (66), (67), and (68) were supplemented by the normalization conditions

$$\int_0^D (n_m(z) + n_{qw}(z)) = \int_0^D (p_m(z) + p_{qw}(z)) = Dn_0, \tag{69}$$

where n_0 is the average carrier density determined by intensity of the photo-excitation.

Numerical solutions of this system of equations proved that it was indeed possible to significantly screen the electric field in the interior of the structure and significantly enhance it at its ends. This conclusion is illustrated in Fig. 14, where the magnitude of the electric field at one end of the structure is plotted versus concentration of photo-excited carriers.

We also simulated reflection spectrum of a short (10 periods) ideal BMQW structure in the presence of the external field and phto-generated carriers in order to illustrate that the photo-induced screening resulted in the shift of the reflection spectrum (see Fig. 15).

C. Enhanced of radiative coupling of excitons via manipulation of structure of Bragg multiple-quantum-wells at macroscopic level

A key to further improvement of technical characteristics of BMQW-based devices lie in enhancing radiative coupling between excitons. We showed that it is possible to achieve

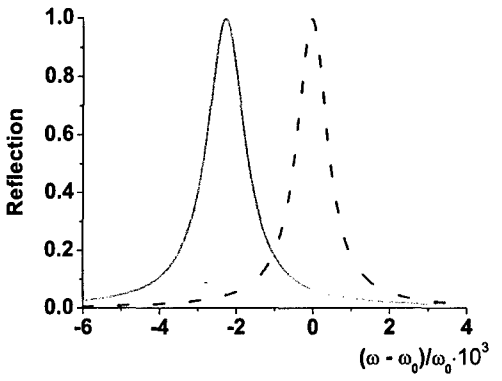

FIG. 15: The reflection spectra of the structure before (solid line) and after (dashed line) the injection of the carriers. The structure is assumed to satisfy the Bragg condition at $\omega_0 = 1.491$ eV, the exciton frequency with absent external field.

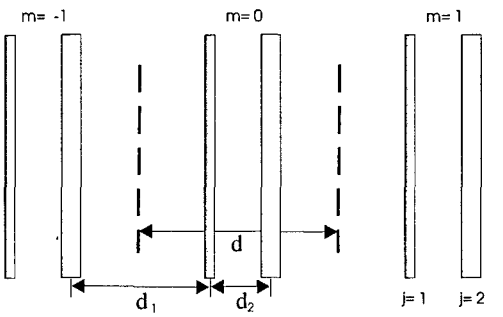

FIG. 16: A complex elementary cell with two different QWs

a significant enhancement of the coupling via structural manipulation of Bragg multiple-quantum-wells at the macroscopical level.

We considered a periodic multiple-quantum-well structure with an elementary cell consisting of two wells with different exciton frequencies (see Fig. 16). We showed that the polariton dispersion law in such a structure can be presented in the following form

$$\cos^2(Kd/2) = G_1(\omega, d/2)G_2(\omega, d/2)\,. \tag{70}$$

where functions G_j $(j = 1, 2)$ are defined as

$$G_j(\omega, d) = \cos kd + \eta_j(\omega)\sin kd\,. \tag{71}$$

Here η_j stands for exciton susceptibility in one or another well, and is characterized by two different exciton frequencies, ω_1 and ω_2. The boundaries between allowed and forbidden

bands in this case are defined by four frequencies, which, assuming that the radiative lifetime of excitons in both wells is the same, Γ_0, and that the period d satisfies the Bragg condition at the average frequency $\bar{\omega} = (\omega_1 + \omega_2)/2$, are defined by following expressions

$$\omega_1^{(\pm)} = \bar{\omega} + \frac{\omega_{21}}{4} \pm \sqrt{\left(\frac{\omega_{21}}{4}\right)^2 + \Delta_B^2}\,, \; \omega_2^{(\pm)} = \bar{\omega} - \frac{\omega_{21}}{4} \pm \sqrt{\left(\frac{\omega_{21}}{4}\right)^2 + \Delta_B^2}\,, \qquad (72)$$

where $\omega_{21} = \omega_2 - \omega_1$ and Δ_B is the width of the polariton stop-band in a BMQW structure with a simple elementary cell. An important conclusion that we drew from these formulas was that by requiring the frequency spacing ω_{21} to satisfy the following condition $\omega_{21} = \sqrt{2}\Delta_B$, one can produce a spectral gap between two polariton branches equal to $2\sqrt{2}\Delta_B$. Thus, the stop-band in the structures with complex elementary cells can be significantly increased compared to simpler structures, which signifies an effective enhancement in the exciton-light coupling.

IV. DEVELOPMENT OF HUMAN RESOURCES

In the course of work on the project we employed two graduate students, Mikhail Erementchouk and Vladimir Schuvayev, as well as two post-doctoral associates, Ilya Ponomarev and Vadim Puller. M. Erementchouk has graduated in 2005 and is currently with Professor H. Cao's group at Northwestern University. (Mikhail Erementchouk's thesis is attached to this report.) He was primarily involved in studies of optical properties of BMQW structures. Vladimir Schuvayev participated in studies of exciton properties of single QWs, his dissertation is under preparation now. Ilya Ponomarev worked with us from 2002 to 2004. He is currently with Naval Research Laboratory. His participation in the project consisted in developing self-consistent approach to calculations of of exciton energies, analysis of quantum confined Stark effect, and the role of electric field in inhomogeneous broadening of the excitons. Vadim Puller worked with us from 2004 to 2005 and was engaged in analysis of screening of electric field by photo-generated carriers.

V. PUBLICATIONS STEMMING FROM THE EFFORTS

In this section we list publications resulting from the research conducted within the framework of the project.

1. "Spectral engineering with multiple quantum well structures," L.I. Deych, M.V. Erementchouk, and A.A. Lisyansky, Appl. Phys. Lett. **83**, 4562 (2003).

2. "Local polariton modes in planar optical microcavities," L.I. Deych and A.A. Lisyansky, Proceed. SPIE, **5023**, 116 (2003).

3. "Effects of inhomogeneous broadening on reflection spectra of Bragg multiple quantum well structures with a defect," L.I. Deych, M.V. Erementchouk, and A.A. Lisyansky, Phys. Rev. B, **69**, 075308 (2004).

4. "Interface disorder and inhomogeneous broadening of quantum well excitons: Do narrow lines always imply high quality interfaces?" I. Ponomarev, L.I. Deych and A.A. Lisyansky, Appl. Phys. Lett., **85**, 2496 (2004).

5. "Multiple-quantum-well-based photonic crystals with simple and compound elementary supercells," E.L Ivchenko, M.M. Voronov, M.E. Erementchouk, L.I. Deych, A.A. Lisyansky, Phys. Rev. B, **70**, 195106 (2004).

6. "Complex scaling approach for the quantum confined Stark effect in quantum wells," L.I. Deych and I. Ponomarev, Phys. Rev. B, **71**, 035342 (2005).

7. "Self-consistent approach for calculations of exciton binding energy in quantum wells," I. Ponomarev, L.I. Deych, V. Shuvaev, and A.A. Lisyansky, Physica E, **25**, 539 (2005).

8. "One-dimensional photonic crystals based on periodic multiple quantum well structures," L. I. Deych, M. V. Erementchouk, E. L. Ivchenko, A. A. Lisyansky, M. M. Voronov, phys. stat. sol. (c) **2**, 805 (2005).

9. "Effect of inter-wall surface roughness correlations on optical spectra of quantum well excitons," I. Ponomarev, L.I. Deych, A.A. Lisyansky, Phys. Rev. B, **71**, 155303 (2005).

10. "Optical properties of one-dimensional photonic crystals based on multiple-quantum-well structures," M.V. Erementchouk, L.I. Deych and A.A. Lisyansky, Phys. Rev. B, **71**, 235335 (2005).

11. "Screening of external electric field by photo-induced carriers in Bragg multiple-quantum-wells," V. I. Puller, L. I. Deych, A. A. Lisyansky, M. V. Erementchouk, Applied Physics Letters, **87**, 052104 (2005).

12. "Electric field induced narrowing of exciton line width," I. Ponomarev, L.I. Deych, A.A. Lisyansky, Phys. Rev. B, **72**, 115304 (2005).

13. "Luminescent properties of MQW-based photonic crystals," M. Erementchouk, L. Deych and A.A. Lisyansky, phys. stat. sol. c, **2**, 3903 (2005).

14. "Spectral properties of exciton polaritons in one-dimensional resonant photonic crystals," M. Erementchouk, L. Deych and A.A. Lisyansky, Phys. Rev. B, **73**, 115321 (2006).

15. "Self-consistent Hartree method for calculations of exciton binding energy in quantum wells" V. Shuvaev, L.I. Deych, I. Ponomarev, and A.A. Lisyansky, Microstructures and Superlattices, submitted.

16. "Photoluminescence Spectroscopy of One-Dimensional Resonant Photonic Crystals" M.M. Voronov, E.L. Ivchenko, M.V. Erementchouk, L.I. Deych, A.A. Lisyansky, J. of Luminescence, submitted.

VI. COLLABORATIONS AND TRANSITIONS

In the course of this project we developed successful collaboration efforts with a group of Professor Ivchenko from Ioffe Institute for Physics and Engineering at St. Petersburg, Russia, which resulted in three publications and one more publication is in preparation. During the last year of the project we also started collaborating with an experimental group of Professor S. Oktyabrsky at SUNY-Albany. Currently we work on experimental verification of some of the effects predicted in this project and realization of device related ideas developed.

The results of our work were also presented at numerous scientific conferences and seminars. The list is given below.

1. Localization of light in one-dimensional disordered photonic crystals: statistics of resonant transmission in the band gap region. L. Deych and A. Lisyansky, invited talk at OSA annual meeting "Frontiers in Optics," Tucson, October, 2003.

2. Mode coupling in random lasers, L. Deych, Norfolk University, September, 2004 - invited. Violation of single parameter scaling in random periodic-on-average systems, L.I. Deych, and A.A. Lisyansky 2003 CLEO/QELS Conference, Maryland, June 2003 - invited.

3. Localization of light in one-dimensional disordered photonic crystals, A.A. Lisyansky, SUNY at Albany, November, 2003 - invited.

4. Violation of single parameter scaling in random periodic-on-average systems, L.I. Deych and A.A. Lisyansky 2003 CLEO/QELS Conference, Maryland, June, 2003 - invited.

5. Self-consistent approach and effective renormalization of band edge in quantum wells, L.I. Deych, V. Shuvayev, A.A. Lisyansky, I. Ponomarev, March Meeting of the APS, Montreal, Canada, March, 2004.

6. The effect of electric field on inhomogeneous broadening of excitons in narrow quantum wells, I. Ponomarev L.I. Deych, A.A. Lisyansky, March Meeting of the APS, Montreal, Canada, March, 2004.

7. Polariton spectrum of 1d photonic crystals based on multiple quantum well structures, M.V. Erementchouk, L.I. Deych, and A.A. Lisyansky, March Meeting of the APS, Montreal, Canada, March, 2004.

8. New efficient approach to calculations of exciton resonance position and width for quantum-confined Stark effect in shallow quantum wells, I. Ponomarev L.I. Deych, and A.A. Lisyansky, March Meeting of the APS, Montreal, Canada, March, 2004.

9. Self-consistent approach to exciton binding energy in quantum wells. "Nanostructures: Physics and Technology," I. Ponomarev, L. Deych, and A.A. Lisyansky, St. Petersburg, Russia, June, 2004.

10. Effect of vertical correlations and electric field on exciton inhomogeneous broadening in quantum wells. "Nanostructures: Physics and Technology," I. Ponomarev, L. Deych, and A.A. Lisyansky , St. Petersburg, Russia, June, 2004.

11. Multiple-quantum-well-based one-dimensional photonic crystals. "Physics of Light Matter Coupling in Nanostructures (PLMCN-4)," L.I. Deych, M.V. Erementchouk, A.A. Lisyansky, E.L. Ivchenko, and M.M. Voronov, St. Petersburg, Russia, July, 2004.

12. The effect of inter-wall correlations and electric field on inhomogeneous broadening of excitons in quantum wells, I.V. Ponomarev, L.I. Deych, and A.A. Lisyansky, 27th Int. Conference on the Physics of Semiconductors, ICPS-27, Flagstaff, AZ, July, 2004.

13. New efficient approach to calculation exciton resonance position and width for quantum-confined Stark effect in shallow quantum wells, I.V. Ponomarev, L. I. Deych, and A.A. Lisyansky, 27th Int. Conference on the Physics of Semiconductors, ICPS-27, Flagstaff, AZ, July, 2004.

14. Polariton spectrum of one-dimensional photonic crystals based on MQW structures. OSA annual meeting "Frontiers in Optics," M.V. Erementchouk and L. Deych, Rochester, October, 2004.

15. Self-Consistent Approach for Calculations of Exciton Binding Energy in Quantum Wells, "March Meeting of the APS," V. Shuvayev, L.I Deych, A.A Lisyansky, and I.V. Ponomarev, March Meeting of the APS, Los Angeles, March, 2005.

16. Screening of External Electric Field by Photo-Induced Carriers in Multiple Quantum Wells, "March Meeting of the APS," V. Puller, L.I. Deych, and A.A. Lisyansky, March Meeting of the APS, Los Angeles, March 2005.

17. Electric field induced narrowing of exciton line width, March Meeting of the APS, Los Angeles, I.V. Ponomarev, L.I. Deych, and A.A. Lisyansky, March 2005.

18. Exciton polaritons in 1d resonant photonic crystals, Invited talk at AMS-IMS-SIAM Summer Research Conderence on Mathematical Modeling of Novel Optical Materials and Devices, M. Erementchouk, L.I. Deych, and A.A. Lisyansky, Snowbird, UT, June, 2005.

19. Luminescent properties of MQW-based photonic crystals. "Physics of Light Matter Coupling in Nanostructures (PLMCN-5)," M.V. Erementchouk and L. Deych, Glasgow, UK, June, 2005.

20. Long-living collective optical excitations in a linear chain of microspheres. "Physics of Light Matter Coupling in Nanostructures (PLMCN-5)," L. Deych and A. Roslyak, Glasgow, UK, June, 2005.

21. Effects of spatial nonuniformity of cavity dielectric constant on lasing dynamics. Invited talk at Conference on Complex Medium VI: Light and complexity, part of the SPIE International Symposium on Optics & Photonics, L. Deych, San Diego, August, 2005.

---

[1] R. C. Miller, D. A. Kleinman, W. T. Tsang, and A. C. Gossard, Phys. Rev. B **24**, 1134 (1981).

[2] G. Bastard, E. E. Mendez, L. L. Chang, and L. Esaki, Phys. Rev. B **26**, 1974 (1982).

[3] R. L. Greene, K. K. Bajaj, and D. E. Phelps, Phys. Rev. B **29**, 1807 (1984).

[4] A. L. Efros, Sov. Phys. Semicond. **20**, 808 (1986).

[5] L. C. Andreani and A. Pasquarello, Phys. Rev. B **42**, 8928 (1990).

[6] B. Gerlach, J. Wusthoff, M. O. Dzero, and M. A. Smondyrev, Phys. Rev. B **58**, 10568 (1998).

[7] R. C. Iotti and L. C. Andreani, Phys. Rev. B **56**, 3922 (1997).

[8] J. Kossut, J. K. Furdyna, and M. Dobrowolska, Phys. Rev. B **56**, 9775 (1997).

[9] P. Harrison, T. Piorek, W. E. Hagston, and T. Stirner, Superlatt. Microstruct. **20**, 45 (1996).

[10] S. de Leon and B. Laikhtman, Phys. Rev. B **61**, 2874 (2000).

[11] U. Ekenberg and M. Altarelli, Phys. Rev. B **35**, 7585 (1987).

[12] S. K. Chang, A. V. Nurmikko, J. W. Wu, L. A. Kolodziejski, and R. L. Gunshor, Phys. Rev. B **37**, 1191 (1988).

[13] J. Warnock, B. T. Jonker, A. Petrou, W. C. Chou, and X. Liu, Phys. Rev. B **48**, 17321 (1993).

[14] T. Piorek, P. Harrison, , and W. E. Hagston, Phys. Rev. B **52**, 14111 (1995).

[15] A. Stahl and I. Balslev, *Electrodynamics of the Semiconductor Band Edge* (Springer, Berlin, 1987).

[16] I. Balslev, R. Zimmermann, and A. Stahl, Phys. Rev. B **40**, 4095 (1989).

[17] D. Merbach, E. Schöll, W. Ebeling, P. Michler, and J. Gutowski, Phys. Rev. B **58**, 10709 (1998).

[18] H. Castella and J. W. Wilkins, Phys. Rev. B **58**, 16186 (1998).

[19] D. Tran Thoai, R. Zimmermann, M. Grundmann, and D. Bimberg, Physical Review B (Condensed Matter) **42**, 5906 (1 Sept. 1990).

[20] G. Bastard, E. Mendez, L. Chang, and L. Esaki, Physical Review B (Condensed Matter) **28**, 3241 (15 Sept. 1983).

[21] D. A. B. Miller, D. S. Chemla, T. C. Damen, A. C. Gossard, W. Wiegmann, T. H. Wood, and C. A. Burrus, Phys. Rev. B **32**, 1043 (1985).

[22] G. Sanders and K. Bajaj, Physical Review B (Condensed Matter) **35**, 2308 (15 Feb. 1987).

[23] D. Ahn and S. Chuang, Physical Review B (Condensed Matter) **35**, 4149 (1987).

[24] W. P. Reinhart, Annu. Rev. Phys. Chem. **33**, 223 (1982).

[25] J. N. Bardsley, Int. J. Quantum Chem. **14**, 343 (1978).

[26] A. L. Efros and M. E. Raikh, *Optical Properties of Mixed Crystals* (North-Holland, Amsterdam, 1988).

[27] M. Herman, D. Bimberg, and J. Christen, Journal of Applied Physics **70**, R1 (15 July 1991).

[28] E. Runge, *Excitons in semiconductor nanostructures,* (????).

[29] S. Baranovskii and A. Efros, Sov. Phys. Semicond. **12**, 1328 (1978).

[30] R. Zimmermann, Physica Status Solidi B **173**, 129 (1992).

[31] A. Efros, C. Wetzel, and J. Worlock, Physical Review B (Condensed Matter) **52**, 8384 (15 Sept. 1995).

[32] R. Zimmermann, F. Grosse, and E. Runge, Pure & Appl. Chem. **69**, 1179 (1997).

[33] A. E. Meyerovich and A. Stepaniants, Phys. Rev. B **60**, 9129 (1999).

[34] L. I. Deych, A. Yamilov, and A. A. Lisyansky, Phys. Rev. B **64**, 75321 (2001).

[35] L. I. Deych, A. Yamilov, and A. A. Lisyansky, Nanotechnology **13**, 114 (2002).

[36] L. Deych, A. Yamilov, and A. Lisyansky, Optics letters **25**, 1705 (2000).

[37] H. C. Casey, Jr and M. B. Panish, *Heterostructure Lasers* (Academic, New York, 1978).

[38] Z. R. Wasilewski, M. M. Dion, D. J. Lockwood, P. Poole, R. W. Streater, and A. J. SpringThorpe, J. Appl. Phys. **81**, 1683 (1997).

[39] N. Grandjean, J. Massies, and M. Leroux, Appl. Phys. Lett. **74**, 2361 (1999).

[40] L. V. Keldysh, Superlattices Microstruct. **4**, 637 (1988).

[41] E. L. Ivchenko, Sov. Phys. Solid State **33**, 1344 (1991).

[42] D. S. Citrin, Solid State Commun. **89**, 139 (1994).

[43] E. L. Ivchenko, A. I. Nesvizhskii, and S. Jorda, Phys. Solid State **36**, 1156 (1994).

APPENDIX A: EXPRESSIONS FOR THE EFFECTIVE POTENTIALS

Choosing the origin of the coordinate system at the center of the QW the expression for effective potential $\overline{V}_r(r)$, which takes into account discontinuity of the dielectric constant in the following form:

$$\overline{V}_r(r) = -\left[V_1(r) + V_2(r) + V_3(r)\right], \tag{A1}$$

where

$$\begin{aligned}
V_1(r) &= \int_0^{L/2}\int_0^{L/2} dz_e\, dz_h\, F(z_e, z_h) \sum_{n=-\infty}^{\infty} q^{|n|} \left\{W_n(r; z_e, -z_h) + W_n(r; z_e, z_h)\right\}, \\
V_2(r) &= 2(1+q)\int_0^{L/2}\int_{L/2}^{\infty} dz_e\, dz_h\, F(z_e, z_h) \sum_{n=0}^{\infty} q^{n} \left\{W_n(r; z_e, -z_h) + W_n(r; z_e, z_h)\right\}, \\
V_3(r) &= \int_{L/2}^{\infty}\int_{L/2}^{\infty} dz_e\, dz_h\, F(z_e, z_h) \left\{\frac{(1+q)}{(1-q)}\left(W_0(r; z_e, -z_h) - qW_{-1}(r, z_e, z_h)\right)\right. \\
&\qquad \left. +(1+q)^2 \sum_{n=0}^{\infty} q^n W_n(r; z_e, z_h)\right\},
\end{aligned} \tag{A2}$$

and

$$F(z_e, z_h) = \chi_e^2(z_e)\chi_h^2(z_h) + \chi_e^2(z_h)\chi_h^2(z_e). \tag{A3}$$

The integrand in the effective potential (A1) has a singularity at $r = 0, z_e = z_h$, therefore we apply a coordinate transformation $\xi = z_e - z_h, \eta = z_e + z_h$, which allows extracting the divergent part and significantly increasing computational efficiency of the calculations. In new coordinates the potential takes the following form:

$$
\begin{aligned}
V_1(r) = &\sum_{n=-\infty}^{\infty} q^{|n|} \int_0^{L/2} d\eta \times \\
&\left[W_{-n}(r;\eta) \int_0^{\eta} d\xi\, \Phi(\xi,\eta) + W_{n-1}(r;\eta) \int_0^{\eta} d\xi\, \Phi(\xi,-\eta+L) \right. \\
&\left. + W_n(r;\eta) \int_{\eta}^{L-\eta} d\xi\, \Phi(\eta,\xi) \right], \\
V_2(r) = &(1+q) \sum_{n=0}^{\infty} q^n \left(V_{21n}(r) + V_{22n}(r) \right), \\
V_{21n}(r) = &\int_0^{L/2} d\eta \left[W_n(r;\eta) \int_0^{\eta} d\xi\, \left(\Phi(\eta,\xi+L) + \Phi(\eta,-\xi+L) \right) \right. \\
&\left. + W_{n+\frac{1}{2}}(r;\eta) \int_0^{\eta} d\xi \left(\Phi\left(\xi+\frac{L}{2},\eta+\frac{L}{2}\right) + \Phi\left(-\xi+\frac{L}{2},\eta+\frac{L}{2}\right) \right) \right], \\
V_{22n}(r) = &\int_{L/2}^{\infty} d\eta \left[W_{n+\frac{1}{2}}(r;\eta) \int_0^{L/2} d\xi \left(\Phi\left(\xi+\eta,\eta+\frac{L}{2}\right) + \Phi\left(-\xi+\eta,\eta+\frac{L}{2}\right) \right) \right. \\
&\left. + W_n(r;\eta) \int_0^{L/2} d\xi \left(\Phi\left(\eta,\xi+\eta+\frac{L}{2}\right) + \Phi\left(\eta,-\xi+\eta+\frac{L}{2}\right) \right) \right], \\
V_3(r) = &\frac{(1+q)}{(1-q)} \int_0^{\infty} d\eta \left[W_0(r;\eta) \int_{\eta}^{\infty} d\xi\, \Phi(\eta,\xi+L) + W_1(r;\eta) \int_0^{\eta} d\xi\, \Phi(\xi,\eta+L) \right. \\
&\left. + \sum_{n=1}^{\infty} q^n \left(W_{n+1}(r;\eta) - W_{n-1}(r;\eta) \right) \int_0^{\eta} d\xi\, \Phi(\xi,\eta+L) \right],
\end{aligned}
\tag{A4}
$$

where we substituted $W_n(r;\eta) \equiv W_n(r;z_e,z_h)$ and

$$
\Phi(\xi,\eta) = F\left(\frac{\xi+\eta}{2}, \frac{\eta-\xi}{2} \right). \tag{A5}
$$

To treat the singularity in $V_{1,2}(r)$ we split the outer integral into two parts: $\int_0^{L/2} d\eta = \int_0^{\delta} d\eta + \int_{\delta}^{L/2} d\eta$, with $\delta \ll 1$. For the first part the inner integral of $\Phi(\xi,\eta)$ can be replaced by the first several terms of its series expansion near $\eta = 0$. It results in the following approximation $\int_0^{\delta} d\eta\, W_n(r,\eta)(y_0 + \alpha\eta + \beta\eta^2)$. Parameters y_0, α, β are the parameters of the quadratic spline. This integral can be found explicitly and it has a logarithmic divergence at small r.

The effective potentials $\overline{V}_{e,h}(z_{e,h})$ in z-directions are free from divergencies. They can be

written down as follows:

$$\overline{V}_{e,h}(z_{e,h}) = \begin{cases} V_{e,h}^{(<)}(z_{e,h}), & \text{for } z_{e,h} \leq \frac{L}{2}, \\ V_{e,h}^{(>)}(z_{e,h}), & \text{for } z_{e,h} \geq \frac{L}{2}, \end{cases} \tag{A6}$$

where

$$\begin{aligned} V_{e,h}^{(<)}(z_{e,h}) &= \int_0^\infty dr\, r\psi^2(r) \\ &\times \left(\int_0^{L/2} dz_{h,e}\, \chi_{h,e}^2(z_{h,e}) \sum_{n=-\infty}^{\infty} q^{|n|} \left(W_n(r; z_{e,h}, -z_{h,e}) + W_n(r; z_{e,h}, z_{h,e}) \right) \right. \\ &+ \left. \int_{L/2}^\infty dz_{h,e}\, \chi_{h,e}^2(z_{h,e})(1+q) \sum_{n=0}^{\infty} q^n \left(W_n(r; z_{h,e}, -z_{e,h}) + W_n(r; z_{h,e}, z_{e,h}) \right) \right), \\ V_{e,h}^{(>)}(z_{e,h}) &= \int_0^\infty dr\, r\psi^2(r) \\ &\left(\int_0^{L/2} dz_{h,e}\, \chi_{h,e}^2(z_{h,e})(1+q) \sum_{n=0}^{\infty} q^n \left(W_n(r; z_{e,h}, -z_{h,e}) + W_n(r; z_{e,h}, z_{h,e}) \right) \right. \\ &+ \int_{L/2}^\infty dz_{h,e}\, \chi_{h,e}^2(z_{h,e}) \left[(1+q)^2 \sum_{n=0}^{\infty} q^n W_n(r; z_{e,h}, z_{h,e}) \right. \\ &+ \left. \left. \frac{(1+q)}{(1-q)} \left(W_0(r; z_{e,h}, -z_{h,e}) - qW_{-1}(r; z_{e,h}, z_{h,e}) \right) \right] \right) \end{aligned} \tag{A7}$$

Optical properties of quantum heterostructures

by

Mikhail V. Erementchouk

A dissertation submitted to the Graduate Faculty in Physics
in partial fulfillment of the requirements for the degree of
Doctor of Philosophy, The City University of New York

2005

Abstract

Optical Properties of Quantum Heterostructures
by
Mikhail Erementchouk
Adviser: Professor Lev I. Deych

The thesis is devoted to consideration of optical properties of quantum heterostructures. These structures are characterized by a spatial modulation of the dielectric function and a periodic arrangement of optically active elements. The coexistence of two different channels of the light interaction with the matter makes the quantum heterostructures belonging to the new class of structures - resonant photonic crystals. In the present thesis effective approaches have been developed for an effective description of the exciton polariton dispersion law and optical spectra of finite structures. In particular, the polariton spectrum is shown to consist of passing bands separated by forbidden gaps. The structure of the gaps essentially depends on the relation between the exciton resonant frequency and the frequencies of the photonic band gaps existing in a passive photonic crystal characterized by the same modulation of the dielectric function. The resonant condition for formation of a wide solid stop-band is obtained and analyzed in detail for different structures. The reflection and transmission spectra are effectively described by effective excitonic susceptibility and effective optical widths of the quantum wells. These effective quantities are determined by the dielectric environment of the quantum wells and naturally take into account the dependence of the reflection and transmission spectra on angle of propagation of the electromagnetic waves and their polarization state. The information obtained for the polariton spectrum and reflection and transmission properties of quantum heterostructures is used for the solution of a problem of the exciton luminescence in resonant photonic crystals. In particular, it is shown that the large scale form of the luminescence spectra is determined by the form of the polariton forbidden gap while its fine structure is the result of a strong frequency dependence of the transmission coefficient near the band edges.

Acknowledgments

Algebra is the offer made by the devil ... The devil says: "I will give you this powerful machine, and it will answer any question you like. All you need to do is give me your soul: give up geometry and you will have this marvellous machine." ... we would probably cheat on the devil, pretend we are selling our soul, and not give it away. Nevertheless the danger to our soul is there, because when you pass over into algebraic calculation, essentially you stop thinking; you stop thinking geometrically, you stop thinking about the meaning.

M. Atiyah, *Mathematics in the 20th century*, Bull. of the London Math. Soc. **34**, 1-15 (2002)

First of all I would like to thank my advisors Professor Lev Deych and Professor Alexander Lisyansky for the invaluable support and encouraging conversations and discussions. This is extremely important to be able to concentrate without other cares on a problem and such a possibility has been provided by my advisors.

I am grateful to professors Steven Schwarz and Azriel Genack for their reading and valuable commenting manuscripts.

I will nostalgically remember the friendly and supportive environment of the Physics Department of Queens College.

I would like to thank all members of our theoretical group, Professor Lev Deych, Professor Alexander Lisyansky, Dr. Ilya Ponomarev, Dr. Vadim Puller, Vladimir Shuvayev and Alexey Roslyak, for their patience during my presentations on Thursday's seminars and valuable discussions.

In my being in a delocalized state I have used research facilities of A. F. Ioffe Physico-Technical Institute (St. Petersburg, Russia) and L. V. Kirensky Institute of Physics (Krasnoyarsk, Russia). I would like to thank Professor Eugenius Ivchenko and Professor Valter Ignatchenko for their warm hospitality.

I would like to thank the participants of the seminar "Geometrical methods in physics" (Spring 2004, L. V. Kirensky Institute of Physics) and especially Dima Dzebisashvili for active discussions of the geometrical background of the approach developed in the thesis.

Last but not least I do not have words to express my deepest appreciation of the endless support and patience of my wife, Marina Bakhmetieva.

Contents

List of Tables

List of Figures

Chapter 1

Introduction

1.1 Quantum heterostructures. Quantum wells vs. superlattices

Quantum heterostructures are structures with modulated composition. A simple example is multilayer structures grown using molecular beam epitaxy or metal organic chemical vapor deposition [2]. In such structures different layers are composed of different materials. There is a great variety of materials which are used for producing such multilayers: GaAs/$Al_{1-x}Ga_xAs$, $In_{1-x}Al_xAs/Ga_{1-y}Al_yAs$, CdTe/$Cd_{1-x}Mn_xTe$, $Zn_{1-x}Cd_xSe/ZnSySe_{1-x}$ to name a few [3]. Here the subscripts show the fraction of atoms of a particular kind at sites of the crystal lattice or one of its sublattices. Building such heterostructures makes it possible to engineer the properties of electron and hole states because the positions of the top of the valence band and the bottom of the conduction band vary with the material used to compose the layer. According to the relative position of the band gap of the materials used for the growth of the heterostructure, one distinguishes heterostructures of three types (see Fig. 1.1).

In the structures of type-I, the gap of one material is situated completely in the band of another. A typical example of such structure is GaAs/$Al_xGa_{1-x}As$ multilayer with $x < 0.4$. Here, the gap of GaAs is covered by the gap of $Al_xGa_{1-x}As$. Such structures sometimes are called direct because in equilibrium the electrons and holes are situated in the same layers. In type-II structures the gaps in different layers are shifted with respect to each other. Fig. 1.1 shows a typical picture of the band structure for a GaInN/GaN multilayer. A distinction is made between such structures (also called type-II staggered lattices) and type-II misaligned structures. In the latter the shift of the gaps is so large that the top of the valence band in one material lies above the bottom of the conduction band in another. An example of such a lattice is the GaSb/InAs heterostructure. Structures of type III are those where one of the layers is a gapless semiconductor. This situation is implemented in HgTe/CdTe heterostructures where the band merging point of HgTe falls inside the gap of CdTe.

The structures of type-I, which are the main objective of the present thesis, are additionally classified according to the widths of the layers. This reflects a strong dependence of physical properties of the heterostructures on this parameter of the system. The physical reason for this dependence is the following: the motion of an electron perpendicular to the growth direction is unaffected by the modulation of the composition. Meanwhile for the motion along the growth direction, the modulation of the profile of the bottom of the conduction band plays the role of an external potential. The layers where the gap is narrower are the potential wells and those with wider gap are the barriers. When the wells are far apart the electron states in a vicinity of one well are independent of the existence of other wells. Indeed, as is shown in any standard textbook for quantum mechanics (see e.g. Ref. [4]) there always exist bound states in a one-dimensional potential well. For a finite well

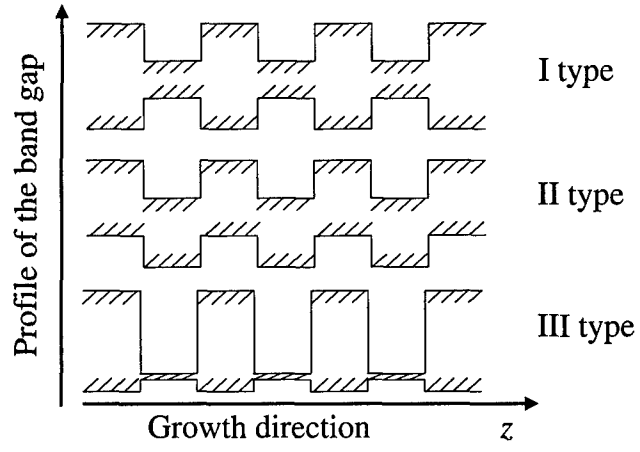

Figure 1.1: Three types of heterostructures classified according to relative position of the band gaps (dashed regions).

for a state to be bound means that outside of the well the wavefunction exponentially decays. This decay determines a characteristic length scale. When the wells are further apart from each other than this length the. overlap of the wavefunctions corresponding to the states in different wells becomes negligibly small. As the result, the electron spectrum at the energies below the edges of the well, i.e. below the bottom of the conduction band of the material with the wider forbidden gap, is discrete and degenerate. The multiplicity of the degeneration is equal to the number of the wells. In this case, one can say that the electrons are free to move in the plane of the layers while there is confinement along the growth direction. Corresponding structures are called long-period or quantum well structures.

When the distance between the wells becomes smaller than the penetration length into the barriers, the overlap of the wave functions corresponding to the levels in different quantum wells becomes noticeable. This removes the degeneration. Eventually, when the number of the layers in the structure is essentially large, a mini-band appears, similarly to what happens when atoms form a solid. Such structures are referred to as superlattices.

There is a qualitative difference between quantum wells and superlattices. Formation of mini-bands in the latter removes the electron confinement in the growth direction. This has a great impact on the physical properties of such structures and optics is not an exception. As will be demonstrated later, the propagation of light in a medium is strongly affected by dipole active bound states. The interaction with such states results in the appearance of a strong resonant dispersion of the effective dielectric function. For the case of the light-exciton interaction, the resonant frequency is related to the recombination energy of the electron-hole pair constituting the exciton. The width of the resonance is determined by the non-radiative decay of the exciton through phonon emission. The observation and applications of the resonance of the dielectric function are hampered by the closeness of the resonant frequency to the semiconductor fundamental absorption edge. The difference between the resonant frequency and the fundamental absorption edge is determined by the exciton binding energy. The binding energy, in turn, strongly depends on the ability of electrons and holes to move freely. Even simple restriction in one direction leads to essential increase of the binding energy

[5, 6]. This circumstance makes quantum well structures more promising from the point of view of observation and application of peculiarities in optical properties which are the result of the exciton-light interaction.

1.2 Light-matter interaction in quantum heterostructures

The interaction between the electrons and the electromagnetic field in quantum heterostructures has its specific features. First is the spatial confinement of the electron states due to the modulation of the profile of the semiconductor forbidden gap. Second is a modulation of the dielectric function that essentially affects the states of the electromagnetic field. These features require a solid understanding of the basic processes occurring in the quantum heterostructures. In this Section we provide a qualitative derivation and the analysis of main equations of motion which will be considered in details in the following chapters.

The interaction of light with the electrons in the materials constituting the structure leads to a non-constant number of the electrons in the conduction band. Therefore, the most suitable frameworks for a description of the dynamics of the electrons and the electromagnetic field are those provided by a quantum field approach. It has been reviewed in a number of publications [5, 7–10] and the consideration below follows a standard procedure. First, to illustrate the basic ideas, we consider a two-band model for the semiconductor. Then, we obtain the modifications produced by a degeneration of the band states. Finally, we discuss the form of the Maxwell equations in the multiple quantum well structures.

1.2.1 Two-band approximation

The interaction between the electrons and the electromagnetic field is described in the most general way by the introduction of the canonical momentum

$$\hat{\mathbf{p}} \to \hat{\mathbf{p}} + \frac{e}{c}\hat{\mathbf{A}}, \tag{1.1}$$

where $\hat{\mathbf{p}}$ is the electron momentum operator and $\hat{\mathbf{A}}$ is the operator of the vector potential. The canonical momentum determines the electron kinetic energy and thereby gives a coupling between the electron states and the states of the electromagnetic field. In the operator of the kinetic energy the term proportional to $\hat{\mathbf{A}}^2$ can be neglected (the dipole approximation)

$$\frac{1}{2}\left(\hat{\mathbf{p}} + \frac{e}{c}\hat{\mathbf{A}}\right) = \frac{\hat{\mathbf{p}}^2}{2m} + \frac{e}{mc}\hat{\mathbf{A}}\cdot\hat{\mathbf{p}}, \tag{1.2}$$

where we have adopted the Coulomb gauge $\nabla\cdot\mathbf{A} = 0$. Under this approximation the total Hamiltonian has the form of a sum of parts responsible for dynamics of the electromagnetic field and electrons alone and the interaction between them

$$\mathscr{H} = \mathscr{H}_{ph} + \mathscr{H}_e + \mathscr{H}_{e-ph}. \tag{1.3}$$

Here, $\mathscr{H}_{ph}$ is the Hamiltonian of the electromagnetic field

$$\mathscr{H}_{ph} = \frac{\epsilon_0 c^2}{2}\int d\mathbf{r}\left[\frac{n^2(\mathbf{r})}{c^2}\dot{\hat{\mathbf{A}}}^2 + (\nabla\times\hat{\mathbf{A}})^2\right], \tag{1.4}$$

where c is the speed of light in vacuum and $n(\mathbf{r})$ is the index of refraction which is not assumed to be homogeneous in space. In the electron Hamiltonian $\mathscr{H}_e$ we explicitly write only the kinetic energy

$$\mathscr{H}_e = \int d\mathbf{r}\,\psi^+(\mathbf{r})\frac{\hat{\mathbf{p}}^2}{2m}\psi(\mathbf{r}) + \mathscr{V}[\psi^+,\psi] \tag{1.5}$$

and use the notation $\mathscr{V}[\psi^+,\psi]$ for the contribution of the Coulomb interaction between the electrons themselves and between the electrons and ions in the lattice. The part of the Hamiltonian responsible for the interaction between the electromagnetic field and the electrons is

$$\mathscr{H}_{e-ph} = \frac{e}{2mc}\int d\mathbf{r}\,\psi^+(\mathbf{r})\hat{\mathbf{A}}(\mathbf{r})\cdot\hat{\mathbf{p}}\psi(\mathbf{r}). \tag{1.6}$$

The self-electron and the field-electron parts of the total Hamiltonian can be simplified taking into account two-band structure of the electron spectrum. For this purpose we represent the electron field operator $\psi(\mathbf{r})$ in the form

$$\psi(\mathbf{r}) = w_c(\mathbf{r})\psi_c(\mathbf{r}) + w_v(\mathbf{r})\psi_v(\mathbf{r}), \tag{1.7}$$

where $w_{c,v}$ are the Bloch functions of the electron states at the edges of the conduction and the valence bands respectively. In Eq. (1.7) the operators, $\psi_{c,v}$ can be thought of as electron annihilation operators in the conduction and the valence band respectively. Such representation allows one to make a distinction between different scales of the spatial variation of $\psi(\mathbf{r})$. The Bloch functions are periodic with the period equal to the lattice constant, a. Meanwhile, for energies E not too far from the edges of the gap $E_{c,v}$, the characteristic scale of the spatial change of electron and hole operators is $\propto a(E-E_{c,v})/E_{c,v} \ll a$. Besides, we are interested in optical properties at frequencies that are close to the semiconductor fundamental absorption edge. The light wavelength at these frequencies is much larger than the lattice constant. Thus, the variation of $\hat{\mathbf{A}}(\mathbf{r})$ over the crystal elementary cell is negligibly small. Such a separation of scales allows performing the integrations in Eqs. (1.5) and (1.6) with respect to the smallest scale. The result of such integration in the term $\mathscr{H}_e$ is the simplest one. For our purposes here it is enough to restrict ourselves to one-particle electron properties. In this approximation $\mathscr{H}_e$ reduces after the integration to

$$\mathscr{H}_e = \frac{1}{2}\sum_{b,b'=c,v}\int d\mathbf{r}\,d\mathbf{r}'\,\psi_b^+(\mathbf{r})\hat{h}_{bb'}(\mathbf{r}-\mathbf{r}')\psi_{b'}(\mathbf{r}'). \tag{1.8}$$

Here, the diagonal terms $\hat{h}_{cc,vv}$ of the Hamiltonian density describe the dynamics of the electrons in the conduction and the valence band respectively. For example, for an electron moving in multiple-quantum-well structure the Hamiltonian density can be written in a standard one-particle form $\hat{h}_{cc}(\mathbf{r}-\mathbf{r}') = \delta(\mathbf{r}-\mathbf{r}')[p^2/2m_e + V_c(\mathbf{r})]$, where m_e is the effective electron mass in the conduction band and the potential $V_c(\mathbf{r})$ is given by the modulation of the bottom of the conduction band in the multilayer structure. The off-diagonal elements eventually give the interaction between the electrons and the holes.

The resultant form of the term describing the electron-photon interaction is more complicated, therefore we will discuss it in more details. The derivative in Eq. (1.6) after substitution of Eq. (1.7) produces two term which correspond to different physical processes. One of them is $\propto w_b^* w_{b'}\hat{\mathbf{A}}\psi_b^+\nabla\psi_{b'}$ and another is $\propto w_b^*(\nabla w_{b'})\hat{\mathbf{A}}\psi_b^+\psi_{b'}$, where the indices b and b' run over all bands. In both these terms during the integration over a particular elementary cell all quantities except the Bloch functions can be considered constant due to the arguments discussed above. Then, one can use the orthogonality properties of the Bloch functions

$$\frac{1}{\Omega}\int\limits_{\Omega} d\mathbf{r}\,w_b^* w_{b'} = \delta_{bb'}, \qquad \frac{1}{\Omega}\int\limits_{\Omega} d\mathbf{r}\,w_b^*\nabla w_{b'} = (1-\delta_{bb'})\frac{id_{bb'}}{\hbar}, \tag{1.9}$$

where Ω is the volume of the elementary cell. The second equation of Eqs. (1.9) is the definition of the matrix elements of the dipole moment d_{cv}. These conditions show that the term $w_b^* w_{b'}\hat{\mathbf{A}}\psi_b^+\nabla\psi_{b'}$ is not zero only when $b = b'$. This corresponds to such electron transitions when the final and initial

states are in the same band. Such transitions are called *intraband*. They affect low-frequency optical properties of semiconductors. The term $\propto w_b^*(\nabla w_{b'})\hat{\mathbf{A}}\psi_b^+\psi_{b'}$, on the contrary, is not zero only for *interband* transitions, between states lying in different bands. Thus, if one is interested in optical properties at frequencies close to the fundamental absorption edge only the second term should be kept. Finally, the interaction term in the whole electron-photon Hamiltonian can be written as

$$\mathscr{H}_{e-ph} = \int d\mathbf{r}\,\left[\psi_e^+(\mathbf{r})\mathbf{d}_{cv}\cdot\hat{\mathbf{A}}(\mathbf{r})\psi_h(\mathbf{r}) + \text{h.c.}\right]. \tag{1.10}$$

The equations of motion of the electron field operators and the electromagnetic field are obtained in the Heisenberg form

$$i\hbar\frac{\partial\widehat{O}}{\partial t} = [\widehat{O},\mathscr{H}] \tag{1.11}$$

taking into account the commutation and anticommutation relations

$$\begin{aligned}[\hat{\mathbf{A}}(\mathbf{r}_1),\hat{\mathbf{A}}(\mathbf{r}_2)] &= i\hbar\frac{4\pi c^2}{n^2(\mathbf{r}_1)}\widehat{\delta}^{\perp}(\mathbf{r}_1-\mathbf{r}_2)\\ \left\{\psi^+(\mathbf{r}_1),\psi(\mathbf{r}_2)\right\} &= \hbar\delta(\mathbf{r}_1-\mathbf{r}_2),\end{aligned} \tag{1.12}$$

where $\widehat{\delta}^{\perp}(\mathbf{r})$ is the transverse delta-function [5, 11]. For pairs of fermionic fields a commutator can be found using a useful relation

$$[ab,cd] = a\{b,c\}d - \{a,c\}bd + ca\{b,d\} - c\{a,d\}b. \tag{1.13}$$

After substitution Eq. (1.3) into Eq. (1.11) one obtains the *quantum* equations of motion

$$\begin{aligned}\frac{n^2(\mathbf{r})}{c^2}\ddot{\hat{\mathbf{A}}} &= -\nabla\times\nabla\times\hat{\mathbf{A}} - 4\pi\int d^3\mathbf{r}'\,\widehat{\delta}^{\perp}(\mathbf{r}-\mathbf{r}')\left[\mathbf{d}_{cv}\psi_e^+(\mathbf{r}')\psi_h(\mathbf{r}') + \text{h.c.}\right],\\ i\hbar\frac{\partial}{\partial t}\psi_b^+\psi_{b'} &= \psi_b^+\left(\hat{h}\psi\right)_{b'} - \left(\hat{h}\psi^+\right)_b\psi_{b'} + \widehat{\mathbf{A}}\cdot\left(\psi_b^+\mathbf{d}_{bb'}\psi_{b'} - \text{h.c.}\right),\end{aligned} \tag{1.14}$$

where $\left(\hat{h}\psi\right)_{b'}$ schematically shows the action of the electron-hole Hamiltonian on the field operator. Formally we have kept the term $\nabla\cdot\mathbf{A}$ in Eq. (1.14) to make later a transition to the electric field description more transparent.

Since, we are interested in macroscopic electromagnetic phenomena the average (in the field theoretical sense, i.e. with respect to an equilibrium state) of products similar to $\langle\widehat{\mathbf{A}}\psi_b^+\psi_{b'}\rangle$ can be decoupled leading to $\langle\widehat{\mathbf{A}}\rangle\langle\psi_b^+\psi_{b'}\rangle$. Thus, one can obtain closed equations with respect to the classical electromagnetic field $\mathbf{A} = \langle\widehat{\mathbf{A}}\rangle$ and the electron density matrix $f_{bb'} = \langle\psi_b^+\psi_{b'}\rangle$. The matrix elements of the density matrix have an independent physical sense. The diagonal elements give the electron distribution functions in the bands. The off-diagonal elements describe the transition amplitudes or the interband polarization. The interpretation of the off-diagonal elements as a polarization follows from the equations of motion

$$\begin{aligned}\frac{n^2(\mathbf{r})}{c^2}\ddot{\mathbf{A}} &= -\nabla\times\nabla\times\mathbf{A} - 4\pi\int d^3\mathbf{r}'\,\widehat{\delta}^{\perp}(\mathbf{r}-\mathbf{r}')\left[\mathbf{d}_{cv}f_{cv}(\mathbf{r}',\mathbf{r}') + \mathbf{d}_{vc}f_{vc}(\mathbf{r}',\mathbf{r}')\right],\\ i\hbar\frac{\partial}{\partial t}f_{cv}(\mathbf{r}_1,\mathbf{r}_2) &= (\hat{h}_c(\mathbf{r}_1) - \hat{h}_v(\mathbf{r}_2))f_{cv}(\mathbf{r}_1,\mathbf{r}_2) +\\ &\quad + f_{cc}(\mathbf{r}_1,\mathbf{r}_2)\mathbf{A}(\mathbf{r}_2)\cdot\mathbf{d}_{vc} - f_{vv}(\mathbf{r}_1,\mathbf{r}_2)\mathbf{A}(\mathbf{r}_1)\cdot\mathbf{d}_{cv}.\end{aligned} \tag{1.15}$$

The second equation has a sense of a Schrödinger equation with a source. One of the particles has negative mass and can be identified as the hole.

Accomplished with the equations with respect to the diagonal elements of the density matrix Eqs. (1.15) give a complete description of a semiconductor near the band edge in the two-band model (aside from the one-body electron approximation and the approximation of the classical electromagnetic field). To make a complete transition to the electron-hole picture one needs to introduce the hole population instead of electron population in the valence band f_{vv}. To do this one can note that the electron and the hole pictures are complimentary in the sense that an electron annihilation operator is a hole creation operator and, therefore, $\psi_{\rm e}^{+}\psi_{\rm e} = \psi_{\rm h}\psi_{\rm h}^{+}$. Using the anticommutation relation $\psi_{\rm h}\psi_{\rm h}^{+} = -\psi_{\rm h}^{+}\psi_{\rm h} + \{\psi_{\rm h}, \psi_{\rm h}^{+}\}$ one can show that $f_{vv}(\mathbf{r}_1, \mathbf{r}_2) = -f_{\rm h}(\mathbf{r}_1, \mathbf{r}_2) + \delta(\mathbf{r}_1 - \mathbf{r}_2)$, where $f_{\rm h}$ is the hole distribution function.

Eqs. (1.15) describe a rich variety of physical phenomena (including, e.g. a transport in semiconductors) and are the subject of extensive investigation for last several decades. Here we are interested in only a small part of this big physics. For our purposes it is enough to assume that the electron and the hole distributions, f_e and f_h, are given by the Fermi distribution in the thermodynamic equilibrium, so that Eqs. (1.15) are closed. After being linearized the second equation of Eqs. (1.15) can be easily solved with respect to the interband polarization allowing to obtain thereby a closed equation for the electric field. To obtain such an equation it is necessary to take a derivative of both equations with respect to time. As the result $\dot{f}_{cv}$ enters the Maxwell equations, however, it satisfies exactly the same equation with the electric field $\mathbf{E}$ in the r.h.s. Now, let us assume, for simplicity, that the Hamiltonian of the electron-hole pair has a single discrete level (exciton) with the energy determined by the frequency ω_0 and the eigenstate, the exciton wavefunction, $\Phi(\mathbf{r}_1, \mathbf{r}_2)$. The polarization created by the electric field of frequency ω is obtained as

$$\dot{f}_{cv}(\mathbf{r}_1, \mathbf{r}_2) = -\frac{S_{cv}\Phi(\mathbf{r}_1, \mathbf{r}_2)}{\omega - \omega_0 - i\gamma}, \tag{1.16}$$

where γ is a phenomenological broadening of the exciton line and

$$\begin{aligned} S_{cv} = \mathbf{d}_{cv} \cdot \int d\mathbf{r}\, \Phi(\mathbf{r}, \mathbf{r})\mathbf{A}(\mathbf{r}) - \\ f_e \mathbf{d}_{vc} \cdot \int d\mathbf{r}_1\, d\mathbf{r}_2\, \Phi(\mathbf{r}_1, \mathbf{r}_2)\mathbf{A}(\mathbf{r}_2) - f_h \mathbf{d}_{cv} \cdot \int d\mathbf{r}_1\, d\mathbf{r}_2\, \Phi(\mathbf{r}_1, \mathbf{r}_2)\mathbf{A}(\mathbf{r}_1), \end{aligned} \tag{1.17}$$

where we have neglected the non-resonant term $(\omega + \omega_0)^{-1}$ (the rotating wave approximation). To obtain the expression for $\dot{f}_{vc}$ one needs to note that by virtue of the anticommutation relation $f_{cv}(\mathbf{r}_1, \mathbf{r}_2) = -f_{cv}(\mathbf{r}_2, \mathbf{r}_1)$.

The expressions similar to Eq. (1.17) describe the dependence of the exciton-light interaction on the population of the valence and the conduction bands. In particular, it is seen that with the increase the population, e.g. due to increase of the temperature or the intensity of a pump field, the oscillator strengths S_{cv} and S_{vc} decrease. Clearly, this is a consequence of the exclusion principle. Indeed, the electron can be excited resonantly by the electromagnetic wave only when the final state is empty otherwise the corresponding transition is prohibited leading to an absent interaction. Thus, the maximum effect of the excitons on the propagation of the electromagnetic waves through the structure is achieved at small populations, e.g. low temperatures. In this case the contributions $\propto f_{e,h}$ can be neglected and the expression for S_{cv} additionally simplifies.

Before we write down the final form of the Maxwell equations for the electromagnetic waves interacting with the excitons we would like to discuss the structure of the polarization term in the r.h.s. of Eq. (1.15). Generally the vector field $\Phi(\mathbf{r}, \mathbf{r})(\mathbf{d}_{cv}S_{cv} + \mathbf{d}_{vc}S_{vc})$ under the integral has a non-zero divergence. Therefore, its convolution with the transverse delta-function is not trivial. This circumstance reflects the fact that there is an electrical dipole moment induced by the exciton polarization. This dipole moment creates a Coulomb field which, generally speaking, affects excitons localized in the same or another quantum wells. As an example of interesting physical

effects produced by the exciton dipole-dipole interaction let us mention its possible important role in the exciton Bose-Einstein condensation [12]. In what follows we primarily are interested in the most pronounced effect of the exciton-light interaction and, therefore, neglect this dipole field. This neglecting is performed by the substitution of the conventional delta-function in the r.h.s. of Eq. (1.15) instead of the transverse delta-function. Thus, finally the Maxwell equations for the electric field can be written in the form

$$\nabla \times \nabla \times \mathbf{E} = \frac{\omega^2}{c^2}[\epsilon_\infty(z)\mathbf{E} + 4\pi \mathbf{P}_{exc}], \tag{1.18}$$

where $\mathbf{P}_{exc}$ is the excitonic contribution to the polarization

$$\mathbf{P}_{exc}(\mathbf{r}) = -\chi(\omega)\widehat{\mathbf{d}}_{cv}\Phi(\mathbf{r}) \int d\mathbf{r}'\, \Phi(\mathbf{r}')\widehat{\mathbf{d}}_{cv} \cdot \mathbf{E}(\mathbf{r}'). \tag{1.19}$$

Here $\widehat{\mathbf{d}}_{cv}$ is the unit vector in the direction of $\mathbf{d}_{cv}$, also for shortness we have denoted $\Phi(\mathbf{r}) = \Phi(\mathbf{r}, \mathbf{r})$ and have introduced the excitonic susceptibility

$$\chi(\omega) = \frac{\alpha}{\omega_0 - \omega - i\gamma} \tag{1.20}$$

with the coupling parameter $\alpha = 2\,\mathrm{Re}(d_{cv})c^2/\omega^2$. The Maxwell equations (1.18) are the basic tool for a semi-phenomenological description of the light propagation in quantum heterostructures in the frameworks of the two-band approximation. They have two specific features. First, this is a resonant response of the medium at a frequency corresponding to a corresponding transition. Second, the interaction with the microscopic dipole active excitations is described by the non-local susceptibility. It is worth noting that the Maxwell equations with a resonant non-local susceptibility accomplished with the Schrödinger equation with respect to the exciton wave function resolve a long lasting problem of additional boundary conditions (ABC problem) [8, 10, 13–15].

1.2.2 Degeneration of the band states

The Maxwell equations with the excitonic susceptibility in the form (1.19) qualitatively reproduce main features of the interaction of the electromagnetic waves with the dipole active excitations. However, they predict some properties of this interaction which are not necessarily true. First, according to Eq. (1.19) the exciton polarization has the fixed direction determined by $\mathbf{d}_{cv}$. Second, only the component of the electric field along this direction interacts with the excitations. These predictions contradict observations of the light interaction with the optically active excitations. For example, such interaction in materials with the cubic symmetry is isotropic. Another example is provided by materials with the zinc-blende structure ($GaAs/Al_xGa_{1-x}As$ heterostructures) where only the component along a particular direction [001] is optically inactive (see e.g. Refs. [16–20] where the optical anisotropy of corresponding structures have been studied).

These predictions are direct results of the two-band approximation. More realistic description of the electron band structure should take into account a degeneration of the states at the edges of the band gap. In semiconductors with the zinc-blende structure the bottom of the conduction band (Γ_6) is twofold degenerate due to the spin of the electron. The form of the top of the valence band is more complicated. It has threefold degeneracy, that is the Bloch functions corresponding to the electron states at the top of the valence band transform according to an irreducible representation of $SU(3)$ (see e.g. Ref. [21]). Additionally, each state is twofold degenerate because of the spin of the electrons. As the result there are six linearly independent Bloch functions for the valence band instead of just two as has been used in Eq. (1.7). The spin-orbit interaction partially removes this degeneracy leading to the appearing of two groups of states (see Fig. 1.2). The first group (Γ_7)

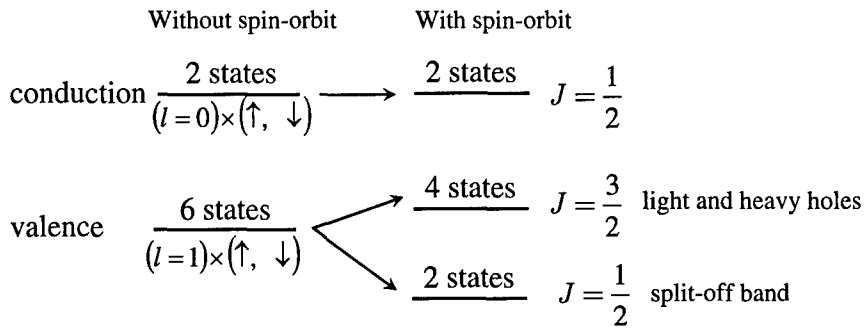

Figure 1.2: The electron states at the edges of the first band gap.

Table 1.1: The normalized matrix elements of the momentum operator for the transition $\Gamma_8 \to \Gamma_6$ [1].

$\frac{\hat{\mathbf{p}}}{p_{cv}}$	$\left\|\frac{3}{2},\frac{3}{2}\right\rangle$	$\left\|\frac{3}{2},\frac{1}{2}\right\rangle$	$\left\|\frac{3}{2},-\frac{1}{2}\right\rangle$	$\left\|\frac{3}{2},-\frac{3}{2}\right\rangle$
$\langle\uparrow\|$	$-\hat{\mathbf{e}}_+$	$\hat{\mathbf{e}}_z\sqrt{2/3}$	$\hat{\mathbf{e}}_z\sqrt{1/3}$	0
$\langle\downarrow\|$	0	$-\hat{\mathbf{e}}_z\sqrt{1/3}$	$\hat{\mathbf{e}}_z\sqrt{2/3}$	$\hat{\mathbf{e}}_-$

has two states and is called split-off band. The second group (Γ_8) has four states and corresponds to heavy and light holes.

The basic steps of the derivation of the Maxwell equation remain the same. The important difference is that the summation over the band states [e.g. in Eqs. (1.8)] now runs over all eight states in the conduction and the valence bands. In particular the density of the electron Hamiltonian $\hat{h}_{bb'}$ is represented generally by 8×8 Kane Hamiltonian [22]. The complete equations of motion describe quite rich variety of physical phenomena. It suffices to mention that there exist different types of the excitons, for example, formed by the bound states of the electrons and heavy and light holes. However, the difference between the masses of the holes leads to different energies of the ground state of these excitons. As the result, one can consider the interaction of light with the excitons of one type in the vicinity of a corresponding resonant frequency neglecting the effect of the interaction with the excitons of other types. This circumstance allows using the one-level approximation in the same way as it has been done above. One only has to modify the calculation of a product similar to $\mathbf{d}_{cv}\,(\mathbf{d}_{vc}\cdot\mathbf{E})$ in the expression for the excitonic polarization $\mathbf{P}_{exc}$. It can be done using Table 1.1 where the matrix elements of the momentum operator are shown for the transition $\Gamma_8 \to \Gamma_6$. The states in the valence band are classified according to the values of the total angular momentum J in the irreducible representation of the symmetry group. The bands Γ_7 and Γ_8 correspond to $J = 1/2$ and $J = 3/2$, respectively. Let us consider the case when the structure is not grown along a low symmetry direction. For example, let the direction of z axis coincide with the principal axis [001]. Then, in the band Γ_8 the heavy and light holes are the states with $|J_z| = 3/2$ and $|J_z| = 1/2$. The states in the conduction band are enumerated by the projection of the electron spin. In Table 1.1 the vectors $\hat{\mathbf{e}}_\pm$ are defined as $\hat{\mathbf{e}}_\pm = (\hat{\mathbf{e}}_x \pm i\hat{\mathbf{e}}_y)/\sqrt{2}$.

In what follows we will be interested in a relatively narrow vicinity of the heavy hole exciton frequency. The contributions of the interaction of the electromagnetic waves with other excitons can

be neglected. As the result in the expression $\mathbf{d}_{cv}\,(\mathbf{d}_{vc}\cdot\mathbf{E})$ the summation over the valence band states should run over the states corresponding to the heavy holes. Substitution of the matrix elements from Table 1.1 yields

$$\langle\uparrow|\,\mathbf{p}\,|3/2\rangle\,\mathbf{E}\,\langle 3/2|\,\mathbf{p}\,|\uparrow\rangle+\langle\downarrow|\,\mathbf{p}\,|-3/2\rangle\,\mathbf{E}\,\langle -3/2|\,\mathbf{p}\,|\downarrow\rangle=p_{cv}\mathbf{E}_{\perp}, \tag{1.21}$$

where we have left only the value of the projection of the total angular momentum and $\mathbf{E}_{\perp}$ is the component of the electric field perpendicular to the growth direction $\hat{\mathbf{e}}_z$. Making use of this result leads to the well-known form of the excitonic contribution to the polarization

$$\mathbf{P}_{exc}(\mathbf{r})=-\chi(\omega)\Phi(\mathbf{r})\int d\mathbf{r}'\,\Phi(\mathbf{r}')\mathbf{E}_{\perp}(\mathbf{r}'), \tag{1.22}$$

where the exciton susceptibility is defined by Eq. (1.20) with ω_0 the resonance frequency of the heavy hole exciton.

1.2.3 Electromagnetic waves in multiple quantum wells structures

To complete the derivation of the basic equations governing the propagation of the electromagnetic waves in quantum heterostructures let us consider the case of multiple quantum well structures. It is clear that the consideration provided in the previous subsections remains valid in this case also with a slight modification in finding the density of the exciton polarization $f_{cv}(\mathbf{r}_1,\mathbf{r}_2)$. As has been discussed above the specific feature of the multiple quantum well structures is the absence of the overlap of the exciton wave functions localized in different quantum wells. As the result the exciton state in one well is not affected by the exciton localized in other wells in the approximation of a small dipole-dipole interaction between the excitons. If we restrict our attention to $1s$-state of the heavy hole excitons then the absence of the interaction between the excitons leads to the fact that there exists only one exciton level in the system with the degeneracy determined by the number of the quantum wells in the structure. Using this fact the Hamiltonian of the electron-heavy hole pair can be written in the spectral representation as

$$H=\omega_0\sum_m|m\rangle\langle m|\,, \tag{1.23}$$

where the summation runs over all quantum wells in the structure and the state $|m\rangle$ is the exciton state localized in the m-th quantum well. Schematically, the equation determining the spatial distribution of the exciton polarization density [the second equation of Eqs. (1.15)] can be written as a Schrödinger equation with a source

$$i\hbar\dot{f}_{cv}=(\omega_0+i\gamma)\sum_m|m\rangle\langle m|\,f_{cv}+\mathcal{S}, \tag{1.24}$$

where we have taken into account a phenomenological broadening γ and $\mathcal{S}$ is the source function. The representation of the density of the exciton polarization in the form $f_{cv}=\sum_m f_m\,|m\rangle$ gives

$$f_m=-\frac{\langle m|\mathcal{S}\rangle}{\omega-\omega_0-i\gamma}. \tag{1.25}$$

The expression for the scalar product $\langle m|\mathcal{S}\rangle$ is similar to Eq. (1.17) where as the exciton wavefunction $\Phi(\mathbf{r}_1,\mathbf{r}_2)$ should be taken $\Phi_m(\mathbf{r}_1,\mathbf{r}_2)$ i.e. that of the exciton localized in the m-th quantum well. As the result the form of the exciton contribution to the polarization in the multiple quantum well structures is merely the sum of the terms similar to Eq. (2.2) or (1.22) over all quantum wells.

The modulation of the exciton polarization and the dielectric function along the growth direction preserves the symmetry of the structure with respect to shifts in the plane of the layers. This allows one to simplify more the integral entering $\mathbf{P}_{exc}$ and to reduce it to the integration along z direction only. The qualitative line of reasoning is the following. First, the in-plane exciton dispersion can be taken into account by the phase factor $e^{i\mathbf{k}\boldsymbol{\rho}}$ only, where $\boldsymbol{\rho}$ is the coordinate in the plane perpendicular to the growth direction. Indeed, because of the separation of variables in the Shrödinger equation the resonant frequency corresponding to an exciton state characterized by the momentum $\hbar\mathbf{k}$ in the plane of the quantum well is simply $\omega_k = \omega_0 + \hbar k^2/2M$, where M is the mass of the exciton. However, for the values of the wave-vectors under the interest the shift of the resonant frequency due to the kinetic energy term is negligibly small. Taking into account this additional degeneracy of the exciton states the exciton polarization can be written as

$$\mathbf{P}_{exc} \propto \int d^2k\, \Phi_m(z) \int d^3r'\, \Phi_m(z') E(\mathbf{r}') e^{i\mathbf{k}(\boldsymbol{\rho}-\boldsymbol{\rho}')}, \tag{1.26}$$

where $\Phi_m(z) = \Phi_m(z,z)$ and $\Phi_m(z,z)$ is the solution of a corresponding one-dimensional Shrödinger equation in the m-th quantum well. After the Fourier transform of the electric field with respect to the in-plane coordinates the integration over both $\boldsymbol{\rho}$ and $\mathbf{k}$ can be performed. Finally, this gives the excitonic contribution to polarization in multiple quantum well structure made of a semiconductor with the zinc-blende structure

$$\mathbf{P}_{exc}(\mathbf{r}) = -\chi(\omega) \sum_m \Phi_m(z) \int dz'\, \Phi_m(z') \mathbf{E}_\perp(z'). \tag{1.27}$$

Eq. (1.27) and the Maxwell equation (1.18) constitute the basic equations describing the propagation of the electromagnetic waves in the multiple quantum well structures and which will be analyzed in detail in the following chapters of the present thesis.

1.3 Resonant photonic crystals

In quantum heterostructures described by the Maxwell equation (1.18) with the polarization given by Eq. (1.27), the spatial modulation of the dielectric function $\epsilon_\infty(z)$ coexists with the periodic arrangement of the optically active elements. This puts the propagation of the electromagnetic waves in quantum heterostructures in a general context of resonant photonic crystals. These structures attract a great deal of attention [23–31]and are the object of intensive investigation.

The optical properties of resonant photonic crystals are still a challenge since an interplay of two scattering channels existing in such structures is not trivial. Different aspects of this problem have been considered in a number of publications. In particular, in Ref. [32] the necessity of a modification of the Bragg resonance condition in comparison with what one has in the case of simple MQW structures has been shown. Later, this result was confirmed [33] and an exact Bragg condition in such structures was found. It is especially interesting to note recent publications Refs. [29] and [31]. In these papers the numerical calculations of the photonic band structure have been provided for a 3D (and 2D) system with periodically modulated resonant dielectric function and for a 3D lattice of quantum dots with the index of refraction different from that of the environment, respectively. These calculations have shown that the existence of the resonance widens the forbidden gap in the spectrum of the electromagnetic waves. There is a definite similarity between the spectral properties of different systems which makes it reasonable to suggest that such widening is a general feature of resonant photonic crystals.

A formal problem which impedes establishing a general framework for description of the resonant photonic crystals is their resonant property. Strong dispersion near the resonance and

accompanying resonant absorption make difficult using a standard technique which has been developed for self-adjoint operators proved its efficiency in quantum mechanics. This circumstance requires a special approach for description of the propagation of the electromagnetic waves which is under active development these days [34, 35]. The basic idea of this approach is the introduction of fictitious degrees of freedom which are responsible for both absorption and dispersion. The general requirement of causality in the form of the Kramers-Kronig relation leads to a unique[1] choice of these additional degrees of freedom. For the new extended system the dynamics turn out to be unitary and this allows applying the machinery of self-adjoint operators.

In the present thesis a similar ideology is implemented naturally since the initial system explicitly contains degrees of freedom additional to the electromagnetic field — the exciton polarization. There are two important differences, though. First, we do not consider dynamics in the extended electromagnetic field – exciton polarization system. Moreover, using the absence of the overlap of the exciton wavefunction we exclude the exciton degrees of freedom from the equations of motion. Second, in order to account the finite exciton lifetime we introduce a phenomenological exciton linewidth broadening and thereby we make the system incomplete from the canonical point of view. The success of our approach is provided by a possibility to describe one-dimensional systems without referring to solutions of some boundary value problems. In Chapter 2 we develop a general approach and apply it for an analysis of the exciton polariton spectrum in different structures. In Chapter 3 we use the same general ideas to consider the reflection and transmission spectra of finite structures. Finally, in Chapter 4 we apply the information we gathered regarding the optical properties of the quantum heterostructures to solve the problem of the exciton luminescence in MQW based photonic crystals.

[1]This is obvious that such a choice is unique up to a trivial extension of the resultant system by degrees of freedom which do not interact with the relevant excitations. Thus, one can talk only about unique irreducible set of the degrees of freedom.

Chapter 2

Polaritons in MQW based photonic crystals

In the present Chapter we obtain and analyze the polariton dispersion law in photonic crystals based on multiple quantum well structures. The main objective is to establish a solid theoretical background for a description of exciton polaritons in resonant photonic crystals with an arbitrary periodic modulation of the dielectric function, propagation angle of the electromagnetic wave and its polarization state. The developed approach is applied for an analysis of the exciton polariton spectrum in different structures.

2.1 Derivation of the transfer matrix

As has been shown in Introduction a propagation of the electromagnetic wave in the structures under discussion is governed by the Maxwell equation

$$\nabla \times \nabla \times \mathbf{E} = \frac{\omega^2}{c^2}[\epsilon_\infty(z)\mathbf{E} + 4\pi \mathbf{P}_{exc}], \tag{2.1}$$

with the excitonic contribution to the polarization

$$\mathbf{P}_{exc} = -\chi(\omega) \sum_m \Phi_m(z) \int dz\, \Phi_m(z')\mathbf{E}_\perp(z'). \tag{2.2}$$

Here z axis is chosen along the growth direction, and $\Phi_m(z) = \Phi(z - z_m)$ is the envelope wave function of an exciton localized in the m-th quantum well. The summation in Eq. (2.2) is taken over all quantum wells and z_m are the positions of their centers. We assume that the distance between the consecutive wells, $d = z_{m+1} - z_m$, coincides with the period of the spatial modulation of the dielectric function, $\epsilon(z + d) = \epsilon(z)$. Also, we assume that the profile of the dielectric function is symmetric with respect to the position of the center of the quantum well, $\epsilon(z_m + z) = \epsilon(z_m - z)$ (see Fig. 2.1). We restrict ourselves to the consideration of $1s$ states of heavy-hole excitons and neglect their in-plane dispersion. Therefore, writing Eq. (2.2) we have taken into account that the component of the electric field parallel to the growth direction is optically inactive. Only $\mathbf{E}_\perp$, the component lying in the plane of the quantum wells, contributes to the exciton polarization.

The frequency dependence of the excitonic susceptibility, $\chi(\omega)$, is given by

$$\chi(\omega) = \frac{\alpha}{\omega_0 - \omega - i\gamma}, \tag{2.3}$$

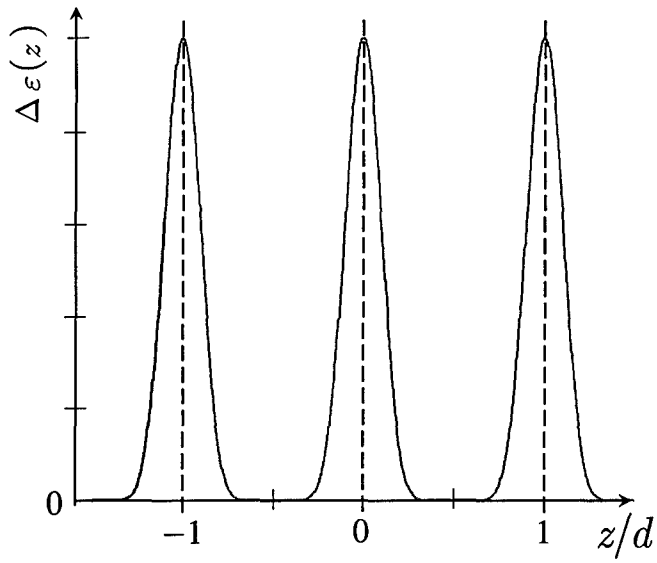

Figure 2.1: An example of the modulation of the dielectric function, $\epsilon(z) = \bar{\epsilon} + \Delta\epsilon(z)$ (solid line). The dashed vertical lines show the positions of the centers of quantum wells.

where ω_0 is the exciton resonance frequency, γ is the non-radiative decay rate of the exciton, and α is the exciton-light coupling parameter.

It is convenient to analyze Eq. (2.1) considering the components of the electric field. To do this it is necessary to make separate considerations of s- and p-polarized fields because these fields satisfy different differential equations. This follows from the fact that for s-polarization one has $\nabla \cdot \mathbf{E} = 0$ while for p-polarized wave this is generally not true because of the spatial modulation of the dielectric function.

2.1.1 S-polarization

In s-polarized wave the electric field $\mathbf{E}$ is perpendicular to the direction of z axis and can be represented in the form

$$\mathbf{E}(z, \boldsymbol{\rho}) = \hat{\mathbf{e}}_s E(z) e^{i\mathbf{k}\boldsymbol{\rho}}, \tag{2.4}$$

where $\boldsymbol{\rho}$ is a coordinate in the (x, y)-plane and $\hat{\mathbf{e}}_s = \hat{\mathbf{e}}_\mathbf{k} \times \hat{\mathbf{e}}_z$ is a unit polarization vector. We use the separability of variables and the symmetry of the equation with respect to infinitesimal shifts in (x, y)-plane to introduce the wave vector $\mathbf{k} = k\,\hat{\mathbf{e}}_\mathbf{k}$ lying in the plane of the layers. For $E(z)$ we obtain an ordinary differential equation

$$\frac{d^2E(z)}{dz^2} + \kappa_s^2(z) = -\chi(\omega)\frac{4\pi\omega^2}{c^2}\sum_m \Phi_m(z)\int dz\,\Phi_m(z')E(z'), \tag{2.5}$$

where $\kappa_s^2(z) = \omega^2\epsilon(z)/c^2 - k^2$.

The absence of an overlap of the exciton wave functions localized in different quantum wells makes it plausible to use the transfer matrix technique. The general idea of this technique, in

summary, is obtaining the field at, say, the right boundary of the elementary cell ($z = z_+$) given by the field at the left boundary ($z = z_-$). Due to linear character of the basic equations it is sufficient to consider each elementary cell separately and then obtain the complete transfer matrix as a product of individual matrices. Without any lost of generality we can choose the position of the origin coinciding with a position of the quantum well in the layer under consideration. Inside a single layer the summation over quantum wells in Eq. (2.5) can be dropped and so is the index of the quantum well. The term with the exciton polarization at the r.h.s. of Eq. (2.5) can be considered as an inhomogeneity in a second order differential equation

$$\frac{d^2E(z)}{dz^2} + \kappa_s^2(z)E = \mathcal{F}(z). \tag{2.6}$$

A general solution of this equation can be written in the form [36]

$$E(z) = c_1 h_1(z) + c_2 h_2(z) + (G \star \mathcal{F})(z), \tag{2.7}$$

where

$$(G \star \mathcal{F})(z) = \int_{z_-}^{z} dz' \mathcal{F}(z') \frac{h_1(z')h_2(z) - h_1(z)h_2(z')}{W(h_1, h_2; z')}. \tag{2.8}$$

Here we have introduced $h_{1,2}(z)$, a pair of linearly independent solutions of the homogeneous equation

$$\frac{d^2E(z)}{dz^2} + \kappa_s^2(z)E = 0, \tag{2.9}$$

and $W(h_1, h_2; z) = h_1 h_2' - h_1' h_2$ is the Wronskian of these solutions. For the case under consideration the Wronskian does not depend on z and will be denoted by W_h in what follows.

Using, next, a standard procedure we obtain the expression for the field (2.7) for points to the right of the quantum well where $\Phi(z) = 0$

$$\begin{aligned} E(z) =& h_1 \left[c_1 + \tilde{\chi} \frac{4\pi\omega^2 \varphi_2}{c^2} (c_1\varphi_1 + c_2\varphi_2) \right] + \\ &+ h_2 \left[c_2 - \tilde{\chi} \frac{4\pi\omega^2 \varphi_1}{c^2} (c_1\varphi_1 + c_2\varphi_2)) \right], \end{aligned} \tag{2.10}$$

where $\varphi_{1,2}$ are "projections" of the solutions $h_{1,2}$ onto the exciton states

$$\varphi_{1,2} = \frac{1}{\sqrt{W_h}} \int_{QW} dz' \Phi(z') h_{1,2}(z'), \tag{2.11}$$

and the modified excitonic susceptibility $\tilde{\chi}$ can be presented as

$$\tilde{\chi} = \frac{\chi}{1 - \Delta\omega\chi/\alpha}, \tag{2.12}$$

where

$$\Delta\omega = \alpha \int_{QW} dz\, \Phi(z)(G \star \Phi)(z) \tag{2.13}$$

gives the radiative shift of the exciton frequency in the photonic crystal. It is useful to compare Eq. (2.13) with well-known expression for the radiative shift in MQW structures with a homogeneous dielectric function [37–39].

Using the general solution (2.10) we can find a relation between the field at different sides of the elementary cells ($z = z_{\pm}$). Because the field is uniquely specified by providing the amplitudes $c_{1,2}$ we have

$$\begin{pmatrix} c_1 \\ c_2 \end{pmatrix}(z_+) = T_h \begin{pmatrix} c_1 \\ c_2 \end{pmatrix}(z_-), \tag{2.14}$$

where T_h is the transfer matrix written in the basis of the linearly independent solutions inside the elementary cell

$$T_h = \mathbf{1} + \frac{4\pi\omega^2\tilde{\chi}}{c^2}\begin{pmatrix} \varphi_2\varphi_1 & \varphi_2^2 \\ -\varphi_1^2 & -\varphi_2\varphi_1 \end{pmatrix}, \tag{2.15}$$

where $\mathbf{1}$ is the unit matrix. It should be noted that Eq. (2.15) is valid for an arbitrary form of the exciton envelope wave function and spatial modulation of the dielectric function as long as the period of the arrangement of the quantum wells coincides with the period of the spatial modulation of the dielectric function.

Now, we use the freedom of choice of the pair of the solution to simplify the expressions obtained. We note that one of $\varphi_{1,2}$ can always be turned to zero by a special choice of $h_{1,2}$.[1] In the case when $\epsilon(z)$ is invariant with respect to mirror reflection relatively to the center of the quantum well such choice of $h_{1,2}$ corresponds to h_1 and h_2 being even and odd solutions with respect to the center of the quantum well. The existence of such solutions with the definite parity is guaranteed by the symmetry of $\epsilon(x)$. Below we will consider only this symmetrical case. The generalization of the consideration is straightforward but requires more complicated analysis.

Sometimes we will call h_1 and h_2 even and odd modes of the photonic crystal. It should be understood that actual modes of the photonic crystal defined as solutions of appropriate boundary problems are not necessarily even and odd functions with respect to the center of the elementary cell. Moreover, due to the Bloch theorem the modes of a photonic crystal have a definite parity only at specific frequencies that are naturally identified with boundaries of the forbidden gap in the spectrum. However, all modes of the photonic crystal can be represented as linear combinations of the even and odd solutions $h_{1,2}$.

It should be noted that after fixing the symmetry the functions $h_{1,2}$ are still determined up to a constant factor only. However, observables, such as, for example, the positions and the widths of forbidden gaps, do not depend on this factor due to appropriate entrance of W_h. For example, the functions $h_{1,2}$ can be found as solutions of a Cauchy problem for Eq. (2.9) with initial conditions (some formal details can be found in Ref. [40] where the spectrum of a Shrödinger equation with a periodic potential is studied using similar approach)

$$\begin{aligned} h_1(0) &= 1, \qquad h_1'(0) = 0, \\ h_2(0) &= 0, \qquad h_2'(0) = 1. \end{aligned} \tag{2.16}$$

With such a choice of the initial conditions we have $W_h = 1$. We will write general results in a covariant form, i.e. independent on a particular choice of the initial conditions in corresponding Cauchy problems. However, discussions will be done having in mind the initial conditions (2.16).

Let h_1 be the even solution then $\varphi_2 \equiv 0$ and the transfer matrix for the coefficients $c_{1,2}$ is

$$T_h = \mathbf{1} + S_s q_s \begin{pmatrix} 0 & 0 \\ 1 & 0 \end{pmatrix}, \tag{2.17}$$

[1] It raises a question is it possible to have both $\varphi_{1,2}$ equal to 0. Generally it can be proven that it is impossible below the frequency of the first photonic band gap, so the latter is always effected by the exciton-light interaction. This impossibility can be proven also for all frequencies for considered here model of symmetric quantum wells and spatial modulation of the dielectric function, and for δ-functional approximation for the envelope wave function. These results make the question about the possibility for the effective exciton-light interaction to be completely inhibited rather academic.

where $q_s = \kappa_s(z_+)$ is the value of $\kappa_s(z)$ at the boundary of the elementary cell and

$$S_s(\omega) = -\tilde{\chi}(\omega)\frac{2\pi\omega^2\varphi_1^2}{q_s c^2}. \tag{2.18}$$

Substitution of $\tilde{\chi}$ yields

$$S_s(\omega) = \frac{\Gamma_s}{\omega - \omega_0 - \Delta\omega + i\gamma}, \tag{2.19}$$

where Γ_s is the radiative decay rate,

$$\Gamma_s = \frac{2\pi\alpha\omega^2\varphi_1^2}{q_s c^2}. \tag{2.20}$$

The function $S_s(\omega)$ plays an important role in determining the effect of the exciton-light interaction on optical properties. In particular, the resonant absorption of light occurs at a frequency $\omega_0 + \Delta\omega$ where the pole of $S_s(\omega)$ is situated. This is important that the main parameters — the resonant frequency and the radiative decay rate — can be found in a single quantum well optical experiment. We note that the radiative shift of the exciton frequency $\Delta\omega$ is small provided by the narrowness of quantum wells and often is neglected. In what follows by the exciton frequency we will mean the resonant frequency of $S_s(\omega)$. Also, for shortness we will refer to the function $S_s(\omega)$ as the excitonic susceptibility.

The basis of a pair of linearly independent functions is clearly convenient to derive the transfer matrix through a single elementary cell staying inside the cell. To obtain the transfer matrix through the period of the structure it is necessary to satisfy the continuity of the field and its derivative at the boundary between different elementary cells. This problem appears since the even and odd solutions in one cell are not necessarily even and odd with respect to the center of the next cell. This problem can be solved but, instead, using the conversion rule (A.9) we convert the matrix to more conventional basis of plane waves

$$E(z) = E_+ e^{iq_s z} + E_- e^{-iq_s z}. \tag{2.21}$$

As will be seen shortly the transfer matrix in the basis of plane waves T is convenient to be represented in the form

$$T = \begin{pmatrix} af & (\bar{a}f - a\bar{f})/2 \\ (a\bar{f} - f\bar{a})/2 & \bar{a}\bar{f} \end{pmatrix}. \tag{2.22}$$

This representation is extensively used in the present paper and, in what follows, we will refer to it as (a, f)-representation. The parameters of this representation, a and f, are found to be

$$\begin{aligned} a &= g_2, \qquad & f &= g_1 - iS_s g_2, \\ \bar{a} &= g_2^*, \qquad & \bar{f} &= g_1^* + iS_s g_2^*, \end{aligned} \tag{2.23}$$

where

$$g_1 = \frac{1}{\sqrt{W_h}}\left[h_1(z_+) + \frac{h_1'(z_+)}{iq_s}\right], \qquad g_2 = \frac{1}{\sqrt{W_h}}\left[iq_s h_2(z_+) + h_2'(z_+)\right]. \tag{2.24}$$

2.1.2 p-polarization

As has been mentioned, the important difference between s- and p-polarized waves is that they satisfy different differential equations since for the latter case $\nabla \cdot \mathbf{E} \neq 0$. For conventional photonic crystals the p-polarized waves are conveniently described in terms of the magnetic field (see e.g. Ref. [41]). However, the existence of dipole active excitations essentially reduces this convenience by the necessity to close the equations by finding the interaction of the excitons with

light in terms of the magnetic field. This problem, of course, can be solved but it leads to quite cumbersome expressions which make it difficult to establish a relation with the results obtained above. Therefore, it is reasonable to stay in the frameworks of the equations with respect to electric field.

The electric field can be represented in a similar to Eq. (2.4) form

$$\mathbf{E}(z,\boldsymbol{\rho}) = \left[\hat{\mathbf{e}}_{\mathbf{k}} E_x(z) + \hat{\mathbf{e}}_z E_z(z)\right] e^{i\mathbf{k}\boldsymbol{\rho}}. \tag{2.25}$$

The amplitudes $E_{x,z}(z)$ satisfy the system of the ordinary differential equations

$$\begin{aligned} &\frac{d^2E_x}{dz^2} - ik\frac{dE_z}{dz} + \kappa_p^2(z)E_x = \\ &\qquad -\chi(\omega)\sum_m \Phi_m(z)\int dz\,\Phi_m(z')E_x(z'), \\ &-ik\frac{dE_x}{dz} + \left[\kappa_p^2(z) - k^2\right]E_z(x) = 0, \end{aligned} \tag{2.26}$$

where $\kappa_p^2(z) = \omega^2\epsilon(z)/c^2$. Deriving these equations we again explicitly have taken into account that only the in-plane component of the electric field interacts with the heavy-hole excitons. Solving the second equation with respect to E_z we obtain the closed equation for $E_x(z)$

$$\begin{aligned} &\frac{d}{dz}\left[p(z)\frac{dE_x}{dz}\right] + \kappa_p^2(z)E_x = \\ &\qquad -\chi(\omega)\frac{4\pi\omega^2}{c^2}\sum_m \Phi_m(z)\int dz\,\Phi_m(z')E_x(z'), \end{aligned} \tag{2.27}$$

where $p(z) = \kappa_p^2(z)/[\kappa_p^2(z) - k^2]$. This function can be seen to be determined by the local angle of propagation of the wave, $p(z) = 1/\cos^2\theta(z)$.

The derivation of the transfer matrix for the p-polarized field follows exactly the same steps as in the previous subsection with an important specific detail. The Wronskian of two solutions of "homogeneous" version of Eq. (2.27) (that is with $\chi \equiv 0$) is not a constant but depends on z [36]. However, writing down this dependence as

$$W(z) = W_h\frac{p(z_+)}{p(z)}. \tag{2.28}$$

one can see that the main results of the previous subsection are immediately applied. In particular, the transfer matrix in the basis of plane waves can also be represented in the form (2.22). There are only simple changes in definitions of the parameters of the (a,f)-representation. First of all, in the definition (2.24) as the pair of functions $h_{1,2}$ there should be even and odd solutions of the "homogeneous" version of Eq. (2.27). Second, the expression for the radiative shift of the exciton frequency (2.13) changes because now, instead of Eq. (2.8) one has

$$(G\star\mathcal{F})(z) = \frac{1}{W_h p(z_+)}\int_{z_-}^{z} dz'\mathcal{F}(z')\left[h_1(z')h_2(z) - h_1(z)h_2(z')\right]. \tag{2.29}$$

Finally, the function $S_p(\omega)$ can be introduced which also has the Lorentz form as in Eq. (2.19) with the modified radiative decay rate that becomes

$$\Gamma_p = \frac{2\pi\alpha\omega^2\varphi_1^2}{q_p c^2 p(z_+)}, \tag{2.30}$$

where $q_p = \kappa_p(z_+)$. It is seen that these expressions and corresponding expressions for an s-polarized wave coincide in the case of normal propagation, i.e. when $k = 0$.

2.2 The structure of the transfer matrices

The fact that the transfer matrices for both polarizations allow the (a, f)-representation is not a coincidence but is related to a structure of the Maxwell equations. To demonstrate this let us consider Eq. (2.5) in a particular case corresponding to the passive structure ($\chi \equiv 0$). Let $E(z)$ be a solution of this equation. Taking complex conjugation of the equation one can see that $E^*(z)$ is also a solution. Then, one finds that

$$\frac{d}{dz}\left(EE^{*\prime} - E'E^*\right) = 0. \tag{2.31}$$

Now, representing the electric field in the form (2.21) the relation

$$\frac{d}{dz}\left[q_s\left(|E_+|^2 - |E_-|^2\right)\right] = 0 \tag{2.32}$$

is found. This relation can be shown to correspond to a constancy of the flux of the Poynting vector through a plane perpendicular to the z-axis and represents the fact that there are no sources or drains of the energy in the system. From Eq. (2.32) follows that the transfer matrix through the period of the structure must preserve the combination $|E_+|^2 - |E_-|^2$. The same can be shown for p-polarization. This proves that the transfer matrix written in the basis of plane waves belongs $SU(1,1)$ [42]. A general form of an element of $SU(1,1)$ is [42]

$$T = \begin{pmatrix} T_1 & T_2 \\ T_2^* & T_1^* \end{pmatrix}, \tag{2.33}$$

where $T_{1,2}$ are complex numbers and $|T_1|^2 - |T_2|^2 = 1$. The (a, f)-representation can be seen to correspond to a particular case of T_2 being purely imaginary. Such transfer matrices describe structures that posses mirror symmetry. Indeed, the condition of this symmetry can be written in the form $\sigma_x T \sigma_x = T^{-1}$, where σ_x is the Pauli matrix. Substitution of Eq. (2.33) into this equation gives $T_2^* = -T_2$. The converse statement can also be easily checked. The corresponding statement regarding the full equations (2.5) and (2.27) can also be proved but the proof is rather technical and we do not provide it here[2].

Structures with the mirror symmetry have a nice property to allow a relatively simple analysis and still demonstrate a rich variety of interesting phenomena. Therefore they attract a lot of attention (see e.g. Ref. [43]). If such a structure is built of blocks that have the mirror symmetry by themselves then the transfer matrix through the entire structure can be easily written in terms of matrix element describing the individual blocks. Indeed, let us look at a structure with the period BAB where the transfer matrices of the blocks A and B have the form $T(a_1, f_1)$ and $T(a_2, f_2)$, respectively, in the (a, f)-representation. Then the transfer matrix through the period is

$$T(a_2, f_2)T(a_1, f_1)T(a_2, f_2) = T(a, f), \tag{2.34}$$

where

$$\begin{aligned} a &= a_1 a_2 f_2 - \frac{\bar{a}_1}{2}\left(\bar{a}_2 f_2 - a_2 \bar{f}_2\right), \\ f &= f_2 f_1 a_2 + \frac{\bar{f}_1}{2}\left(\bar{a}_2 f_2 - a_2 \bar{f}_2\right). \end{aligned} \tag{2.35}$$

[2]The non-locality of the equations with the exciton polarization seems to be a problem for a straightforward derivation of a relation (2.31). This problem can be resolved in several ways. One of the simplest is a consideration of an equivalent local equation. The equivalence is understood here in terms of transfer matrices.

To establish a connection with well-known results let us consider several important examples. The first example is when the blocks B are homogeneous barriers whose the transfer matrix is $T_b(\phi_b) = \mathrm{diag}\,[\exp(i\phi_b), \exp(-i\phi_b)]$. In this case one has $a_2 = f_2 = \exp(i\phi_b/2)$ in Eq. (2.34) and thus

$$T_b(\phi_b)T(a,f)T_b(\phi_b) = T(ae^{i\phi_b}, fe^{i\phi_b}). \tag{2.36}$$

Another example is when a mismatch of the indices of refraction at the boundaries of the block A and the surrounding barriers is taken into account. In this case one has

$$T_\rho(\rho)^{-1}T(a,f)T_\rho(\rho) = \frac{1}{1-\rho^2}T(a+\bar{a}\rho, f-\bar{f}\rho). \tag{2.37}$$

where ρ is the Fresnel reflection coefficient [44] (see below Eq. (2.45)), and T_ρ is the matrix describing the interfacial scattering

$$T_\rho = \frac{1}{1+\rho}\begin{pmatrix} 1 & \rho \\ \rho & 1 \end{pmatrix}. \tag{2.38}$$

The real factor in Eq. (2.37) can be incorporated into a and f due to the useful relation (with real λ)

$$\lambda T(a,f) = T(\lambda a, f) = T(a, \lambda f). \tag{2.39}$$

The formulas (2.34), (2.36) and (2.37) are basic tools for obtaining the (a,f)-representation of a matrix in terms of more elementary transfer matrices. This method is often more practical than solving corresponding differential equations. It is interesting, however, to note the reverse: the parameters of the (a,f)-representation are boundary values of solutions of a corresponding Cauchy problem.

2.3 The dispersion equation

In the formalism of a transfer matrix in the basis of plane waves the polariton dispersion law can be obtained using [45]

$$\cos Kd = \frac{1}{2}\mathrm{Tr}\,T, \tag{2.40}$$

where K is the Bloch wave number and d is the period of the structure. From the fact that $\det T = 1$ follows that $f\bar{a} + \bar{f}a = 2$. Using this identity we can write the polariton dispersion law in the form

$$\cos^2\left(\frac{Kd}{2}\right) = \mathrm{Re}(a)\mathrm{Re}(f), \tag{2.41}$$

where the real part is defined as $\mathrm{Re}(a) = (a+\bar{a})/2$. The forbidden gap is determined as such a frequency region where the r.h.s. of this equation becomes negative or bigger than 1 because in these cases the Bloch wave-number becomes complex and this corresponds to evanescent modes. These conditions, being the r.h.s. negative or bigger than 1, can be seen to determine different parts of the forbidden gap and this makes an analysis of the structure of the spectrum somewhat cumbersome. However, the consideration can be easily unified noting that the dispersion equation can be equivalently written as

$$\sin^2\left(\frac{Kd}{2}\right) = \mathrm{Im}(a)\mathrm{Im}(f), \tag{2.42}$$

with $\mathrm{Im}(a) = (a-\bar{a})/2i$. Now, the gaps that are at the frequencies where the r.h.s. of Eq. (2.41) is bigger than 1 correspond to frequencies where the r.h.s. of Eq. (2.42) is negative. This circumstance allows one to consider all gaps in the same way.

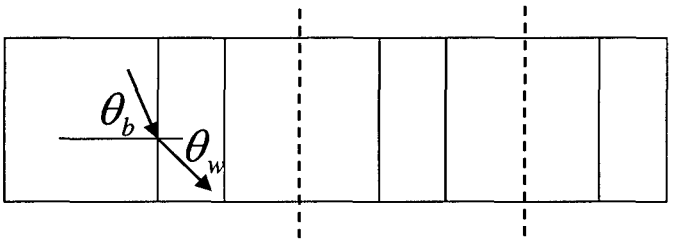

Figure 2.2: The periodic structure built of two blocks. Vertical dashed lines show the boundary of the elementary cell. The angles of propagation inside the blocks are related by Snell's law.

The representation of the dispersion equation in the form (2.41) or (2.42) [and, hence, the transfer matrix in the form (2.22)] has that advantage that the polariton forbidden gap corresponds to frequencies where *one* of the terms is negative. Such factorization of the equation drastically simplifies the analysis of the spectrum. We demonstrate how it works for the examples of known structures and apply the results obtained for more general situation.

2.3.1 Passive multilayer structure

Let us consider a structure built of a periodic sequence of two blocks characterized by the widths $d_{b,w}$ and the indices of refraction $n_{b,w}$. To emphasize the mirror symmetry we choose the elementary cell as shown in Fig. 2.2. The transfer matrix through the period of the structure has the form

$$T = T_b^{1/2} T_\rho^{-1} T_w T_\rho T_b^{1/2}, \tag{2.43}$$

where

$$T_{b,w} = \begin{pmatrix} e^{i\phi_{b,w}} & 0 \\ 0 & e^{-i\phi_{b,w}}, \end{pmatrix} \tag{2.44}$$

$\phi_{b,w} = \omega n_{b,w} d_{b,w} \cos\theta_{b,w}/c$ and $\theta_{b,w}$ are the angles of propagation of the wave.

The scattering of the electromagnetic wave at the interface between different blocks depends on both the angle of incidence of the wave and its polarization state. These effects are described by using Fresnel coefficients ρ_s and ρ_p

$$\begin{aligned} \rho_s &= \frac{n_w \cos\theta_w - n_b \cos\theta_b}{n_w \cos\theta_w + n_b \cos\theta_b}, \\ \rho_p &= \frac{n_w \cos\theta_b - n_b \cos\theta_w}{n_w \cos\theta_b + n_b \cos\theta_w} \end{aligned} \tag{2.45}$$

for s and p polarizations respectively. Below we denote the Fresnel coefficients simply by ρ having in mind that for a particular polarization one of these expressions should be used.

Using Eqs. (2.36) and (2.37) we can obtain the (a, f)-representation of the transfer matrix. Then making use of Eq. (2.39) we can factor out the term $1/(1-\rho^2)$ and write

$$a = e^{i\omega\tau_+} + \rho e^{i\omega\tau_-}, \qquad f = e^{i\omega\tau_+} - \rho e^{i\omega\tau_-}, \tag{2.46}$$

where $\tau_\pm = (\phi_b \pm \phi_w)/2\omega$. For this case Eqs. (2.41) and (2.42) turn to

$$\cos^2\left(\frac{Kd}{2}\right) = \frac{\mathrm{Re}(a)\mathrm{Re}(f)}{1-\rho^2}, \quad \sin^2\left(\frac{Kd}{2}\right) = \frac{\mathrm{Im}(a)\mathrm{Im}(f)}{1-\rho^2}. \tag{2.47}$$

As follows from these equations there exist forbidden gaps of two types. First, where the r.h.s. of the first equation becomes negative, $\mathrm{Re}\,(a)\mathrm{Re}\,(f) < 0$, and, second, where the same is valid for the second equation, $\mathrm{Im}\,(a)\mathrm{Im}\,(f) < 0$. If τ_+ and τ_- are incommensurate these gaps alternate along the frequency axis and correspond to the gaps appearing in vicinity of the odd and even Brillouin boundaries. For the convenience we will call these gaps odd and even respectively.

The edges of the forbidden gaps are situated at the frequencies where different terms in these equations vanish[3]. For example, if $\rho > 0$ than $\mathrm{Re}\,(a)$ changes its sign at the low frequency boundary, Ω_-, of the first gap and the same occurs with $\mathrm{Re}\,(f)$ at the high frequency boundary, Ω_+. That is the edges of the forbidden gap satisfy the equations

$$\mathrm{Re}\,[a(\Omega_+)] = 0, \qquad \mathrm{Re}\,[f(\Omega_-)] = 0. \tag{2.48}$$

The center of the gap is situated at $\Omega_c = (\Omega_+ + \Omega_-)/2$ and its width is $\Delta_{PC} = \Omega_+ - \Omega_-$. The left and right edges of the next *odd* gap are given by $\mathrm{Re}\,(f) = 0$ and $\mathrm{Re}\,(a) = 0$, respectively, and so on. The explicit form of these equations is obtained using definitions (2.46)

$$\begin{aligned} \cos(\Omega_-\tau_+) - \rho\cos(\Omega_-\tau_-) = 0, \\ \cos(\Omega_+\tau_+) + \rho\cos(\Omega_+\tau_-) = 0. \end{aligned} \tag{2.49}$$

In the simplest case when the layers have the same optical width one has $\tau_- = 0$ and the positions of the edges of the forbidden gap are $\omega_r(1 \pm 2\arcsin(\rho)/\pi)$, where

$$\omega_r\tau_+ = \frac{\pi}{2}. \tag{2.50}$$

While this case gives a convenient reference point, however, having in mind applications to multiple quantum well structures (MQW) an opposite case, when the optical widths of the layers are different, is of more interest. Generally, as one can see from Eq. (2.49) the boundaries of the gap are situated asymmetrically with respect to ω_r and in the assumption of narrow gap, that is fulfilled for angles not too close to the angle of the total internal reflection, are given by

$$\Omega_\pm = \omega_r\left(1 \pm \frac{2\rho\sin\phi_w}{\pi(1 \pm \rho\cos\phi_w)}\right). \tag{2.51}$$

2.3.2 Multiple quantum well structure

An opposite limiting case is when all layers in the structure have the same index of refraction, n, but there are optically active excitations in the quantum wells. The propagation of light through a quantum well is described by the transfer matrix of the form

$$T_w = \begin{pmatrix} e^{i\phi_w}(1 - iS) & -iS \\ iS & e^{-i\phi_w}(1 + iS) \end{pmatrix}. \tag{2.52}$$

Here $\phi_w = \omega n d_w \cos\theta_w/c$. The excitonic contribution to the scattering of the light is described by [compare with Eq. (2.19)]

$$S = \frac{\Gamma_0}{\omega - \omega_0 + i\gamma}. \tag{2.53}$$

The radiative decay rate, Γ_0, depends on the angle of incidence. As follows from Eqs. (2.20) and (2.30) for structures with homogeneous dielectric function these dependencies for different polarizations are [32, 46, 47]

$$\Gamma_0^{(s)} = \Gamma_0/\cos\theta_w, \qquad \Gamma_0^{(p)} = \Gamma_0\cos\theta_w. \tag{2.54}$$

[3]It can be shown that if τ_+ and τ_- are commensurate then at some frequencies both terms become zero simultaneously. That is the corresponding gaps collapse and a continuity of the band establishes.

The transfer matrix through the period of the structure, thereby, is

$$T = T_b^{1/2} T_w T_b^{1/2}. \tag{2.55}$$

The parameters of the (a, f)-representation of the transfer matrix through the quantum well are

$$a = e^{i\phi_w/2}, \qquad f = e^{i\phi_w/2}(1 - iS) \tag{2.56}$$

[it is useful to compare them with those given by Eqs. (2.23)]. The dispersion equation is, thus, [48–50]

$$\cos^2\left(\frac{Kd}{2}\right) = \cos\omega\tau_+(\cos\omega\tau_+ + S\sin\omega\tau_+). \tag{2.57}$$

A straightforward application of the approach from the previous subsection is complicated by the fact that the second term in this equation has a singularity at the exciton frequency ω_0. This singularity, however, is cancelled by the first term if the condition $\cos(\omega_0\tau_+) = 0$ is met. It is seen that this condition is equivalent for the photonic half-wavelength at the exciton frequency to be equal to an odd multiplier of the period of the structure

$$\omega_0\tau_+ = \frac{\pi}{2} + \pi n \tag{2.58}$$

and is called the Bragg resonance. The spectrum of such structures is characterized by a relatively wide gap with the width

$$\Delta_\Gamma = 2\sqrt{\frac{\Gamma_0}{\tau_+}} = 2\sqrt{\frac{2\Gamma_0\omega_0}{\pi(1+2n)}} \tag{2.59}$$

indicating enhanced coupling between light and QW excitons.

2.3.3 MQW structures with a mismatch of the indices of refraction

Now, we consider the situation which is a combination of the two just analyzed. In this case we assume that quantum wells in a MQW have the index of refraction different from that of the barriers. Different aspects of this case have been considered in a number of publications [32, 33, 37, 51–54] including the polariton spectrum in such structures [32, 33]. However, here we consider this case in details since it gives perfect illustration of analysis of factorized complicate dispersion equations.

The transfer matrix for this structure is obtained from Eq. (2.55) by taking into account the scattering at the interfaces between the quantum wells and the barriers,

$$T = T_b^{1/2} T_\rho^{-1} T_w T_\rho T_b^{1/2}. \tag{2.60}$$

The dispersion equation following from the (a, f)-representation of the transfer matrix has the form

$$\cos^2\left(\frac{Kd}{2}\right) = \frac{1}{1-\rho^2}\mathrm{Re}(a_{PC})[\mathrm{Re}(f_{PC}) + S\,\mathrm{Im}(a_{PC})], \tag{2.61}$$

where a_{PC} and f_{PC} are calculated for a passive multilayer structure and are given by Eqs. (2.46).

Similarly to what we had before, the structure of the gap near the exciton frequency is complicated by the singular character of the excitonic susceptibility that compels taking into account both conditions of the existence of the gap (see Fig. 2.3). However, as one can see from Eq. (2.42) when the exciton frequency coincides with the position of the right edge of the photonic band gap

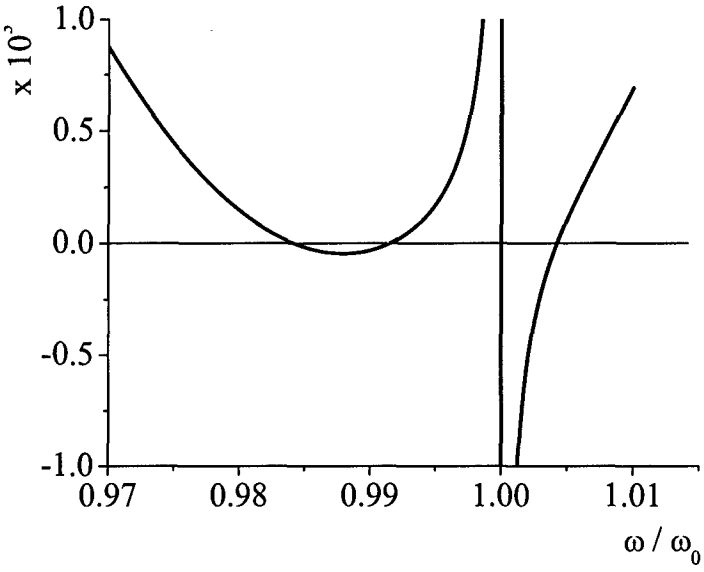

Figure 2.3: The dependence of r.h.s. of Eq. (2.61) scaled by 10^3 on frequency for slightly off-Bragg structure. The material parameters are chosen to be close to typical parameters of $GaAs/Al_xGa_{1-x}As$ structures: $\rho = 0.03$, $\Gamma_0 = 60$ μeV, $\omega_0 = 1.5$ eV.The frequencies where it is negative correspond to forbidden gaps. The vertical line shows the position of the exciton frequency. There is an additional contribution to the forbidden gap where graph exceeds 1 (not shown in this scale). This addition is given by Ω_δ, Eq. (2.71) and, as can be seen, is small.

Ω_+ the singularity of the excitonic susceptibility cancels and the only contribution to the gap is that given by being the r.h.s. of Eq. (2.61) negative.

Assuming a smallness of the gap we can expand a_{PC} and f_{PC} near the frequencies $\Omega_\pm$

$$\mathrm{Re}[a_{PC}(\omega)] = (\Omega_+ - \omega)t_+, \qquad \mathrm{Re}[f_{PC}(\omega)] = (\Omega_- - \omega)t_-, \tag{2.62}$$

and write the equation for the boundaries of the forbidden gaps in the form

$$(\omega - \Omega_+)(\omega - \Omega_-) - \Gamma_0 \frac{\mathrm{Im}(a_{PC})}{t_-} = 0, \tag{2.63}$$

where

$$t_+ = \left|\frac{d}{d\omega}\mathrm{Re}\left[a_{PC}(\omega)\right]\right|_{\Omega_+}, \qquad t_- = \left|\frac{d}{d\omega}\mathrm{Re}[f_{PC}(\omega)]\right|_{\Omega_-}. \tag{2.64}$$

In Eqs. (2.62) we explicitly have taken into account the negative sign of these derivatives. The radiative decay rate, Γ_0 in Eq. (2.63), should be taken according to the polarization of the wave and the angle of propagation as given in Eqs. (2.54).

The imaginary parts of a_{PC} and f_{PC} can be approximated using the following argument. Since

$$|a_{PC}|^2 = (1+\rho)^2 - 4\rho \sin^2\left(\omega \frac{\tau_+ - \tau_-}{2}\right) \tag{2.65}$$

and $\mathrm{Re}(a_{PC}) \sim 0$, then taking into account the narrowness of the quantum wells we obtain

$$\mathrm{Im}(a_{PC}) \approx 1 + \rho, \qquad \mathrm{Im}(f_{PC}) \approx 1 - \rho. \tag{2.66}$$

The approximation $t_- \approx \tau_+ \mathrm{Im}(f_{PC})$ can be derived using the similar reasoning.

Using these approximations the solutions of (2.63) can be found in the form

$$\omega_\pm = \Omega_c \pm \frac{1}{2}\Delta. \tag{2.67}$$

It follows that the forbidden gap is situated symmetrically with respect to the center of the *photonic* gap with the width

$$\Delta = \sqrt{\Delta_{PC}^2 + \tilde{\Delta}_\Gamma^2} \tag{2.68}$$

equal to "Pythagorean sum" of the widths of the passive photonic and the modified excitonic gaps,

$$\tilde{\Delta}_\Gamma^2 = \Gamma_0 \frac{4\mathrm{Im}(a_{PC})}{t_-} \approx \Delta_\Gamma^2 \frac{1+\rho}{1-\rho}. \tag{2.69}$$

This is important that in order to have a solid gap the exciton frequency must be situated not at the center of the gap but rather be shifted towards the higher frequencies. Comparison of the properties of the solutions of Eq. (2.63) with a consideration of MQW structures without the mismatch of the indices of refraction [55] shows that the case of the gap being solid must be identified with the Bragg resonance. That is the condition of the Bragg resonance in a MQW-based photonic crystal has the form

$$\omega_0 = \Omega_+. \tag{2.70}$$

The reason for the necessity of modification of this condition is clear. Indeed, to provide an effective optical coupling between the excitons in different quantum wells the distance between the quantum wells must be multiple of half-wavelength of the electromagnetic wave at the exciton frequency. However, in structures with a modulation of the dielectric function the dispersion relation of the waves is essentially modified in the vicinity of the boundary of a Brillouin zone [Eq. (2.47)]. Therefore, to find the wavelength of the wave at the exciton frequency it is necessary to use the dispersion law of the structure with the modulated dielectric function rather than a homogeneous one.

While the results presented have been obtained using the assumption that $\rho > 0$ (that is, for the normal propagation, $n_w > n_b$) they remain valid in the opposite case due to the symmetry of the transfer matrix under the transformations $\rho \to -\rho$ and $a_{PC} \leftrightarrow f_{PC}$. In other words, when we have the opposite relation between n_w and n_b all the arguments used above can be repeated with the mirror reflection of the frequency axis with respect to the center of the photonic gap. In particular, the Bragg resonance occurs when the exciton frequency coincides with the left (low frequency) edge of the photonic band gap.

For the case of the normal propagation, when $\rho = (n_w - n_b)/(n_w + n_b)$, these solutions were obtained in Ref. [33]. In a general case Eq. (2.69) yields the dependence of the excitonic contribution to the forbidden gap on the angle of propagation and the polarization state of the electromagnetic wave. When the angular dependence of the spectrum is considered it is necessary additionally to take into account that the position and the width of the photonic band gap depends on the angle of propagation and the polarization. Both these effects are taken into account by Eqs. (2.49) with the Fresnel coefficients given by Eqs. (2.45).

It is natural to consider two problems regarding the angular dependence of the spectrum. First one corresponds to the situation when the system is tuned to the Bragg resonance at an oblique propagation of the electromagnetic waves in the structure. The second one describes the fixed structure tuned to the Bragg resonance at normal propagation.

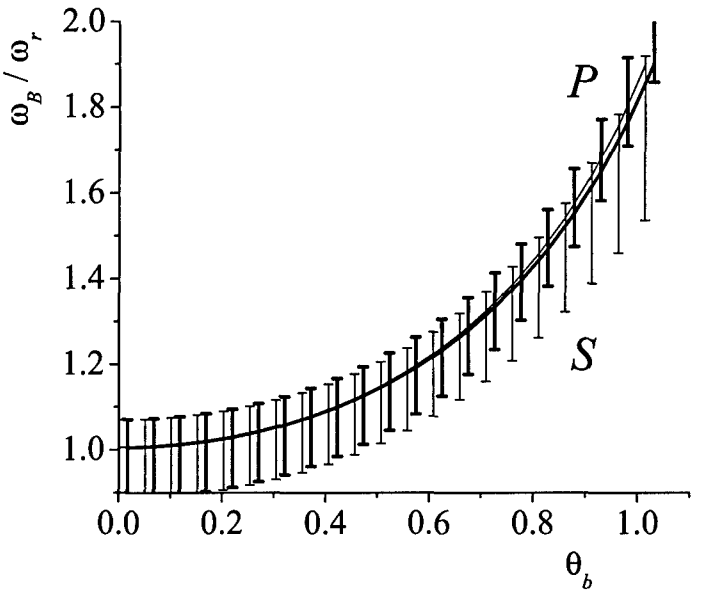

Figure 2.4: Dependence of the Bragg resonance frequency ω_B/ω_r [see Eq. (2.50)] on the angle of propagation θ_b measured in the barriers. The material parameters are the same as in Fig. 2.3. Bold and thin lines correspond to $p-$ and s-polarizations, respectively. The vertical lines (the error bars) show the forbidden gap for each polarization. For better visibility the gap is scaled by the factor of 5.

On Fig. 2.4 the dependence of the Bragg frequency on the angle of propagation is shown for both s- and p-polarizations. Due to the narrowness of the quantum wells the position of the Bragg resonance approximately follows the renormalization of the optical width of the period of the structure $\propto \cos(\theta_b)$ for both polarizations. Meanwhile, the change of the width of the gap with the angle of propagation essentially depends on the polarization. The width monotonously increases with the angle for s-polarization. For p-polarization it first, decreases, reaches its minimum at Brewster's angle, where the only contribution to the gap is due to the exciton-light interaction, and then increases. It should be noted that at Brewster's angle, found from the equation $\sin\theta_b = n_w/\sqrt{n_b^2+n_w^2}$, the Fresnel coefficient ρ_p changes its sign [it corresponds to $\theta_b \approx 0.8$ in Fig. 2.4]. Thus, the symmetry argument pointed above says that the Bragg resonance condition corresponds to coinciding the lower frequency edge of the photonic band gap for p-polarized wave.

When the exciton frequency is not tuned to Ω_+, so that $\delta = \omega_0 - \Omega_+ \neq 0$, in addition to the contributions to the gap found from the condition of being the r.h.s. Eq. (2.41) negative there is one more. It is caused by the singularity of the excitonic susceptibility and can be found looking at the frequencies where the r.h.s. of Eq. (2.42) is negative. In the same approximation as above, we find that this patch is between ω_0 and $\omega_0 + \Omega_\delta$, where

$$\Omega_\delta = \frac{\pi}{2}\tau_+\delta\tilde{\Delta}_\Gamma^2, \tag{2.71}$$

extending to the left or to the right from ω_0 depending on whether ω_0 is smaller or bigger than Ω_+. For slightly off-Bragg structures this frequency is small and in what follows we neglect this

correction to the structure of the band gap.

Thus, the gap is determined by zeros of r.h.s. of Eq. (2.41) and as the result the structure of the gap is determined by four frequencies: ω_0 and the roots of the equation

$$(\omega - \Omega_+)\left[(\omega - \Omega_-)(\omega - \omega_0) - \frac{\tilde{\Delta}_\Gamma^2}{4}\right] = 0. \tag{2.72}$$

If we put these four frequencies in ascending order the gap is determined by the first and second pairs of frequencies with a transparency window between them (see Fig. 2.3). The exact order depends on relation between ω_0 and Ω_+. If $\omega_0 < \Omega_+$ then the gap is between ω'_- and ω_0 and between Ω_+ and ω'_+, where

$$\omega'_\pm = \Omega_c + \frac{\delta}{2} \pm \frac{1}{2}\sqrt{(\Delta_{PC} - \delta)^2 + \tilde{\Delta}_\Gamma^2}, \tag{2.73}$$

while there is a window between ω_0 and Ω_+. Thus, detuning the exciton resonance frequency away from Ω_+ leads to the appearance of the transparency window between ω_0 and Ω_+ in the forbidden gap obtained before for the case $\omega_0 = \Omega_+$ and slight modification of the external edges of the gap. Taking into account Ω_δ results in shifting the edge of the window from ω_0 to $\omega_0 + \Omega_\delta$. This result is in a qualitative agreement with the analysis of off-resonant MQW structures [55] and this additionally confirms the consistency of the modification of the condition of the Bragg resonance to have the form (2.70). Moreover, now it is clear that the situation when the exciton frequency satisfies a "standard" Bragg condition actually means having a system detuned from the resonance. Such a detuning shows up as a transparency window in the forbidden gap [26] or as a dip on the reflection spectrum [54, 56, 57].

With detuning of the system away from the Bragg resonance the second question about the angular dependence of the spectrum is related. This is the situation when the system is tuned to the Bragg resonance at normal propagation, the exciton frequency and the period of the structure are fixed, and the polariton spectrum is considered for different angles of propagation. As follows from Fig. 2.4 the Bragg frequency increases with the angle of propagation and, therefore, the structure becomes detuned from the Bragg resonance. Two gaps appear separated by the transparency window. One of the gaps is adjacent to the exciton frequency and another one is detached. Fig. 2.5 shows the angular dependence of the forbidden gap for the case of s-polarization. The behavior of the detached band-gap essentially depends on polarization. For both polarizations there is a collapse of the detached gap occurring at the angle where $\Omega_+ = \omega'_+$ (slightly different for different polarizations). This collapse is a specific feature of the resonant photonic crystals and is absent in either purely passive structures or MQW. The dependence of the adjacent gap on the polarization is rather weak. This is clear from the following reasoning. A noticeable difference between the polarizations, as seen from Fig. 2.4, should appear at such angles where $\omega_B - \omega_0 \gg \tilde{\Delta}_\Gamma, \Delta_{PC}$. As follows from Eq. (2.73) the width of the adjacent gap in this case is

$$\Delta_{\text{adj}} \approx \frac{\tilde{\Delta}_\Gamma^2}{\Omega_- - \omega_0} \tag{2.74}$$

and, up to terms $\propto \Delta_{\text{adj}}\Delta_{PC}/(\omega_B - \omega_0)$, is the same for both polarizations. This weak dependence accomplished with the relation between the polariton's dispersion law and the optical properties of finite structures [54] leads to the omnidirectional reflectivity of the structures under consideration. It follows from the notion that usual scattering problem is set up for a structure embedded in a medium with essentially lower index of refraction (air or vacuum). As the result the angles of propagation inside the structure can not exceed the angle of the internal reflection θ_c at the boundary between the structure and surrounding medium. Therefore, for all angles of incidence

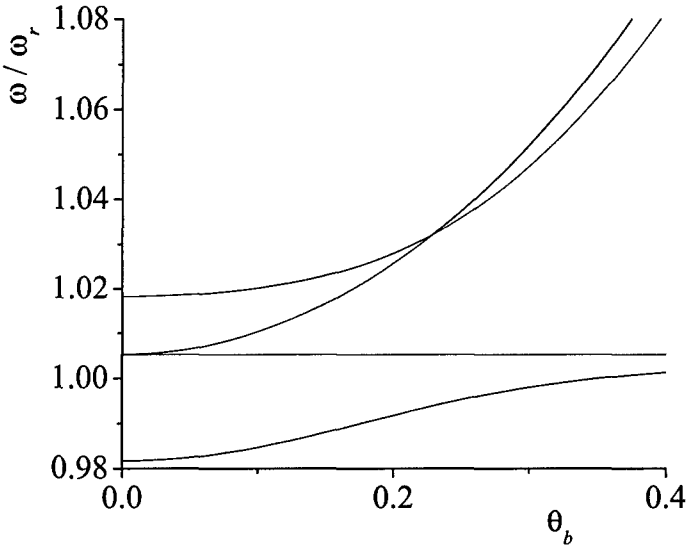

Figure 2.5: The dependence of the band-gap structure of the s-polarized wave on the angle of propagation θ_b measured in the barriers. The material parameters are the same as in Fig. 2.3. The dashed regions correspond to the forbidden gaps. The structure is assumed to be tuned to the Bragg resonance at normal propagation.

the range of frequencies between ω_0 and $\omega'_-(\theta_c)$ corresponds to the forbidden gap and, therefore, to a resonant reflection. The similar effect has been considered for the case of passive photonic crystals in a number of publications [58–61]. Here we would like to emphasize the feature specific for resonant photonic crystals. Assuming a smallness of the angle of total internal reflection (for a air-GaAs interface $\theta_c \approx 0.28$) we can describe change of the edges of the photonic band gap by a simple renormalization of the optical width of the period $\Omega_\pm \to \Omega_\pm/\cos\theta$. It results in the width of the region corresponding to the omnidirectional reflection in the form

$$\Delta_{\text{omni}} \approx \frac{1}{2}\frac{\tilde{\Delta}_\Gamma^2}{\Omega_+ \sin^2\theta_c - 2\Delta_{PC}}, \tag{2.75}$$

where we have assumed that the photonic forbidden gap is not too wide, i.e. $\Omega_+ \sin^2\theta_c > 2\Delta_{PC}$. It is seen that the presence of quantum wells essentially weakens the condition of the omnidirectionality in comparison with passive photonic crystals.

2.3.4 General modulation of the dielectric function

Using the formalism developed and the expressions for the parameters a and f obtained before [Eqs. (2.23)] we can derive the dispersion equation in the form Eq. (2.41)

$$\cos^2\left(\frac{Kd}{2}\right) = \frac{h_2'(z_+)}{W_h}\left[h_1(z_+) + Sqh_2(z_+)\right] \tag{2.76}$$

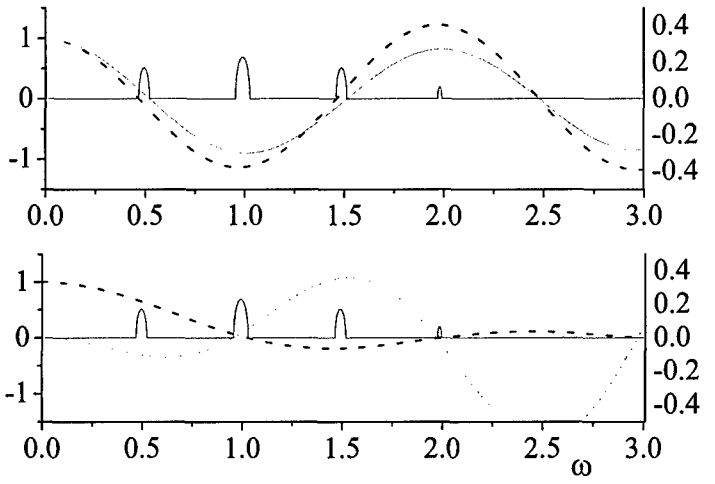

Figure 2.6: Dependence on frequency of $\mathrm{Im}(Kd)$ (solid lines, left scales) for a passive structure ($S \equiv 0$) and the boundary values of the solutions of Eq. (2.9) (right scales). The modulation of the dielectric function is chosen in such a way that $n(z) = 3 + \cos^{20}(\pi z/2d)$, for calculations the value $d = 1$ has been used. (a) $h_1(\omega)$ (dashed line), $h_2'(\omega)$ (dotted line), Kd is the solution of Eq. (2.76). (b) $h_2(\omega)$ (dashed line), $h_1'(\omega)/5$ (dotted line), Kd has been found from Eq. (2.77). Different dispersion equations give the same result, but the conditions of being r.h.s. of these equations negative determine different forbidden gaps.

or Eq. (2.42)

$$\sin^2\left(\frac{Kd}{2}\right) = -\frac{h_2(z_+)}{W_h}\left[h_1'(z_+) + Sqh_2'(z_+)\right]. \tag{2.77}$$

The dispersion equations have this form for all polarization. The only difference is using S, q and $f_{1,2}$ appropriate for particular polarization. Eqs. (2.76) and (2.77) are ready for using the general procedure. In particular, the photonic contribution to the forbidden gap is obtained by setting $\chi \equiv 0$ in Eq. (2.76), so that the frequencies $\Omega_\pm$ corresponding to the edges of the gap satisfy the equations

$$h_1(z_+, \Omega_-) = 0, \qquad h_2'(z_+, \Omega_+) = 0, \tag{2.78}$$

where $\Omega_\mp$ as arguments denote that the functions $h_{1,2}$ are solutions of corresponding homogenous equations [Eqs. (2.5) or (2.27) with $\chi \equiv 0$] when $\omega = \Omega_\mp$ respectively.

Thus the boundaries of the forbidden gap lie at points of zero of even and the maximum of odd solutions. This puts the result about the gaps in the spectrum of a photonic crystal in a perspective of the oscillating theorem about the number of zeros of an n-th eigenfunction of a Sturm-Liouville problem [62] (see Fig. 2.6). In Eqs. (2.78) we implicitly assumed that the odd solution reaches the maximum at a frequency which is bigger than that where the even solution vanishes. Of course, the exact answer depends on details of the modulation of the dielectric function. This assumption is true for such $\epsilon(z)$ that monotonously decreases, for $z > 0$, from the position of the quantum well up to the boundary of the elementary cell and this is enough for our consideration here.

The analysis of the full dispersion equations repeats the one provided in the previous subsection, with the substitutions $a_{PC} = g_2$ and $f_{PC} = g_1$. In particular, the parameters, $t_\pm$, of the

equation for the boundaries of the forbidden gap, Eq. (2.63) are defined in terms of boundary values of $f_{1,2}$ as

$$t_- = \frac{1}{\sqrt{W_h}}\left|\frac{\partial h_1(\Omega_-)}{\partial\omega}\right|, \qquad t_+ = \frac{1}{\sqrt{W_h}}\left|\frac{\partial h_2'(\Omega_+)}{\partial\omega}\right|. \tag{2.79}$$

Following the outlined procedure we immediately obtain the necessity of the modification of the Bragg resonance obtained before for the case of a piece-wise constant modulation of the dielectric function. In order to have a solid forbidden gap, the singularity of the excitonic susceptibility at the exciton frequency must be cancelled by the first term $f_2'(z_+)$ in Eq. (2.76). This corresponds to coinciding of the exciton frequency and the high frequency boundary of the photonic gap, Ω_+. Eqs. (2.78) prove the representation of the Bragg resonance condition in terms of the effective optical width of the period of the structure, $\tilde{\phi}$, defined by Eq. (3.16) (see Chapter 3). At the point where $f_2' = 0$ one has $a/\bar{a} = -1$ yielding $\tilde{\phi}(\Omega_+) = \pi$. This allows one to write down the Bragg condition in the form similar to what one has in the case of pure MQW structure, $\tilde{\phi}(\omega_0) = \pi$. This form is convenient for practical calculations.

The second result is the width of the forbidden gap in the case of the Bragg resonance. Performing the expansion similar to Eqs. (2.62) we can obtain the equation for boundaries of the forbidden gap

$$(\omega - \Omega_+)\left(\omega - \Omega_- - \frac{\tilde{\Delta}_\Gamma^2/4}{\omega - \omega_0}\right) = 0, \tag{2.80}$$

with $\tilde{\Delta}_\Gamma^2$ given by the first part of Eq. (2.69). The analysis of Eq. (2.80) completely repeats that of Eq. (2.63). In particular the width of the forbidden gap is determined by the Pythagorean sum of the photonic and excitonic contributions

$$\Delta^2 = \Delta_{PC}^2 + \tilde{\Delta}_\Gamma^2, \tag{2.81}$$

where $\Delta_{PC} = |\Omega_+ - \Omega_-|$. The relation between the parameters a_{PC} and f_{PC} and the solutions of corresponding differential equations allows us to express the renormalization of the excitonic contribution to the forbidden gap in terms of a quantity having a direct physics sense. Using the standard procedure of differentiating of a solution of a differential equation with respect to parameter one obtains for s- and p-polarizations

$$\left(\frac{\tilde{\Delta}_\Gamma}{\Delta_\Gamma}\right)^2 = \frac{\pi c^2 q_s W_h}{4\Omega_-\omega_0 u_s^{(1)}}, \quad \text{and} \quad \left(\frac{\tilde{\Delta}_\Gamma}{\Delta_\Gamma}\right)^2 = \frac{\pi c^2 q_p W_h p(z_+)}{4\Omega_-\omega_0 u_p^{(1)}}, \tag{2.82}$$

respectively. Here we have introduced

$$u_{s,p}^{(1)} = \frac{1}{2}\int dz\, \epsilon(z)\mathbf{E}_{s,p}^{(1)2}, \tag{2.83}$$

where $\mathbf{E}_{s,p}^{(1)}$ is the s- and p-polarized electric fields corresponding to the even mode of the photonic crystal. Eq. (2.82) describes the effect of the modulation of the dielectric function on the exciton contribution to the exciton-polariton spectrum. First, as could be expected, only even mode of the photonic crystal contributes to the exciton-photon interaction and, second, the modification can be estimated to be proportional to $u_{qw}^{(1)}/u^{(1)}$, where $u_{qw}^{(1)}$ and $u^{(1)}$ are the energies of the even mode of the photonic crystal in the quantum well and the whole elementary cell, respectively. This means that the modification of the exciton-light interaction depends on the distribution of the electric field inside the elementary cell at the frequency corresponding to Ω_-. If the electric field is pushed out of the center of the elementary cell, i.e. the quantum well, then the excitonic effects are reduced and vice versa.

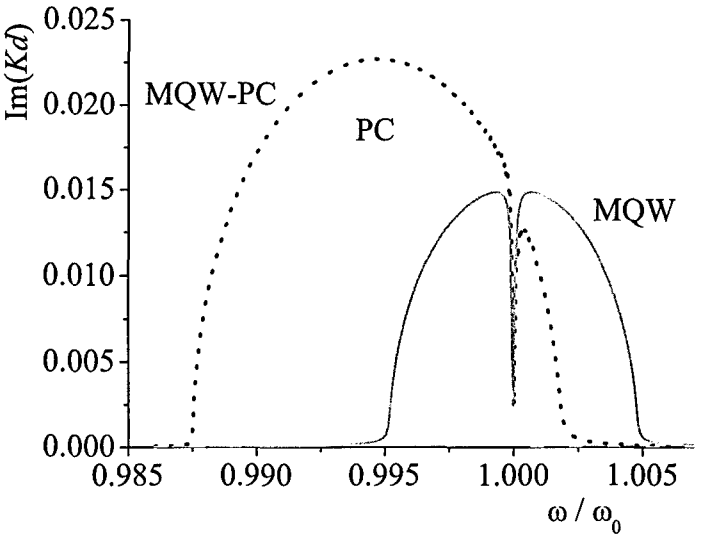

Figure 2.7: Dependence of $\mathrm{Im}(Kd)$ on frequency for different structures in a vicinity of the first forbidden gap when the exciton homogeneous broadening is taken into account. Dashed line represents the passive structure from Fig. 2.6. Solid line shows a Bragg-MQW structure with a homogeneous dielectric function. Dotted line represents the structure with combination of quantum wells and the smooth modulation of the dielectric function. The characteristic feature is a divergence of the penetration length $(\mathrm{Im}\, K)^{-1}$ at the exciton frequency.

Consideration of off-Bragg structures is exactly the same as in Section 2.3.3 with the same main results. Therefore, we do not repeat it here. We supplement the analysis provided in the previous subsection by a discussion of an effect of homogeneous broadening on the spectrum of the exciton polaritons. We assume that the only source of the dissipation of the energy of the electromagnetic wave is a broadening of the exciton line. In the presence of losses the conception of band gaps becomes ill-defined because the imaginary part of the Bloch wave-number, generally speaking, is not zero at all frequencies. Therefore it is necessary to consider directly solutions of Eq. (2.76). Representing Kd in the form

$$Kd = \pi + i\lambda \tag{2.84}$$

and assuming a smallness of λ we can write

$$\lambda^2 = 4t_+t_-(\Omega_+ - \omega)\left(\omega - \Omega_- - \frac{\tilde{\Delta}_\Gamma^2/4}{\omega - \omega_0 - i\gamma}\right). \tag{2.85}$$

As one can see from this expression λ vanishes at the frequency corresponding to the right edge of the photonic band gap. The similar effect of divergence of the penetration length of polaritons in media with homogeneous broadening takes place in MQW [55] structures without the contrast. The important difference, however, is that in the latter case it happens at the exciton frequency that lies at the center of the forbidden gap. Fig. 2.7 shows the comparison of the solutions of the dispersion equation for different structures with taken into account the exciton homogenous broadening.

To complete the consideration of the exciton polaritons in the resonant photonic crystals let us briefly discuss the dispersion law $\omega(K)$ of the polaritons near frequencies corresponding to the

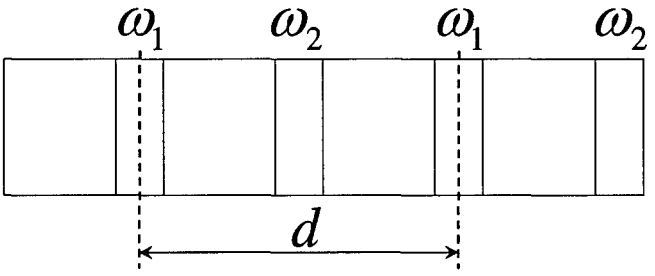

Figure 2.8: The periodic structure with two quantum wells (dark rectangulars) in the elementary cell. Dash lines show the boundaries of an elementary cell having the mirror symmetry. The quantum well with the exciton frequency ω_2 is assumed to have the index of refraction different from other elements of the structure.

band edges. The polariton's dispersion law can be obtained resolving Eq. (2.76) with respect to ω. In the case of the Bragg resonance it reduces to a quadratic equation with the solutions

$$\omega_{\pm}(K) = \Omega_c \pm \frac{1}{2}\sqrt{\Delta^2 + \zeta^2(K - K_B)^2}, \tag{2.86}$$

where $K_B = \pi/d$ is the Bloch wave-number corresponding to the boundary of the first Brillouin zone and $\zeta = d/t_+t_-$. These two branches with positive and negative masses, $m_{\pm} = \pm 2\hbar^2\Delta/\zeta^2$, lie in the bands that are above and below the forbidden gap, respectively. In addition to these branches there is one more dispersionless branch at the exciton frequency $\omega_B(K) = \omega_0$.

Let now the system be detuned from the Bragg resonance with the parameter of the detuning $\delta = \omega_0 - \Omega_+$. If the detuning is not too big, $|\delta| \lesssim \tilde{\Delta}_\Gamma$, it leads to only a slight modification of the polariton branches (2.86). In particular, the magnitudes of their masses are little bit different in this case

$$m_{\pm}(\delta) = m_{\pm}\left(1 - \frac{\Delta_{PC}\delta}{\Delta^2} \pm \frac{2\delta}{\Delta \mp \Delta_{PC}}\right). \tag{2.87}$$

Near the band edges the dispersion laws of these branches become $\omega_{\pm}(K) = \omega'_{\pm} + \hbar^2(K - K_b)^2/2m_{\pm}$, where $\omega'_{\pm}$ are given by Eq. (2.73).

What is more important is that the third branch acquires the dispersion

$$\omega_B(K) = \Omega_+ + \frac{\zeta^2\delta}{\tilde{\Delta}_\Gamma^2}(K - K_B)^2. \tag{2.88}$$

That is the mass of the third branch (the braggaritons [26]) becomes finite in the off-Bragg structures $m_B = \hbar^2\tilde{\Delta}_\Gamma^2/2\zeta\delta$. Let us note that the extremum point of the dispersion curve lies at Ω_+ and the mass of the braggaritons, particularly its sign, depends on the parameter of detuning.

2.3.5 MQW structures with complex elementary cells

Here we illustrate the application of the developed technique to structures with complex elementary cells studied in Ref. [33]. We consider only one particular example when the elementary cell contains two quantum wells half-period apart and these quantum wells differ by the value of the exciton frequency, ω_1 and ω_2 (see Fig. 2.8). One of the interesting results obtained in Ref. [33]

for such structures was that the condition of having a solid gap involves all excitonic frequencies in the system. That is, this is *not* enough just to tune the period of the system according to, for example, the mean value of the frequencies. It is necessary to have the special separation between the frequencies. Second, at the same value of the period as Bragg MQW structure with a simple cell it turns out to be possible to increase the effective interaction between excitons and photons by the factor of $\sqrt{2}$. More formally, this is expressed by the fact that the half-width of the forbidden gap for such structures is

$$\Delta_{CS} = \sqrt{2}\Delta_{\Gamma}. \tag{2.89}$$

This eventually means that it is possible to increase the exciton-photon interaction thanks to increasing density of quantum wells in the structure. However, special conditions on the exciton frequencies must be imposed, while "random" rearrangement of the quantum wells will most likely lead to a crumbly structure of the forbidden gap and, as the result, to a complicated and rather not favorable optical spectra.

Here we would like to consider the effect of the mismatch of the indices of the refraction on the spectral properties of such structures. For this purposes we consider a simple case when all elements of the structure, except the wells with the exciton frequency ω_2, have the same exciton frequency. Formally, the dispersion equation for such structure in the case of normal propagation has been obtained in Ref. [33] by more conventional methods, but that equation turned out to be too cumbersome to allow non-numerical analysis.

To apply the technique developed in the present paper it is necessary to choose the elementary cell with the explicit mirror symmetry. It can be done as shown in Fig. 2.8. The problem of writing the transfer matrices through the right and left halves of the quantum well can be resolved in the following way. We note that the quantum well transfer matrix T_w determined by Eq. (2.52) can be written in a factorized form

$$T_w = T_b(\phi_w/2)\tilde{T}_w T_b(\phi_w/2), \tag{2.90}$$

where $\tilde{T}_w$ is derived from the expression for T_w by setting $\phi_w = 0$. Using this factorization the transfer matrix through the elementary cell can be written in the form similar to Eq. (2.34)

$$T = \sqrt{\tilde{T}_w^{(1)}}\, T_b(\phi_b + \phi_w/2)\, T_\rho^{-1} T_w^{(2)}\, T_\rho T_b(\phi_b + \phi_w/2)\, \sqrt{\tilde{T}_w^{(1)}}. \tag{2.91}$$

The difference between the indices of refraction is taken into account by introduction corresponding Fresnel coefficient entering T_ρ. The transfer matrices through different quantum wells $T_w^{(1,2)}$ are obtained from Eq. (2.52) by substitution of the different excitonic susceptibilities

$$S_{1,2} = \frac{\Gamma_0}{\omega - \omega_{1,2} + i\gamma}. \tag{2.92}$$

The square root $\sqrt{\tilde{T}_w^{(1)}}$ can be found to be

$$\sqrt{\tilde{T}_w^{(1)}} = \begin{pmatrix} 1 - iS_1/2 & -iS_1/2 \\ iS_1/2 & 1 + iS_1/2 \end{pmatrix}. \tag{2.93}$$

Now, we can apply Eqs. (2.35), (2.36) and (2.37) to derive (a, f)-representation for T. The dispersion equation following from this representation has a relatively simple form

$$\cos^2\left(\frac{Kd}{2}\right) = \frac{1}{1-\rho^2}\left[\mathrm{Re}(a) + S_1\,\mathrm{Im}(a)\right]\left[\mathrm{Re}(b) + S_2\,\mathrm{Im}(b)\right], \tag{2.94}$$

where $a = \exp(i\phi_+) - \rho\exp(i\phi_-)$, $b = \exp(i\phi_+) + \rho\exp(i\phi_-)$ [compare with Eqs. (2.46)], and $\phi_\pm = \omega(2d_b n + d_w n \pm d_w n_2)/2c$. Comparison with Eq. (2.61) shows that Eq. (2.94) is proportional to the product of dispersion equations for MQW structures with a mismatch of indices of refraction considered in details in Subsection 2.3.3. This fact makes it reasonable to interpret this equation as an interaction of polariton branches in different sublattices.

It is seen that the structure of the forbidden gap is determined by six characteristic frequencies where r.h.s. of Eq. (2.94) changes its sign, so that, generally, the gap has two transparency windows. This makes the analysis of the equation somewhat long but straightforward. We restrict ourselves to detailed consideration of the resonant case when the solid forbidden gap is formed. As we already know from previously considered examples the solid gap is formed when the exciton frequencies coincide with one of characteristic frequencies of the system without the corresponding excitonic contribution. Such frequencies in the case under consideration are the boundaries of the polariton branches. Let for concreteness one have $\omega_2 > \omega_1$, then for a solid gap to form ω_1 should fall to the low-frequency boundary of the second branch gap and ω_2 should coincide with high-frequency boundary of the first branch gap.

Let us denote these frequencies by $\omega_{1,2}^{\pm}$. The lower index shows which branch we consider and $\pm$ denotes high- and low-frequency boundaries, respectively. The frequencies $\omega_{1,2}^{\pm}$ are determined by

$$\begin{aligned} \omega_1^{\pm} &= \frac{1}{2}(\omega_1 + \Omega_-) \pm \frac{1}{2}\sqrt{(\omega_1 - \Omega_-)^2 + \Delta_\Gamma^2}, \\ \omega_2^{\pm} &= \frac{1}{2}(\omega_2 + \Omega_+) \pm \frac{1}{2}\sqrt{(\omega_2 - \Omega_+)^2 + \Delta_\Gamma^2}, \end{aligned} \tag{2.95}$$

where $\Omega_\mp$ are determined by Eqs. (2.49), and, for simplicity, we assumed the same value of the effective exciton-light interaction for both branches, i.e. we have neglected possible difference between the exciton radiative decay rates in different wells and have neglected the renormalization of Γ_0 due to the spatial modulation of the dielectric function [see Eqs. (2.69) and (2.82)]. The generalization is straightforward but leads to nothing new except cumbersome expressions.

Let us, first, consider the case when the index of refraction of the wells of the second type is higher, i.e. $\rho > 0$. The condition of absence of transparency windows inside the gap (the Bragg resonance condition) is formulated as $\omega_1^+ = \omega_2$ and $\omega_2^- = \omega_1$. Resolving these equations with respect to the exciton frequencies one obtains

$$\omega_0 = \Omega_c, \qquad \delta = \frac{1}{2}\left(\sqrt{2\Delta_\Gamma^2 + \Delta_{PC}^2} - \Delta_{PC}\right), \tag{2.96}$$

where ω_0 and δ are determined by $\omega_{1,2} = \omega_0 \mp \delta/2$. Substitution of found relations into the expression for the width of the gap $\Delta = \omega_2^+ - \omega_1^-$ gives familiar result

$$\Delta = \sqrt{\Delta_{CS}^2 + \Delta_{PC}^2}. \tag{2.97}$$

The opposite relation between the indices of refraction can be considered using transformation $\Delta_{PC} \to -\Delta_{PC}$. It changes the Bragg condition [the second equation of Eqs. (2.96)] but leaves the width of the gap (2.97) the same.

Thus, taking into account the mismatch of the indices of refraction in the system with complex elementary cell leads to modification of the Bragg condition in comparison with what one has in the case of absent mismatch. This modification has a different character then in structures with a simple cell. The mean value of the exciton frequencies stays at the center of the forbidden gap and only the difference between the frequencies must be corrected to take into account the mismatch. The resultant gap is, as well as in the case of simple cell, again the Pythagorean sum of the photonic and the excitonic contributions.

2.4 The effect of a complex structure of the exciton states

In the previous Section we essentially use the (a, f)-representation of the transfer matrix. As has been discussed the necessary condition of existence of the (a, f)-representation is the mirror symmetry of the elementary cell. It should be noted that such symmetry is a property of two characteristics of the medium, the modulation of the dielectric function and the profile of the exciton wave function. The symmetry of the dielectric function is specified during the growing process and can be considered fixed. The symmetrical properties of the exciton wave function are the consequences of those of the confining potential and can be relatively easy changed. For example, one of the possible applications of multiple quantum well structures is related to the possibility of the tuning the exciton frequency using the quantum confined Stark effect [63–65]. The applied electric field obviously breaks the mirror symmetry of the potential and as the result the exciton wave function does not have a definite parity.

Another deviation from the situation considered in the previous sections is a multilevel property of the exciton levels. Generally, the different exciton states, $1s$, $2s$ and so on, either have energies well separated from each other (in comparison with the width of the gap Δ) or have small oscillator strength. As the result, in a vicinity of a particular exciton frequency the contributions of other exciton states are negligibly small. However, in specially engineered structures the situation can be completely different. As an example let us consider structures with two identical quantum wells in the elementary cell. If the wells are sufficiently close to each other then the hybridization of the exciton in these wells leads to splitting of the exciton level with the value of the split determined by the distance between the wells.

All these deviations lead to changes of the picture of the exciton polariton spectrum in comparison with that established above. A complete analysis of these changes requires a special approach different from used above. In present Section we briefly consider the effect of a non-trivial structure of the exciton states on the polariton spectrum in cases when this effect is in some sense small. We will consider explicitly the case of an s-polarized electromagnetic wave. Using the results of Section 2.1 a similar analysis of the case of the p polarization can be provided.

2.4.1 The transfer matrix and the dispersion equation

When the mirror symmetry is absent the transfer matrix does not have the property $T_{21} = -T_{12}$ (see Section 2.2). As the result the transfer matrices can not be represented in the form (2.22). However, the basic steps to obtain the transfer matrix remain the same. The only difference is the form of the exciton contribution to the polarization $\mathbf{P}_{exc}$ because of existence of multiple exciton levels. The interaction of light with each exciton state is given by Eq. (2.2). Thus, to obtain the total polarization one has to sum all these contributions. This gives

$$\mathbf{P}_{exc} = \sum_{\ell} \chi_{\ell} \sum_{m} \Phi_m^{(\ell)}(z) \int dz' \, \overline{\Phi_m^{(\ell)}}(z') \mathbf{E}_{\perp}(z'), \tag{2.98}$$

where the index m runs over all quantum wells in the structure and the index ℓ accounts the exciton states. The interaction of light with the ℓ-th exciton state is specified by the projection of the electric field on the wave function of the ℓ-th state $\Phi_m^{(\ell)}(z)$ and the corresponding susceptibility $\chi_{\ell} = \alpha_{\ell}/(\omega_{\ell} - \omega + \gamma_{\ell})$. The latter is conveniently represented by a diagonal matrix $\widehat{\chi}$ (below the hat is used to denote a matrix in the "space" of the exciton states) with the matrix elements $\widehat{\chi}_{\ell\ell'} = \delta_{\ell\ell'}\chi_{\ell}$. In Eq. (2.98) and in what follows the bar denotes the complex conjugation. We provide formulas with generally complex exciton wave functions to resolve the problem of transformation properties of main quantities under the unitary transformation of the exciton states.

The derivation of the transfer matrix follows the same steps as in Section 2.1. In the basis of the functions $h_{1,2}$ one has

$$T_h = \mathbf{1} + 2q \begin{pmatrix} -S_{12} & -S_{22} \\ S_{11} & S_{21} \end{pmatrix}, \tag{2.99}$$

where $S_{ij} = -2\pi\omega^2 \operatorname{Tr}(\widehat{\widetilde{\chi}}\widehat{\varphi}_{ij})/qc^2W_h$. Here we introduced the matrices $\widehat{\varphi}_{ij}$, the tensor products of the vectors

$$\varphi_i^{(\ell)} = \frac{1}{\sqrt{W_h}} \int dz\, \Phi^{(\ell)}(z) h_i(z), \tag{2.100}$$

with the elements $(\widehat{\varphi}_{ij})_{\ell\ell'} = \overline{\varphi_i^{(\ell)}}\varphi_j^{(\ell')}$. The effective susceptibility $\widehat{\widetilde{\chi}}$ in Eq. (2.99) is found to be

$$\widehat{\widetilde{\chi}} = \sqrt{\widehat{\chi}} \frac{1}{\mathbf{1} + \frac{4\pi\omega^2}{c^2}\sqrt{\widehat{\chi}}\widehat{\mathcal{G}}\sqrt{\widehat{\chi}}} \sqrt{\widehat{\chi}}, \tag{2.101}$$

where the matrix $\widehat{\mathcal{G}}$ has the elements

$$\widehat{\mathcal{G}}_{\ell\ell'} = \int dz\, \overline{\Phi^{(\ell)}}(z)(G \star \Phi^{(\ell')})(z). \tag{2.102}$$

The transfer matrix in the basis of the plane waves can be obtained using mapping (A.9).

We would like to discuss a general structure of the effective susceptibility. As well as in the one-level case one has a radiative shift of the exciton frequency. In addition to this $\widehat{\widetilde{\chi}}$ has off-diagonal elements which lead to a weak radiative mixing of the exciton levels [see below Eqs. (2.108) and (2.110)]. It is convenient to separate the diagonal and the off-diagonal parts of $\widehat{\mathcal{G}}$ writing the latter as $\widehat{\mathcal{G}} = \widehat{\mathcal{G}}_d + \widehat{\mathcal{G}}_o$ (clearly only the symmetric part of $\mathcal{G}$ contributes to $\widehat{\mathcal{G}}_d$). Using this representation the effective susceptibility (2.101) can be approximated by

$$\widehat{\widetilde{\chi}} \approx \widehat{\sigma} - \frac{4\pi\omega^2}{c^2}\widehat{\sigma}\widehat{\mathcal{G}}_o\widehat{\sigma}, \tag{2.103}$$

where the diagonal matrix $\widehat{\sigma}$ takes into account the radiative shifts of the exciton levels

$$\widehat{\sigma} = \frac{1}{\widehat{\chi}^{-1} + \frac{4\pi\omega^2}{c^2}\widehat{\mathcal{G}}_d}. \tag{2.104}$$

For usual long-period MQW structures both the radiative shift of the exciton resonant frequency and the off-diagonal part of the effective susceptibility are small. The smallness of latter is provided by the narrowness of the quantum wells, so that $\varphi_2^{(\ell)}$ are small. The radiative shift (and the whole symmetric part of $\widehat{\mathcal{G}}$) is small for narrow quantum wells because of the same reasoning and also because of the fact that for narrow quantum wells the terms $h_2(z_1)h_1(z_2)$ and $h_2(z_2)h_1(z_1)$ are close. To these arguments it should be added that if the difference between the energies of the exciton levels is bigger than the width of exciton related peculiarities in the polariton spectrum then the off-diagonal part of the effective susceptibility is additionally subsided by the factor $\propto |\omega_\ell - \omega_{\ell'}|^{-1}$. It should be noted, thereupon, that the situation can be different in special MQW structures. For example, in mentioned above structures with two sufficiently close quantum wells in the elementary cell. In such structures the off-diagonal part of the effective susceptibility becomes essential.

The dispersion equation following from the transfer matrix can be written in the form

$$\cos^2\left(\frac{Kd}{2}\right) = \frac{1}{W_h}(h_1 + S_{11}qh_2)(h_2' - S_{22}qh_1') + \frac{h_1'h_2}{W_h}S_{21}S_{12} + \frac{h_2'h_1}{2W_h}(S_{21} - S_{12}). \tag{2.105}$$

It is seen that if the exciton wave function has a definite symmetry (either odd or even with respect to the center of the elementary cells) $S_{12,21} \equiv 0$ and an equation with the structure of Eq. (2.76) is restored. It should be noted that the absence of the mirror symmetry itself does not imply an impossibility to factorize the dispersion equation. However, it can be shown that generally the factorization can not be done similarly to Eq. (2.76), i.e. in terms of a linear combination of the boundary values of the linearly independent solutions of the corresponding Cauchy problems.

2.4.2 Single-level excitonic susceptibility

First we consider the simplest case when there is only single exciton level interacting with light but the corresponding wavefunction does not have definite symmetry, i.e. for even and odd h_1 and h_2 both projections $\varphi_{1,2}$ do not turn to zero. In this case the dispersion equation can be simplified noting that $S_{ij} = \tilde{\chi} 2\pi\omega^2 \varphi_i \varphi_j / qc^2 W_h$ [see also Eq. (2.15)] where $\tilde{\chi}$ is given by Eq. (2.12).

Let us assume that the non-symmetricity of the wave function is small as it takes place, for example, in structures placed in a uniform electric field. To emphasize this circumstance the dispersion equation is convenient to write down in the form

$$\cos^2\left(\frac{Kd}{2}\right) = \frac{h_2'}{W_h}(h_1 + S_{11} q h_2) - \frac{h_1}{W_h} h_1' S_{22} q. \tag{2.106}$$

As follows from this equation the non-symmetricity is quantified by $\Delta_a^2 = \alpha 2\pi\omega_0^2 \varphi_2^2 / qc^2$ [compare with Eqs. (2.69) and (2.20)]. So that the smallness can be understood as $\Delta_a \ll \tilde{\Delta}_\Gamma$.

It is clear that because of the absence of the mirror symmetry the optimal coupling between the excitons localized in different quantum wells can not be provided by the modes of the photonic crystal at an edge of the forbidden gap, i.e. with $K = K_B$. Instead, the states inside the band should be involved. Indeed, as follows from Eq. (2.106) the condition of the Bragg resonance in this case has the form

$$\omega_0 = \Omega_+ + \frac{\Delta_a^2}{4} \frac{\Delta_{PC}}{(\Omega_+ - \omega_-)(\omega_+ - \Omega_+)}, \tag{2.107}$$

where the frequencies $\omega_\pm$ are determined by Eq. (2.67). When this condition is fulfilled there is a solid gap in the polariton spectrum with the width of the gap reduced in comparison with the symmetric case by the value $\sim \Delta_a^2/\Delta$.

2.4.3 Multilevel excitonic susceptibility

If the exciton states can be characterized by a definite parity then, as follows from the expression for the effective susceptibility, Eq. (2.103), the multilevel structure of the excitonic susceptibility leads to multiple poles of the function $S(\omega)$ in the dispersion equation (2.76). The main consequence of having several poles is that generally speaking the polariton gap has at least one transparency window. Changing the period of the structure one can cancel a peculiarity at most one resonant frequency by placing it at the high-frequency boundary of the photonic gap. The complete cancellation of the resonances in r.h.s. of Eq. (2.76) requires a special relation between the oscillator strengths corresponding to different resonances which is quite improbable in a general case.

More interesting situation appears when the different exciton levels correspond to the wave functions with different parity. In this case the effective susceptibility has non-zero off-diagonal part what leads to an optical mixing of the exciton states. To emphasize this effect we consider the case when only two exciton levels characterized by the frequencies $\omega_{1,2}$ (already modified by the radiative shifts) are involved. In this case the effective susceptibility can explicitly be written down

in a relatively simple form

$$\widehat{\widetilde{\chi}} = \frac{1}{\eta - (\omega-\omega_1)(\omega-\omega_2)} \begin{pmatrix} \alpha_1(\omega-\omega_2) & \frac{4\pi\omega^2}{c^2}\alpha_1\alpha_2\widehat{\mathcal{G}}_{12} \\ \frac{4\pi\omega^2}{c^2}\alpha_1\alpha_2\widehat{\mathcal{G}}_{21} & \alpha_2(\omega-\omega_1) \end{pmatrix}, \tag{2.108}$$

where $\alpha_{1,2}$ are the coupling parameters between light and corresponding exciton states, $\widehat{\mathcal{G}}_{12,21}$ are the matrix elements of $\widehat{\mathcal{G}}$ given by Eq. (2.102) and the mixing parameter η is defined as

$$\eta = \widehat{\mathcal{G}}_{12}\widehat{\mathcal{G}}_{21}\alpha_1\alpha_2\left(\frac{4\pi\omega^2}{c^2}\right)^2. \tag{2.109}$$

We also assume that each level has a definite parity, namely, the state 1 is even and the state 2 is odd. As the result, only two of the parameters $\varphi_i^{(\ell)}$ are not zero, $\varphi_1^{(1)}$ and $\varphi_2^{(2)}$. Substitution of the effective susceptibility into Eq. (2.105) gives the dispersion equation

$$\cos^2\left(\frac{Kd}{2}\right) = \frac{h_2'}{W_h}(h_1 + S_1 q h_2) - \frac{h_1}{W_h}S_2 q h_1' + \frac{(h_1h_2)'}{W_h}S_{12}q, \tag{2.110}$$

where

$$\begin{aligned} S_{1,2} &= \alpha_{1,2}\left(\varphi_{1,2}^{(1,2)}\right)^2 \frac{2\pi\omega^2}{c^2}\frac{\omega-\omega_{2,1}}{(\omega-\omega_1)(\omega-\omega_2)-\eta}, \\ S_{12} &= \alpha_1\alpha_2\varphi_1^{(1)}\varphi_2^{(2)}\left(\frac{2\pi\omega^2}{c^2}\right)^2 \frac{\widehat{\mathcal{G}}_{12}-\widehat{\mathcal{G}}_{21}}{(\omega-\omega_1)(\omega-\omega_2)-\eta}. \end{aligned} \tag{2.111}$$

Without going into a detailed technical analysis of the polariton spectrum in this case let us note the most interesting feature of Eq. (2.110). If one formally neglects terms $\propto \varphi_2^{(2)}$ in this equation the spectrum turns to that one has in the case of a multilevel excitonic susceptibility discussed above. The important difference is that the exciton peculiarities are situated at the frequencies ω_s and ω_a which are determined by zeros of the denominator in Eq. (2.111). These frequencies have a structure of a result of an additional interaction between the exciton states induced by the electromagnetic wave. This interaction with the intensity $\propto \sqrt{\eta}$ repels the exciton levels (if $\eta > 0$) or brings them closer to each other (if $\eta < 0$). However, the interaction of the excitons with an electromagnetic wave does not lead to a modification of the actual exciton levels because this interaction enters as a source in the exciton Shrödinger equation (see e.g. Ref. [8]). Thus, the change of the resonant frequencies is the effect of the same nature as the usual radiative shift of the exciton frequency [Eq. (2.13)]. We would like to note that the optical mixing disappears if the exciton wave functions do not overlap. It can be shown using the fact that in this case by an appropriate unitary transformation one of the matrix elements $\widehat{\mathcal{G}}_{12,21}$ can be turned to zero implying $\eta \equiv 0$. In this connection the resonance frequencies $\omega_{q,b}$ should be defined without a reference to a particular form of the matrix elements of the effective susceptibility. It can be shown, however, that these frequencies correspond to poles of $\det\widehat{\widetilde{\chi}}$ which are not altered by unitary transformations.

To conclude the consideration of the effect of the complex structure of the exciton levels on the polariton spectrum we would like to note that a distinction should be made between the structures with coupled quantum wells in the elementary cell and structures with a complex elementary cells (see Refs. [33, 66, 67] and also Section 2.3.5). The first are characterized by the hybridized exciton states i.e. the electromagnetic wave interacts with the exciton localized over both quantum wells. In the structures with the complex elementary cell the excitons are localized in their own quantum wells. The different microscopical pictures of the exciton states lead to the different form of the exciton contributions to the polarization in the Maxwell equations (2.5) and, eventually, to

different features of electromagnetic waves propagating through the structures. In particular, in the structures with the complex elementary cell the effective exciton susceptibility remains diagonal after transition to a pair of non-overlapping wave functions and therefore there is no the radiative mixing of the exciton levels.

2.5 Discussion

This technique developed in the present Chapter has two key features. First of all this is a relation between the parameters of the representation and solutions of appropriate Cauchy problems. It relates results regarding properties of solutions of the differential equations and the spectral properties. In particular, it puts the result about the forbidden gaps in the perspective of the oscillating theorem. We would like to emphasize that this relation automatically establishes the correctness of a problem of propagation of electromagnetic waves in 1D structures with dispersion and absorbtion. In particular, it makes it possible to avoid the question about eigenmodes of the system (which are well defined only when the operator governing the spatial distribution of the electric field is self-adjoint) and still obtain all necessary information for an analysis of optical and spectral properties of the system. This relation sets up a complete framework for description of 1D systems.

The second feature is a special representation of the transfer matrix for structures with an elementary cell possessing mirror symmetry. This representation yields the dispersion equation in a factorized form. It drastically simplifies the analysis of the spectrum.

Thus, these two features open a number of problems for a detailed constructive analysis. In addition to the questions considered in the present Chapter these are reflection and transmission properties of finite structures (see Chapter 3), excitation of the field by external sources such as embedded excited atoms or radiative exciton recombination (see Chapter 4), polariton density of states and other. We also believe that the constructed general setup allows one to apply the results obtained for more complicated systems, e.g. quantum graphs [68, 69].

Chapter 3

Optics of finite structures

3.1 Single quantum well in a dielectric environment

It is constructive to start an analysis from consideration of a simple case of a single quantum well in a dielectric environment. We consider the situation when the indices of refraction of the well and the surrounding barriers are n_w and n_b respectively. Using the usual Maxwell boundary conditions the transfer matrix through one period of the structure in the basis of incoming and outgoing plane waves can be written in the form

$$T = T_b^{1/2} T_{bw} T_w T_{wb} T_b^{1/2}, \tag{3.1}$$

where

$$T_b^{1/2} = \begin{pmatrix} e^{i\phi_b/2} & 0 \\ 0 & e^{-i\phi_b/2} \end{pmatrix} \tag{3.2}$$

is the transfer matrix through the halves of the barriers surrounding the quantum well. Here $\phi_b = \omega n_b d_b \cos\theta_b / c$ with d_b being the width of the barrier and θ_b being an angle between the wave vector $\mathbf{k}$ inside the barrier and the direction of the z-axis, $\hat{\mathbf{e}}_z$.

The scattering of the electromagnetic wave at the interface between the quantum well and the barrier caused by the mismatch of the indices of refraction of their materials is described by

$$T_{bw} = T_{wb}^{-1} = T_\rho(\rho) \equiv \frac{1}{1+\rho} \begin{pmatrix} 1 & \rho \\ \rho & 1 \end{pmatrix}, \tag{3.3}$$

where ρ is the Fresnel reflection coefficient (see, e.g. Ref. [44]). The interface scattering depends upon both the angle of incidence of the wave and its polarization state. These effects are effectively described by an introduction of corresponding Fresnel coefficients ρ_s and ρ_p

$$\begin{aligned} \rho_s &= \frac{n_w \cos\theta_w - n_b \cos\theta_b}{n_w \cos\theta_w + n_b \cos\theta_b}, \\ \rho_p &= \frac{n_w \cos\theta_b - n_b \cos\theta_w}{n_w \cos\theta_b + n_b \cos\theta_w} \end{aligned} \tag{3.4}$$

for s ($\mathbf{E} \perp (\mathbf{k}, \hat{\mathbf{e}}_z)$) and p ($\mathbf{E} \parallel (\mathbf{k}, \hat{\mathbf{e}}_z)$) polarizations respectively. The angular dependence of these coefficients upon the angle of incidence measured inside the barrier is schematically shown in Fig. 3.1.

Finally,

$$T_w = \begin{pmatrix} e^{i\phi_w}(1 - iS) & -iS \\ iS & e^{-i\phi_w}(1 + iS) \end{pmatrix} \tag{3.5}$$

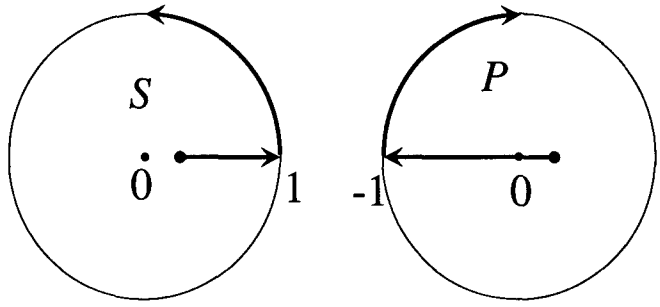

Figure 3.1: A scheme of the angular dependence of the Fresnel coefficients ρ_s and ρ_p upon the angle θ_w is shown on the complex plane. At normal incidence the coefficients have values shown by small filled circles (the same for both polarizations). When the angle of incidence increases the coefficients follow the arrows on the lines. ρ_p passes through 0 at the Brewster's angle, both coefficients reach the unit circle at the angle of total internal reflection. When the angle increases further the Fresnel coefficients become complex with the unit modulus and increasing argument.

is the transfer matrix through the quantum well. Here $\phi_w = \omega n_w d_w \cos\theta_w / c$, where d_w is the width of the quantum well and θ_w is the angle between the wave vector $\mathbf{k}$ inside the quantum well and the growth direction $\hat{\mathbf{e}}_z$. The excitonic contribution to the scattering of the light is described by the function

$$S = \frac{\Gamma_0}{\omega - \omega_0 + i\gamma}, \tag{3.6}$$

which we will call the excitonic susceptibility in what follows. The radiative decay rate, Γ_0, at normal incidence is determined in the case under consideration by

$$\Gamma_0 = \frac{1}{2}\pi k \omega_{LT} a_B^3 \left(\int \Phi(z) \cos kz \, dz \right)^2 . \tag{3.7}$$

For oblique incidence the radiative decay rates are renormalized in different ways for different polarizations [see Eqs. (2.20) and (2.30)]. For p-polarization in addition to this renormalization it is also necessary to take into account a possible splitting of Z- and L-exciton modes [46, 47, 70] that gives rise to a two-pole form of S. However, in materials with the zinc-blend structure, as has been shown in Introduction, the Z-mode of the heavy-hole excitons is optically inactive. Thereby, one can describe angle dependencies of the radiative decay rate for s- and p-polarizations respectively by simple expressions [32, 46, 47]

$$\Gamma_0^{(s)} = \Gamma_0 / \cos\theta_w, \qquad \Gamma_0^{(p)} = \Gamma_0 \cos\theta_w. \tag{3.8}$$

Thus, the propagation of light in the structures under consideration depends upon a number of natural parameters such as Fresnel coefficients, exciton frequencies and radiative decay rate, and optical widths, which (with the exception of ω_0) depend upon the angle of incidence of the wave and its polarization state.

Our next step is to simplify the presentation of the total transfer matrix through the period of the structure in such a way that makes the relations between the elements of the transfer

matrix and the natural parameters of the structure more apparent. The most complicated part of the transfer matrix is the product $T_{bw}T_wT_{wb}$, which describes the reflection of the wave from the interface and its interaction with quantum well excitons. We simplify it by noting that this product can be presented as $T_{bw}T_wT_{wb} = \widetilde{T}_w$, where $\widetilde{T}_w$ has the same form as T_w, Eq. (3.5), but with renormalized parameters

$$\widetilde{T}_w = T_{bw}T_wT_{wb} = \begin{pmatrix} e^{i\tilde{\phi}_w}(1-i\tilde{S}) & -i\tilde{S} \\ i\tilde{S} & e^{-i\tilde{\phi}_w}(1+i\tilde{S}) \end{pmatrix}, \tag{3.9}$$

where the effective excitonic susceptibility, $\tilde{S}$, and the phase shift, $\tilde{\phi}_w$, are defined as

$$\tilde{S} = S\frac{1+\rho^2-2\rho\cos\phi_w}{1-\rho^2} + 2\rho\frac{\sin\phi_w}{1-\rho^2}, \qquad e^{i(\tilde{\phi}_w-\phi_w)} = \frac{1-\rho e^{-i\phi_w}}{1-\rho e^{i\phi_w}}. \tag{3.10}$$

Here ρ denotes the Fresnel coefficient for the wave of a respective polarization. Taking into account the diagonal form of the transfer matrix through the barrier T_b one can see that the total transfer matrix through the period of the structure again has the form of a single quantum well transfer matrix and is determined by Eq. (3.5) where the phase $\tilde{\phi}_w$ is replaced by a total phase $\phi = \phi_b + \tilde{\phi}_w$.

Thus, we have shown that the propagation of the wave in MQW based photonic crystals can be described in terms of properties of a respective optical lattice with renormalized parameters. The renormalization of the phase is the simplest one: the expression for $\tilde{\phi}_w$ can be rewritten as

$$\tilde{\phi}_w = \phi_w\frac{1+\rho}{1-\rho} \tag{3.11}$$

provided that the change of phase ϕ_w across the well is much smaller than 2π, which is usually true for long period MQW structures. Hence, one of the effects of the index of refraction contrast is reduced to a simple renormalization of the optical width of the quantum well.

The effective susceptibility, $\tilde{S}$, consists of two terms. One of them has a singularity at the exciton frequency while the second varies slowly in a wide frequency region. The relation between these terms essentially depends upon the frequency and near the exciton resonance the second term is negligibly small. The frequency region where the nonsingular addition is negligible can be found from Eq. (3.10) and is determined by

$$|\omega-\omega_0| < \omega_{\min} = \frac{\Delta_\Gamma^2}{2\Delta_{PC}}\frac{1+\rho^2-2\rho\cos\phi_w}{1-\rho^2}. \tag{3.12}$$

Here $\Delta_\Gamma = \sqrt{2\Gamma_0\omega_0/\pi}$ is the half-width of the forbidden gap in a Bragg MQW without a mismatch of the indices of refraction, and $\Delta_{PC} = 2\omega_r\rho\sin[\phi_w(\omega_0)]/\pi(1-\rho^2)$ is the half-width of the forbidden gap in a non-resonant (passive) photonic crystal with the same mismatch calculated in the limit $\Delta_{PC} \ll \omega_r$, where ω_r is the central frequency of the gap. In the presence of broadening (both homogeneous and inhomogeneous) there is an additional restriction on this frequency interval: $|\omega_0-\omega| > \gamma$, and for large enough γ it may cease to exist. This will mean that the exciton resonances play very little role in the system, which, in this case, can be considered as a regular passive photonic crystals. In real GaAs/GaAlAs systems, this happens when γ exceeds the value of about $10meV$, which is significantly larger than inhomogeneous broadening in most QW structures, and corresponds to room temperatures for homogeneous broadening. Thus, in good quality samples and at sufficiently low temperatures there always exists a frequency region determined by Eq. (3.12), where the non-singular addition to the effective susceptibility, Eq. (3.10) is negligible regardless of how strong is the mismatch between refractive indexes. Depending on the strength of the mismatch, this region, however, can cover all or only part of the spectral interval affected by excitons. In the case of a single

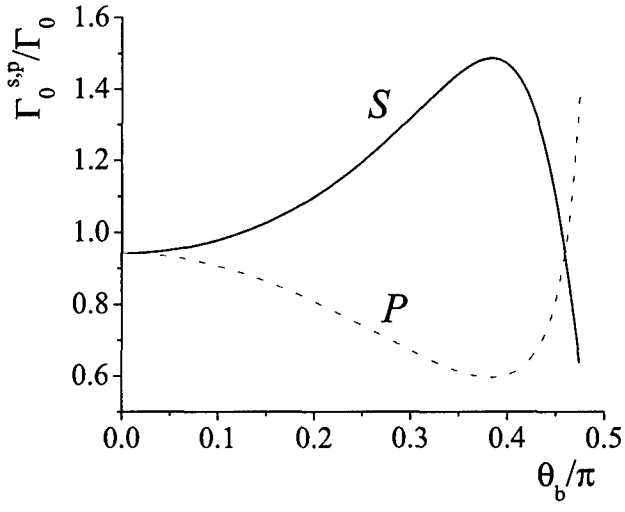

Figure 3.2: Change of the effective radiative decay rates Γ_s (solid line) and Γ_p (dotted line) with the angle of incidence for a single quantum well.

quantum well or of a MQW with a small number of periods, the frequency region of interest is of the order of Γ_0, which is typically much smaller than ω_{min} in Eq.(3.12). In this case the refractive index mismatch can be described in the resonant approximation with only the first term in Eq. (3.10) for the effective susceptibility retained. In this approximation, the effects of the mismatch of the indices of refraction, non-perpendicular incidence, and the polarization are reduced to a renormalization of the radiative decay rate. This means that these effects can be taken into account by using standard expressions obtained for normal incidence in the absence of the mismatch with the radiative decay rate replaced with its effective value

$$\Gamma_{s,p} = \Gamma_0^{(s,p)} \frac{1+\rho^2-2\rho\cos\phi_w}{1-\rho^2}. \tag{3.13}$$

Depending on the value of the Fresnel coefficient one can observe either an enhancement (when $\rho < 0$) or a reduction (when $\rho > 0$) of the exciton radiative recombination. Since usually $n_w > n_b$, the Fresnel coefficient for the normal incidence is positive and therefore the oscillator strength is diminished compared to the case of the absence of the contrast. When the angle of incidence increases, in addition to different dependencies of the Fresnel coefficients corresponding to different polarization states following from Eqs. (3.4), it is necessary to take into account direct modification of the oscillator strength given by Eqs. (3.8). Fig. 3.2 shows the dependence of the factor modifying the radiative decay rate upon the angle of incidence.

3.2 Reflection spectra of simple structures

The representation of the transfer matrix through the period of MQW structure introduced in the previous Chapter in Eq. (2.22) was convenient for an analysis of the band structure because

it solved the problem of the factorization of the dispersion equation. However, for the reflection coefficient it gives an additive form $r \propto \exp(i\arg(a)) + \exp(i\arg(f))$. This form labors establishing the relation between the parameters of the system and the form of the reflection spectrum. Therefore, it is sensible to introduce a special representation for the transfer matrix

$$T(\theta,\beta) = \begin{pmatrix} \cos\theta - i\sin\theta\cosh\beta & -i\sin\theta\sinh\beta \\ i\sin\theta\sinh\beta & \cos\theta + i\sin\theta\cosh\beta \end{pmatrix}, \tag{3.14}$$

where the parameters of the representation, θ and β, are related to the "material" parameters S and ϕ by

$$\cos\theta = \mathrm{Tr}\,T/2 = \cos\phi + S\sin\phi, \qquad \coth\beta = \cos\phi - S^{-1}\sin\phi. \tag{3.15}$$

This representation is valid for an arbitrary system that possesses a mirror symmetry with respect to a plane passing through the middle of the structure. It can be easily derived taking into account the equality of the determinant of the matrix to one, and the circumstance that the mirror symmetry requires off-diagonal elements to be imaginary. Due to the general character of the representations (3.14), the material parameters entering Eq. (3.15) can be either the parameters of a single quantum well, Eq. (3.5) or the effective parameters $\tilde{S}$ and $\tilde{\phi}$, Eqs. (3.9) and (3.10), of a barrier-well sandwich, or even parameters characterizing the entire MQW structure as long as the latter possess the mirror symmetry.

It is useful to compare this representations with the (a,f)-representation [Eq. (2.22)]. Of course, there is a direct relation between all these representations. To see this it is enough to note that for arbitrary matrix in the form (a,f)-representation one can introduce an effective optical width of the period of the structure, $\tilde{\phi}$, and an effective exciton susceptibility, $\tilde{S}$. The relation between the parameters of the (a,f)-representation and these effective parameters can be found comparing Eqs. (2.22) and (3.5)

$$\tilde{S} = \frac{1}{2i}(a\bar{f} - \bar{a}f), \qquad e^{i\tilde{\phi}} = \frac{a}{\bar{a}}. \tag{3.16}$$

This relation can be used to generalize the result of present Chapter for a case of general periodic modulation of the dielectric function. It should be noted that the (a,f)-representation itself is not convenient for an analysis of finite structures since the relation between the parameters of the representation of a transfer matrix through a single layer and the whole structure becomes quite cumbersome [see Eq. (3.52)]. This is where the representation (3.14) becomes very convenient. The latter representation, in turn, misses the possibility to factorize the dispersion equation what makes it barely suitable for a constructive analysis of the dispersion law.

Using the representation (3.14) we can introduce the following transformation rule for transfer matrices

$$T_H(\psi)T(\theta,\beta)T_H^{-1}(\psi) = T(\theta,\beta+2\psi), \tag{3.17}$$

where matrix T_H describes a hyperbolic rotation with a dilation and has the form of

$$T_H(\psi) = e^{\psi}\begin{pmatrix} \cosh\psi & -\sinh\psi \\ -\sinh\psi & \cosh\psi \end{pmatrix}. \tag{3.18}$$

This transformation rule can be used, for instance, for diagonalization of transfer matrices, which can be achieved by choosing parameter $\psi = -\beta/2$. Matrix T_H can be turned into matrix T_{bw}, Eq. (3.3), which describes propagation of waves through interface between two media with different refraction coefficients by using the following relation between ψ and the Fresnel parameter ρ: $\rho = -\tanh(\psi)$ (a detailed discussion of a relation between interface scattering and the hyperbolic rotation can be found in Ref. [71]). This means that the transformation, Eq. (3.17), can be either used to describe the interface between two different structures, or in order to present any type of non-diagonality

of the transfer-matrix as resulting from some effective interface. With the help of Eq. (3.17), any symmetric multilayer structure can be replaced by a uniform slab with the width given by θ and the index of refraction determined by ψ. Therefore, it can be used to describe structures which are more complicated than a simple three layer barrier-well sandwich considered in the previous section. For instance, using Eq. (3.17) we can immediately derive an expression for the transfer matrix T_N of a sequence of identical blocks described by $T(\theta, \beta)$:

$$T_N = T(\theta, \beta)^N = T(N\theta, \beta). \tag{3.19}$$

Because the reflection from the structure described by the transfer matrix T given in the basis of incoming and outgoing waves is $r = -T_{21}/T_{22}$, then for a structure containing N blocks we have

$$r_N = -\frac{i \sinh \beta}{\cot N\theta + i \cosh \beta}. \tag{3.20}$$

The reflection coefficient written in terms of the parameters θ and β does not depend upon the specific form of the transfer matrix and therefore Eq.(3.20) can be applied to a variety of different structures. In the case of $\Gamma_0 = 0$, Eq. (3.20) can be easily shown to reproduce the result well-known for a passive multilayer structure [43, 45, 72].

To find a relation between the quantities entering this expression and the elements of the transfer matrix through the period of the structure it is convenient to multiply both the numerator and the denominator by $\sin\theta$ and to use Eq. (3.15). If each block is characterized by an effective susceptibility $\tilde{S}$ and the phase $\phi = \phi_b + \tilde{\phi}_w$, then we obtain for the reflection coefficient an exact expression

$$r_N = \frac{i\tilde{S}}{\cot(N\theta)\sin\theta + i(\tilde{S}\cos\phi - \sin\phi)}. \tag{3.21}$$

Below we analyze the reflection coefficient for Bragg and slightly off-Bragg structures. For frequencies close to ω_0 we can use $\theta = \pi + i\lambda$, where λ is a complex number with a small modulus. Moreover, in most applications of MQW structures it is naturally to assume that structures are not too long, that is $N \ll N_c = (\mathrm{Re}\,\lambda)^{-1}$. In this approximation, $\coth(N\lambda)\sinh\lambda \approx N$ and the reflection can be written directly in terms of the material parameters

$$r_N = \frac{iN\tilde{S}}{1 + iN(\tilde{S}\cos\phi - \sin\phi)}. \tag{3.22}$$

The amplitude of reflection, $|r|^2$, has the typical form shown in Fig. 3.3. It is characterized by a strong reflection band around the exciton frequency, which is a manifestation of the strong resonant exciton-light interaction. The reflection has an asymmetric form since it is a sum of two terms: one of them is even with respect to the frequency ω_0 and the second is odd. The latter is due to nonzero mismatch and in the approximation used above does not vanish at infinity. Both these terms have a typical width

$$\delta = \frac{N\Gamma_0(1-\rho)^2\cos\phi_+}{(1-\rho^2)^2 + N^2(\sin\phi_+ - \rho^2\sin\phi_-)^2}, \tag{3.23}$$

where $\phi_\pm = \phi_b \pm \phi_w$. It should be noted that the actual optical width of the quantum well determined by ϕ_w enters the definition of $\phi_\pm$, rather than the modified $\tilde{\phi}_w$. We are interested in maximizing exciton related effects in the reflection spectra of our structures, which means designing structures with as large a width δ as possible.

One can see from Eq. (3.23) that the width demonstrates essentially non-monotonous dependence upon the number of quantum wells in the structure: it grows linearly for small N, but starts decreasing as N^2 for larger N. If the coefficient in front of the N^2-term in the denominator of

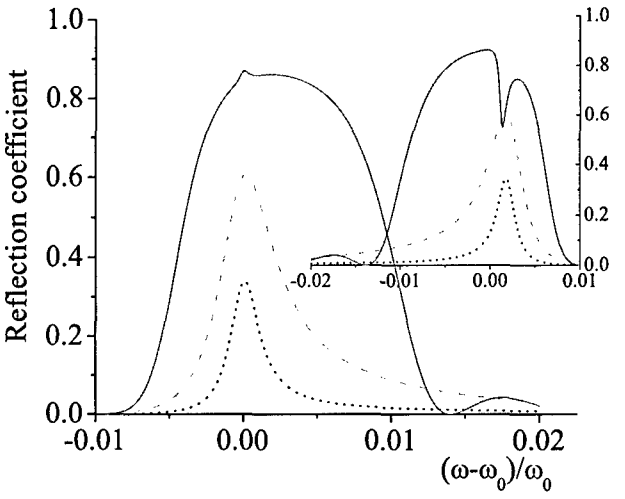

Figure 3.3: Dependence of the amplitude reflection coefficient $|r_N|^2$ upon the frequency. The main plot shows the reflection of structure satisfying the modified Bragg condition with $\rho = 0.005$, the radiative decay rate $\Gamma_0 = 67$ μeV, the exciton frequency $\omega_0 = 1.491$ eV, the homogeneous broadening $\gamma = 500$ μeV and the length $N = 10, 25, 100$ (dot, dash, solid lines, respectively). On the inset reflection spectra of structures which satisfy the standard Bragg condition are shown. To make the correspondence with the experimental results clearer we chose $\rho = -0.005$.

Eq. (3.23) vanishes, then the linear growth of δ would go unchecked as long as N does not exceed N_c. Thus, the condition for maximizing the excitonic effects in the reflection spectrum can be formulated as

$$\rho^2 = \sin\phi_+(\omega_0)/\sin\phi_-(\omega_0). \tag{3.24}$$

If one neglects the mismatch of the indices of refraction, this equation takes a well known form of a condition for the Bragg resonance between the period of the structure and the exciton radiation [49]. One can consider Eq. (3.24) as an equation for the period of the structure, d, for a given ρ. Then for the case of small ρ it gives approximately the same results as that obtained from

$$\rho = \cos(\phi_+/2)/\cos(\phi_-/2), \tag{3.25}$$

which coincides with a modified Bragg condition introduced in previous Chapter (see also Ref. [33]). This condition actually requires that the exciton frequency is equal to the low frequency boundary of the passive (without excitons) photonic crystals' stop band. This consideration shows that the most prominent effect of the light-exciton interaction on the optical properties of long MQW structures with a mismatch of the indices of refraction occurs when the modified Bragg condition is met.

To establish the relation between the modified Bragg condition and the reflection spectrum of the structure, it is convenient to obtain the dispersion equation from the transfer matrix written in terms of $\tilde{S}$ and $\tilde{\phi}_w$, Eq. (3.9). Using the relation $\cos Kd = \mathrm{Tr}\,T/2$, where K is the Bloch wavenumber, d is the period of the structure, one obtains the dispersion equation in the standard form

$$\cos Kd = \cos\phi + \tilde{S}\sin\phi, \tag{3.26}$$

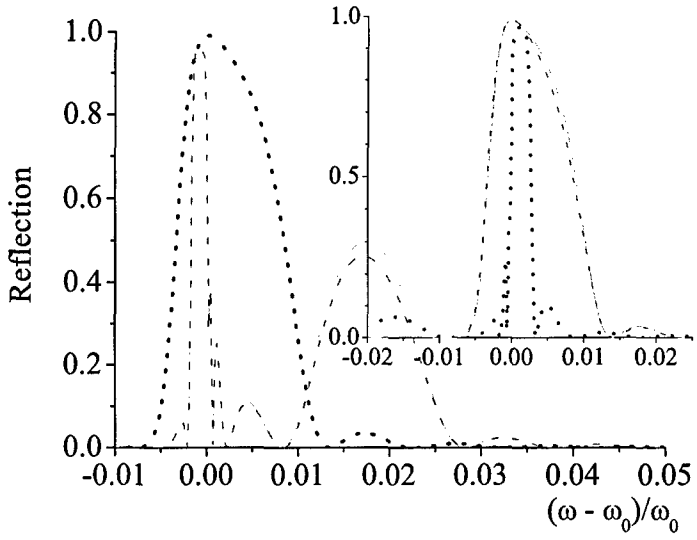

Figure 3.4: The change of the reflection spectrum with the angle of incidence. The parameters of the structure are the same as those used in Fig. 3.3 except: $\gamma = 25$ μeV, $\rho = 0.01$. The dotted line shows the reflection at normal incidence. The solid and dashed lines show the reflection at $\theta_b = \pi/18$ of s- and p-polarized waves, respectively. The main plot corresponds to the structure that is tuned to the Bragg resonance at normal incidence. The inset shows the reflection of a structure which is tuned to the Bragg resonance at $\theta_b = \pi/18$.

where the change of the phase on the period of the structure, ϕ, is determined by the modified optical width of the quantum well, i.e. $\phi = \phi_b + \tilde{\phi}_w$. The Bragg resonance condition is written in a usual form $\phi(\omega_0) = \pi$ as has been shown in previous Chapter coincides with the modified Bragg condition. Thus, for Bragg MQWs the expression for the reflection coefficient, Eq. (3.21), is essentially simplified and can be approximated as

$$r_N = \frac{iN\tilde{S}}{1 + iN\tilde{S}}. \tag{3.27}$$

This expression gives a generalization of a well known result about the linear dependence of the width of the exciton-polariton reflection band on the number of quantum wells in Bragg MQW structures [73].

When the system is detuned from the Bragg resonance, the transparency window appears in the band gap. It shows up in the form of a dip near the exciton frequency in the reflection spectrum (see inset in Fig. 3.3). For example, in Ref. [57] the reflection was measured for MQW structures that satisfied the Bragg condition for structures without the mismatch. In other words, the period of those structures was made to coincide with the half-wavelength at the exciton frequency calculated without taking into account photonic crystal modification of light dispersion. These effects, however, significantly modify the wavelength of light resulting in a detuning of the structures studied in Ref. [57] from actual Bragg resonance. As a result, spectra observed in that paper demonstrate features specific for slightly off-resonance structures [see Fig. (3.3)].

The general results presented in this section allow one to analyze qualitatively modifications in spectra of MQW structures caused by changes of the angle of incidence or polarization state of

the wave. Indeed, using Eq. (3.11) we can write an expression for the renormalized phase, ϕ, in the form

$$\phi = \frac{\omega}{c}\left(n_b d_b \cos\theta_b + n_w d_w \frac{1+\rho}{1-\rho}\cos\theta_w\right). \tag{3.28}$$

This expression shows that the dependence of the Bragg condition on the angle of incidence differs significantly from the intuitive assumption that it can be accounted for by a simple replacement of the wave number k with $k\cos\theta$, which was suggested in some earlier works [56, 57]. While the latter assumption is true in the optical lattice approximation, the presence of the refractive index contrast makes this dependence more complicated. Eq. (3.28) also describes dependence of the Bragg condition on polarization.

Fig. 3.4 demonstrates changes in the reflection spectrum for the structure tuned to the Bragg resonance for the normal incidence with the change of the angle. First, the spectrum for the oblique incidence looks as a typical spectrum for slightly off-Bragg structures. On the other hand, if a structure has a period, which is bigger than what is required by the Bragg condition for normal incidence, i.e. $\phi(\omega_0, \theta = 0) > \pi$, it can be tuned to the resonance by increasing the angle of incidence (see inset in Fig. 3.4). An interesting result apparent from these figures is that tuning the structure to the Bragg resonance by changing the angle preserves to a great extent the shape of the spectrum. This fact opens a possibility for shifting the position of the reflection band of these structures by changing the exciton frequency with the help of, for instance, quantum confined Stark effect [63–65] with consecutive tuning of the structure back to the Bragg resonance by adjusting the angle of incidence. Estimates show that for the available Stark shifts of the exciton frequencies required changes in the angle do not exceed $10-15°$, which is similar to the angles used in Fig. 3.4.

The difference between reflection spectra of waves with s- and p-polarizations remains rather insignificant for angles used in Fig. 3.4. In order to observe it one has to consider much larger angles. Fig. 3.5 shows the reflection spectra of a structure which is tuned to the Bragg resonance at the angle $\theta_b = \pi/4$. The difference between the two polarizations occurs due to two circumstances. First is the different renormalization of the optical width of the quantum wells for different polarizations [Eq. (3.11)]. As a result, the angle at which the structure is tuned to the Bragg resonance depends on the polarization. In Fig. 3.5 the Bragg condition is met for s-polarization. Therefore, one has a typical Bragg profile for the reflection spectrum of the s-polarized wave and off-Bragg profile for the p-polarized wave. The second circumstance is the difference between the effective radiative decay rates [see Eq. (3.13)] for different polarizations. Therefore, the exciton related feature on the reflection spectrum of the p-polarized wave is weaker compared to the s-polarization.

It should be noted, however, that such big angles of propagation inside the barriers are not accessible for a usual experimental setup when the wave is emitted and detected outside the structure. The reason is a high contrast of the indices of refraction of the vacuum and the barriers. However, such angles become relevant when the problem of luminescence is considered.

Another prominent effects caused by the refractive index mismatch consists in vanishing of the reflection coefficient $|r_N|^2$ at $\omega = \omega_0 - \omega_{\min}$ [see Eq. (3.12)] where $\tilde{S} = 0$. This is the consequence of an interference of two channels of scattering of light – by the excitons and by the barrier-well interfaces. For Bragg MQW structures, r_N can be written in a form that explicitly expresses the Fano-like profile of the reflection

$$r_N = r_N^{(0)} \frac{\omega - \omega_0 + \omega_{min}}{\omega - \omega_0 + \omega_{min} r_N^{(0)}}, \tag{3.29}$$

where

$$r_N^{(0)} = \frac{i\pi N \Delta_{PC}}{\omega_r + iN\pi\Delta_{PC}} \tag{3.30}$$

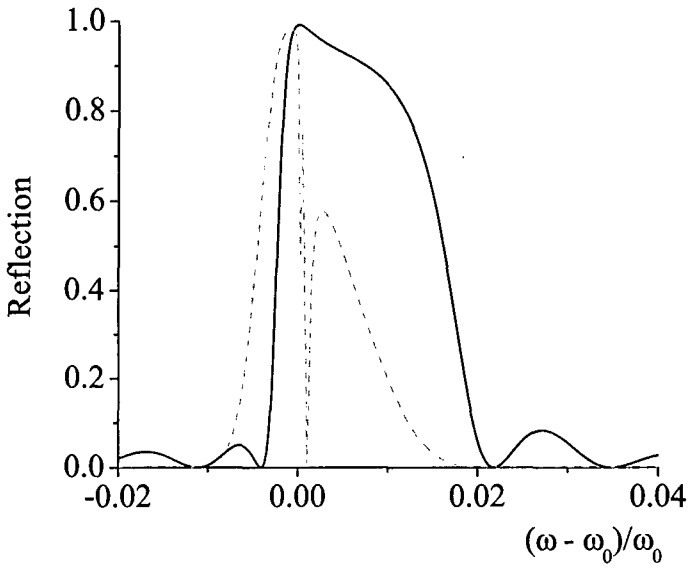

Figure 3.5: The reflection spectrum of s- and p-polarized waves (solid and dashed lines, respectively) of a structure which is tuned to the Bragg resonance at $\theta_b = \pi/4$. The Bragg condition is met for s-polarized wave.

is the reflection in a vicinity of the photonic band gap of a passive, $\Gamma_0 = 0$, N-layer structure which is not too long compared to the penetration length. When the mismatch of the indices of refraction vanishes, ω_{min} turns to infinity and the reflection restores the Wigner-like form with the width $\propto N\Gamma$. This is similar to what one has in the standard Fano resonance case when the Fano parameter tends to infinity [11]. In the other limiting case, $\Gamma_0 = 0$, the reflection turns to what one has for a purely passive multilayer structure.

Due to discussed above relation between different contributions to the scattering of light in regular MQW structures, this resonant drop of reflection occurs at the tail of the excitonic susceptibility where the general smallness of the reflectivity masks this effect. In Section 3.4 we consider a situation where the vanishing of the reflectivity has a much more profound effect on the spectrum.

3.3 Effect of broadenings

So far we have considered ideal systems. In this subsection we discuss the effect of broadenings on the results obtained. There are different sources of broadening of the exciton line. First of all this is the exciton life-time which is finite due to processes of electron-phonon scattering. Such kind of broadening is called homogeneous and is taken into account phenomenologically by adding an imaginary part to the exciton frequency: $\omega_0 \to \omega_0 - i\gamma$.

The second source of the broadening is scattering on interface and bulk inhomogeneities and imperfections. It is necessary to make a distinction between contributions to these processes from inhomogeneities of different spatial scales. There are long-scaled inhomogeneities with the correlation length of the order of magnitude of the distance between the quantum wells and comparable to

wavelength of light in a typical experimental situation. For this scale each quantum well is ideal but different wells have different characteristics: the width, the exciton frequency, the oscillator strength and so on. Inhomogeneities of such scale are called the vertical disorder. The description of structures with the vertical disorder in terms of transfer matrices is straightforward and they are intensively studied in the context of random Kronig-Penny model and Anderson localization of light.

There are, also, inhomogeneities of the scale of the exciton Bohr radius. Such inhomogeneities are non-controllable and caused by, for example, a roughness of the quantum well - barrier interface [74–79]. While in average the quantum wells have the same widths such fluctuations lead to a variety of physical effects. For example, the speckle structure of the scattered electromagnetic waves [80, 81], enhanced resonant backscattering [82, 83], inhomogeneous broadening of exciton lines [38, 84–86] to name only a few. These phenomena can be classified making use a simple phenomenological model. The basic assumption of the model is that the effect of the inhomogeneities on the exciton dynamics can be described by introducing a local exciton frequency $\omega(\rho)$ considered being a random function of the in-plane coordinate ρ. Thus, the frequency dependence of P_{exc} is given by

$$\chi(\rho,\omega) = \frac{\alpha}{\omega(\rho) - \omega - i\gamma}. \tag{3.31}$$

We consider, for simplicity, a perpendicular incidence of the electromagnetic wave with wavelength much longer than the width of QW so we can use the δ-functional approximation for the exciton envelope wave function $\Phi(z)$ and neglect the mismatch of the indices of refraction of the barrier and the quantum well materials. These approximations are sufficient for our particular goals here, but the results obtained will remain valid for more rigorous treatment of the excitonic wave functions as well, within the usual approximation of neglecting the radiative shift of the exciton frequency that vanishes identically in the δ-functional approximation.

After substitution of P_{exc} into Maxwell equations (2.1) and the Fourier transformation with respect to the in-plane coordinates these equations take the form

$$-\left(\kappa_q^2 + \frac{d^2}{dz^2}\right) E_x(q,z) = \frac{2\omega^2\delta(z)}{c^2} \int d^2q\, \chi(q-q',\omega) E(q',z), \tag{3.32}$$

where $\kappa_q^2 = k^2 - q^2$ and $k = \omega\sqrt{\epsilon_\infty}/c$.

One can represent $\chi(\rho,\omega)$ as a sum of its average value and a fluctuating part

$$\chi(q,\omega) = \langle\chi(\omega)\rangle\delta(q) + \tilde{\chi}(q,\omega), \tag{3.33}$$

where, assuming the independence of the distribution function of the exciton frequencies, $f(\omega_0)$, upon the in-plane coordinate, $\langle\chi(\omega)\rangle$ can be written in the form

$$\langle\chi(\omega)\rangle = \int d\omega_0 f(\omega_0) \frac{\alpha}{\omega_0 - \omega - i\gamma}. \tag{3.34}$$

The structure of the Maxwell equation dictates that the reflection and transmission coefficients have a δ-functional singularity in the specular direction [87], $q = 0$. Thus the wave at the left-hand side of the quantum well, E_-, and at the right-hand side, E_+, can be presented in the following form

$$\begin{aligned} E_-(q,z) &= \left(E_0 e^{ikz} + E_0 r_0 e^{-ikz}\right)\delta(q) + E_0 r(q) e^{-i\kappa_q z}, \\ E_+(\rho,z) &= E_0 t_0 e^{ikz}\delta(q) + E_0 t(q) e^{i\kappa_q z}. \end{aligned} \tag{3.35}$$

After the substitution of Eqs. (3.34), and (3.35) into Eq. (3.32) we obtain an integral equation for the reflection and transmission coefficients, $r(q)$, and $t(q)$. Assuming that the random

process representing the fluctuating part of χ does not include constant or almost periodic realizations, we can conclude that $\tilde{\chi}(q,\omega)$, does not have δ-like singularities in almost all realizations. In this case, the terms proportional to $\delta(q)$ in this equation must cancel each other independently of other terms. This leads to splitting of the initial system of equation to

$$\begin{aligned} r_0 &= -iS\,t_0, \\ r(q)\left(1+\frac{ik}{\kappa_q}S\right) &= -\frac{ik}{\kappa_q}\left[\tilde{S}(q)t_0 - \int dq'\tilde{S}(q-q')r(q')\right] \end{aligned} \tag{3.36}$$

with the relation between the reflection and transmission coefficients following from the boundary conditions

$$r_0 + 1 = t_0, \qquad r(q) = t(q). \tag{3.37}$$

Here we have introduced the effective excitonic susceptibilities, $S = -\langle\chi\rangle/k$ and $\tilde{S} = -\tilde{\chi}/k$.

Eqs. (3.36) and (3.37) can be resolved with respect to r_0 and t_0 yielding

$$r_0 = \frac{i\eta}{1-i\eta}, \qquad t_0 = \frac{1}{1-i\eta}. \tag{3.38}$$

Comparison of these results with those obtained for the case of ideal QW [Eq. (3.5) shows that r_0 and t_0 can be obtained from the Maxwell equations (2.1) and, hence, from standard transfer matrix approach, with the susceptibility χ averaged over the distribution of the exciton frequency $f(\omega_0)$. Such a representation constitutes the effective medium approximation and is widely used for the description of the inhomogeneous broadening with the parameter of latter proportional to the variance σ of the distribution (see e.g. Refs. [38, 74, 85, 86]).

This consideration shows that the horizontal disorder leads to appearance of two components in the spectrum of the scattered electromagnetic waves: deterministic (singular), described by r_0 and t_0, and random ($r(q)$ and $t(q)$). An investigation of these components implies addressing to different classes of physical phenomena. The deterministic contribution is most prominent and can be considered as the main contribution to the scattering, while the random component is, generally speaking, small and is responsible for the fine structure of the spectrum (speckles, splitting of the exciton peaks and others).

Staying in the frameworks of present Chapter we restrict ourselves to consideration of the specular component of the scattered light. First of all it should be noted that the inhomogeneous broadening affects optical properties at frequencies that are not too far away from the exciton frequency. Indeed, the broadening enters into expressions for the reflection through the susceptibility S defined by Eq. (3.34). The definition of inhomogeneously broadened susceptibility can be rewritten in the form

$$S = \int d\nu f(\nu)\frac{\tilde{\Gamma}}{(\omega-\bar{\omega})/\bar{\omega} - \nu + i\tilde{\gamma}}, \tag{3.39}$$

where we have introduced $\tilde{\Gamma} = \Gamma_0/\bar{\omega}$, $\tilde{\gamma} = \gamma/\bar{\omega}$, $\nu = (\omega_0 - \bar{\omega})/\bar{\omega}$, and $\bar{\omega}$ is the mean value of the exciton frequency. If the function $f(\nu)$ falls off with increasing ν fast enough we can approximate the integral for the frequencies $|\omega-\bar{\omega}|/\sigma$, $|\omega-\bar{\omega}|/\gamma \gg 1$, as

$$S \approx \bar{S}\int d\nu f(\nu)\left(1 + \frac{\nu}{(\omega-\bar{\omega})/\bar{\omega} + i\tilde{\gamma}} + \ldots\right), \tag{3.40}$$

where

$$\bar{S} = \frac{\Gamma_0}{\omega - \bar{\omega} + i\gamma} \tag{3.41}$$

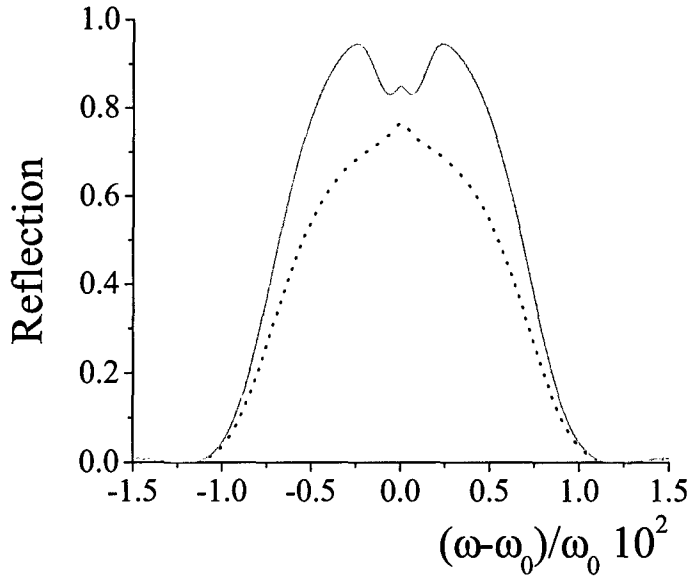

Figure 3.6: The dependence of the reflection of a long Bragg structure, $N = 100$, on frequency. The solid line shows the situation when the inhomogeneous broadening is predominant, $\gamma = 50$ μeV, $\sigma = 1000$ μeV. The dash line shows the reflection for an opposite relation, $\gamma = 1000$ μeV, $\sigma = 50$ μeV. It is seen that homogeneous and inhomogeneous broadenings are not interchangeable.

is the susceptibility in the absence of the inhomogeneous broadening. Noting that now integration of each term in the parentheses gives an appropriate central moment of ν we obtain

$$S \approx \bar{S}\left(1 + \frac{\sigma^2}{|\omega - \bar{\omega}|^2} + \ldots\right). \tag{3.42}$$

Therefore, the corrections due to the inhomogeneous broadening become small for frequencies, which are farther away from the central frequency than the inhomogeneous width σ. Significant inhibition of the effects due to disorder in optical spectra of periodic MQW for frequencies away from the resonance exciton frequency was obtained theoretically in Ref. [85] and observed experimentally in Ref. [88].

In an immediate vicinity of the exciton frequency the effect of the inhomogeneous broadening is, on the contrary, very important. An exact expression of the effect depends upon details of the distribution function of the exciton frequency. To illustrate the main point we model the function by the Gaussian distribution

$$S = \frac{\Gamma_0}{\sigma\sqrt{\pi}} \int_{-\infty}^{\infty} d\omega_0 \, \frac{e^{-(\omega_0 - \bar{\omega})^2/\sigma^2}}{\omega - \omega_0 + i\gamma}. \tag{3.43}$$

Using the function $w(\mu) = e^{-\mu^2}\mathrm{erfc}(-i\mu)$, this expression can be written as $S = \Gamma_0 w(\mu)\sqrt{\pi}/i\sigma$, where $\mu = (\omega - \bar{\omega} + i\gamma)/\sigma$. The small μ expansion [89] $w(\mu) \approx 1 + 2i\mu/\sqrt{\pi}$ allows us to obtain:

$$S = \frac{\Gamma_0 \pi/2}{\omega - \bar{\omega} + i\tilde{\gamma}}, \tag{3.44}$$

where $\tilde{\gamma}$ is the effective broadening,

$$\tilde{\gamma} = \gamma + \frac{\sqrt{\pi}}{2}\sigma. \tag{3.45}$$

One can see that in this case the inhomogeneous and homogeneous broadening combine to form a single broadening parameter $\tilde{\gamma}$, as it is assumed in the linear dispersion theory. However, more detailed analysis shows that, because of fast decay of contribution to the susceptibility, the inhomogeneous broadening results in a peculiarity on reflection that is absolutely opposite to that caused by homogeneous broadening. To illustrate this we consider a Bragg MQW structure in the vicinity of the center of the forbidden gap where

$$|r|^2 = \frac{\Gamma_0^2 N^2}{(\omega - \omega_0)^2 + [\Gamma_0 N + \tilde{\gamma}(\omega)]^2}, \tag{3.46}$$

where we have switched back to the notation ω_0 for the (mean) exciton frequency and neglected the change of the renormalization of the radiative decay rate since its changes slowly with frequency in comparison with $\tilde{\gamma}(\omega)$. The positions of the extremis of the reflection are determined by the solution of the equation

$$\omega - \omega_0 + [\Gamma_0 N + \tilde{\gamma}(\omega)]\frac{d\tilde{\gamma}}{d\omega} = 0. \tag{3.47}$$

For symmetric distribution functions $f(\nu)$ the effective broadening $\tilde{\gamma}$ achieves its maximum at $\omega = \omega_0$. Thus, one extremum is situated at ω_0. Additionally there might be two more extremis (which obviously would be maxima) that are solutions of the equations

$$|\omega - \omega_0| = [\gamma(\omega) + \Gamma_0 N]\left|\frac{d\tilde{\gamma}(\omega)}{d\omega}\right|, \tag{3.48}$$

where it is taken into account that $d\tilde{\gamma}/d\omega$ changes its sign at ω_0.

The solutions of these equations can be quite complicated depending upon the distribution function. As an extreme case it is enough to note that there are no reasons to prohibit as complex $\tilde{\gamma}(\omega)$ as possible (e.g. non-monotonous). However, we exclude such exotic cases from the consideration. Then, due to the fast fall of $|d\tilde{\gamma}/d\omega|$, the condition of existence of solutions of Eq. (3.48) is

$$(\tilde{\gamma} + \Gamma_0 N)|d^2\tilde{\gamma}/d\omega^2| > 1. \tag{3.49}$$

From this expression follows that almost independently on details of the distribution function for long enough structures this condition is satisfied and two additional maxima on the reflection appear.

Thus, the effects of homogeneous and inhomogeneous broadenings on reflection spectra are principally different: the former leads to an appearance of a sudden grow of the reflection in the vicinity of the exciton frequency, while the second, on the contrary, results in a dip. These distinctions are illustrated in Fig. 3.6.

3.4 MQW structures with defect

The results obtained in the previous sections are quite general and can be applied directly to more complicated situations. As an example, in this section we consider a reflection spectrum of a system in which one of the barrier-well-barrier elements has properties different from those of all other elements of the structure. These structures can be described as MQW structures with a "defect." In infinite systems such a defect results in appearance of a new, local state, which arises in a band-gap of the host structure. Then the transmission of light through finite but sufficiently long structures can be conveniently described in terms of resonant tunneling via such a state. This effect

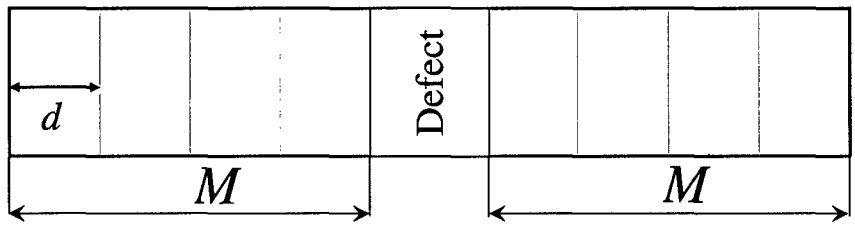

Figure 3.7: A multiple quantum well structure with a defect layer.

was studied in regular passive one-dimensional photonic crystals [90–94], and in Bragg MQWs in the optical lattice approximation [95, 96]. In shorter systems, however, which are the main object of study in this paper, the concept of the resonant tunneling via a local state becomes ill-defined, and therefore, we will interpret results of our calculations without resorting to this concept.

We will consider a structure, in which the defect is placed in its center (see Fig. 3.7): such an arrangement is known to result in strongest modifications of the optical spectra [96]. In this case, the system demonstrates the mirror symmetry and the results of the previous sections can be used. Indeed, for a structure ABA built of blocks A and B described by the transfer matrices (3.14) with parameters $\theta_{A,B}$ and $\beta_{A,B}$, one has

$$T(\theta_A,\beta_A)T(\theta_B,\beta_B)T(\theta_A,\beta_A) = T(\theta,\beta). \tag{3.50}$$

That is, the whole structure can also be described by the matrix (3.14) with

$$\begin{aligned} \cos\theta &= \cos\varphi_+ \cosh^2\delta\beta - \cos\varphi_- \sinh^2\delta\beta, \\ \coth(\beta-\beta_A) &= \cos(2\theta_A)\coth\delta\beta + \frac{\sin\varphi_-}{\sin\theta_N \sinh(2\delta\beta)}, \end{aligned} \tag{3.51}$$

where $\varphi_\pm = 2\theta_A \pm \theta_B$ and $\delta\beta = (\beta_B - \beta_A)/2$. Applying now relations (3.15) one can express the result in terms of parameters S and ϕ, and use the results for reflection described above.

In some particular cases, however, the problem of scattering of light can be solved without resorting to the transformation rule (3.51). Let us consider a situation when the block B is a single quantum well surrounded by barriers so it can be described by the matrix similar to that given by Eq. (3.9) with parameters S_d and ϕ_d. Let the block A be an MQW structure described by θ and β. Thus, the transfer matrix through the whole structure is

$$T = T(\theta,\beta)T_\rho(\rho)T(S_d,\phi)T_\rho^{-1}(\rho)T(\theta,\beta), \tag{3.52}$$

where $T_\rho(\rho)$ takes into account a possible mismatch of the indices of refraction of the defect layer and the host and, ρ is the corresponding Fresnel coefficient.

The transfer matrix (3.52) can be simplified in several steps. First, as has been described before, we can treat β as an addition to the mismatch noting that

$$T_H^{-1}(\beta/2)T_\rho(\rho) = T_\rho(\tilde\rho), \tag{3.53}$$

where $\tilde\rho = (\rho+\rho')/(1+\rho\rho')$ and $\rho' = \tanh(\beta/2)$. Then, similar to Eq. (3.9) we can introduce effective quantities $\tilde S$ and $\tilde\phi$

$$\tilde S = S_d\frac{1+\tilde\rho^2-2\tilde\rho\cos\phi}{1-\tilde\rho^2} + 2\tilde\rho\frac{\sin\phi}{1-\tilde\rho^2}, \qquad e^{i(\tilde\phi-\phi)} = \frac{1-\tilde\rho e^{-i\phi}}{1-\tilde\rho e^{i\phi}}. \tag{3.54}$$

The next step is a multiplication of $T(\tilde{S},\tilde{\phi})$ by the diagonal matrices $T(\theta,0)$ what leads to a simple shift of the phase, $T(\tilde{S},\tilde{\phi}+2\theta)$. Finally, the terminating matrices, $T_H(\beta/2)$ and $T_H^{-1}(\beta/2)$, are taken into account by modifying $\tilde{S}$ and $\tilde{\phi}$. Thus the resultant transfer matrix T takes the form (3.9), i.e. $T=T(\tilde{\tilde{S}},\tilde{\tilde{\phi}})$ with

$$\begin{aligned}\tilde{\tilde{S}} &= \tilde{S}\frac{1+\rho'^2+2\rho'\cos(\tilde{\phi}+2\theta)}{1-\rho'^2}-2\rho'\frac{\sin(\tilde{\phi}+2\theta)}{1-\rho'^2},\\ e^{i(\tilde{\tilde{\phi}}-\tilde{\phi}-2\theta)} &= \frac{1+\rho' e^{-i\tilde{\phi}-2i\theta}}{1+\rho' e^{i\tilde{\phi}+2i\theta}}.\end{aligned} \tag{3.55}$$

These expressions together with Eq. (3.20) give a complete solution of the problem of propagation of light through the MQW structure with an arbitrary defect in the middle.

One can consider several particular types of defects. An example is a well with the exciton frequency different from the frequencies of all other wells, an Ω-defect. Another possible example could be a defect element with the width of the barriers different from the rest of the structure. It is interesting to note that a standard optical microcavity with a quantum well at its center can also be considered within the same formalism. For example, after substitution of $\tilde{S}$ from (3.54) into Eq. (3.55) one obtains an expression that contains a singular term (proportional to S_d) and regular terms. Choosing such widths of the barriers surrounding the quantum well so that the regular terms vanish in the vicinity of the exciton frequency one has the reflection determined by the exciton susceptibility with renormalized oscillator strength. The excitonic contribution to the scattering in such a structure will not be obscured by the interface scattering.

We demonstrate the application of the results obtained above by a detailed consideration of Ω-defect. Different aspects of the optical properties of structures with this type of defect were analyzed in Refs. [96–100] in the scalar model for the electromagnetic wave in MQW structures without a mismatch of the indices of refraction. It has been shown there that in the presence of homogeneous and inhomogeneous broadening of excitons, the effect of the defect is prominent when the frequency of the exciton resonance in the defect layer, ω_d, is close to the boundary of the forbidden gap in the host system, and the length of the system is not too big. The reflection spectrum in this case has the characteristic Fano-like dependence with a minimum followed by a closely located maximum. Such a spectrum makes this structure a potential candidate for novel types of devices such as optical switches or modulators [99, 100]. It is interesting, therefore, to find out how broadenings and the mismatch of the refractive index affect spectral properties of such a structure.

For the frequencies within the polariton stop-band of the host structure one has $\theta=M(\pi+i\lambda)$, where M is the number of quantum wells in the parts of the structures surrounding the defect. The relation between the length of the system $2Md$ and the penetration length $(\mathrm{Re}\,\lambda)^{-1}$ determines how deep the defect layer is situated in the structure. Two limiting cases naturally appear. The first limit corresponds to the situation when the penetration length of the electromagnetic wave at the frequency of the defect is much smaller than the length of the structure (we call it a deep defect), and the second is realized in the opposite case, when the system is much shorter than the penetration length (shallow defect).

3.4.1 Deep defect

First we consider the situation when $(\mathrm{Re}\,\lambda)^{-1} \ll 2Md$ for the example of a structure without the mismatch of the indices of refraction. Such situation was analyzed in Ref. [96] for the case of a lossless system. To determine the range of validity of these results in the case of broadened systems we represent the broadening as a sum of the homogeneous and inhomogeneous ones as in

linear dispersion theory. The estimation of the effect of the broadenings on the reflection spectrum shows that when

$$\gamma + \sigma \lesssim 8\pi e^{-4M\lambda} \frac{\Delta_\omega^3}{\omega_h \Delta_\Gamma^2} \sqrt{\Delta_\Gamma^2 - \Delta_\omega^2}, \tag{3.56}$$

where $\Delta_\omega = (\omega_d - \omega_h)$ is the difference between the defect and the host exciton frequencies (we assume for concreteness that $\omega_h > \omega_d$), the effect of the broadenings can be neglected, and the results of Ref. [96] are valid. This inequality, however, becomes broken for long systems, and the broadenings must be taken into account. In this case the exponentially small non-resonant terms in Eq. (3.55) can be neglected and the reflection in the vicinity of ω_d can be presented in the form

$$r = r_0 \frac{\Omega_d - \Gamma_0 D_d}{\Omega_d + \Gamma_0 D_d - 2ie^{-2M\lambda} \Delta_\omega^2 \omega_h^2}, \tag{3.57}$$

where $D_{d,h} = 1/S_{d,h}$, S_h is the exciton susceptibility of the host layers and

$$r_0 = \frac{1}{1 + D_h \left[\pi(\omega - \omega_h)/\omega_h + i\lambda\left(1 + 2e^{-4M\lambda}\right)\right]} \tag{3.58}$$

is the approximation for the reflection coefficient of the structure without the defect for frequencies deeply inside the forbidden gap. We keep the term $\exp(-4M\lambda)$ in this expression in order to preserve the correct dependence of the reflection coefficient of the pure structure on its length. The frequency Ω_d,

$$\Omega_d = \pi\Gamma_0 \frac{\Delta_\omega}{\omega_h \lambda}, \tag{3.59}$$

describes the shift of the position of the reflection resonance from the initial defect frequency ω_d. This shift is an important property of our structure, which takes place in both ideal and broadened systems. Deriving Eq. (3.57) we dropped the frequency dependence of the non-resonant terms.

Eq. (3.57) shows that when the defect well exciton frequency lies deeply inside the forbidden gap the effect of the defect on the reflection spectrum of the system exponentially decreases when the length of the MQW structure increases. This behavior is strikingly different from that of the respective ideal systems, where resonant tunneling results in the transmission equal to unity at the resonance regardless of the length of the system. One can see that homogeneous broadening severely suppresses this effect, as was anticipated in Ref. [96].

If the shift, Ω_d, of the resonance frequency away from ω_d is large enough, so that ω_r is well separated from ω_d, the effects of the inhomogeneous broadening can be neglected. In this case, we can derive a simple approximate expression for the reflection coefficient in the vicinity of ω_r. The condition $\Omega_d \gg \Delta$ can, in principle, be fulfilled because $\lambda(\omega_d)$ decreases when the frequency goes to the edge of the stop band where λ is determined by

$$\lambda(\omega_h + \Delta_\Gamma) = (1 + i)\pi \sqrt{\frac{\gamma \Delta_\Gamma}{2\omega_h^2}}. \tag{3.60}$$

For GaAs/AlGaAs MQW structures with $\omega_h = 1.49\,\text{eV}$, $\Gamma_0 = 67\,\mu\text{eV}$, $\gamma = 12.6\,\mu\text{eV}$ and $\Delta = 290\,\mu\text{eV}$ we obtain $\text{Re}[\Omega_d(\omega_h + \Delta_\Gamma)]/\sigma \approx 6.3$.

In this case, in the vicinity of the resonance frequency we can approximate the susceptibility S_d by

$$S_d = \frac{\Gamma_0}{\omega - \omega_d + i\gamma} \tag{3.61}$$

and obtain that the resonance has a form of the Lorentz-type dip on the dependence of the reflection spectrum positioned at $\omega = \omega_d - \Omega_d$ with the depth, H, and the width, W, determined by the

expressions

$$H = |r_0|^2 \frac{1 + \gamma\omega_h e^{2M\lambda}/\Delta_\omega^2}{\left(1 + \gamma\omega_h e^{2M\lambda}/2\Delta_\omega^2\right)^2}, \qquad W = \gamma + e^{-2M\lambda}\Delta_\omega^2/\omega_h. \tag{3.62}$$

It should be noted, however, that while formally this approximation is valid even when ω_d is close to the edge of the forbidden gap, the deep defect approximation requires that $2M\lambda \gg 1$. For GaAs/AlGaAs structures this means that $N > (\mathrm{Re}\,\lambda)^{-1} \sim 2000$. The structures of this length are far beyond current technological capabilities, so this case presents mostly theoretical interest.

In the opposite situation, when the frequency shift is small ($\Omega_d < \sigma$), i.e. when ω_d is not too close to the edge of the gap, the inhomogeneous broadening becomes important. In order to estimate its contribution we use the approximation for S_d given by Eq. (3.44), i.e.

$$D_d = \frac{2}{\Gamma_0 \pi}\left(\omega - \omega_d + i\tilde{\gamma}\right). \tag{3.63}$$

One can see that in this case the inhomogeneous and homogeneous broadening combine to form a single broadening parameter $\tilde{\gamma}$, as it is assumed in the linear dispersion theory. The resonance on the reflection curve also has, in this case, a Lorentz-type dip centered at

$$\omega = \omega_h + \frac{\pi\Gamma_0\Delta_\omega}{2\sqrt{\Delta_\Gamma^2 - \Delta_\omega^2}}, \tag{3.64}$$

with the depth and the width, respectively, equal to

$$H = |r_0|^2 \frac{2\pi e^{-2M\lambda}\Delta_\omega^2}{\omega_h\tilde{\gamma}}, \qquad W = \tilde{\gamma} + \frac{\pi e^{-2M\lambda}\Delta_\omega^2}{\omega_h}. \tag{3.65}$$

Because of the contribution of the inhomogeneous broadening, the effective parameter $\tilde{\gamma}$ becomes so large that $\pi e^{-2M\lambda}\Delta_\omega^2 \ll \tilde{\gamma}$, and the defect-induced reflection resonance becomes rather weak compared to the case considered previously.

3.4.2 Shallow defect

From the experimental point of view, a more attractive situation arises when the length of the structure is smaller than the penetration length. The description becomes much simpler if we assume that the width of the defect layer is tuned to the Bragg resonance at the frequency ω_d, that is if $\phi(\omega_d) = \pi$. That makes the second term in the expression for $\tilde{S}$, Eq. (3.54), negligible in a wide region of frequencies and the expression for $\tilde{\tilde{S}}$ takes a very simple form

$$\tilde{\tilde{S}} = S_d\frac{1+\rho}{1-\rho} + 2M\tilde{S}_h. \tag{3.66}$$

In derivation of this expression we have neglected the small term $\propto S_d\tilde{S}_h$. The reflection coefficient can be obtained by substituting this expression into Eq. (3.27) with $N = 1$. The reflection has peculiarities near the exciton frequencies of the host and the defect, and in the absence of broadening becomes 0 at the frequency where $\tilde{\tilde{S}} = 0$. Generally, this equation is suitable for finding the resonance frequency for any value of the photonic band gap, Δ_{PC}, not much bigger than the excitonic forbidden gap, Δ_Γ. Here, however, we only consider the perturbation of the spectrum analyzed in Ref. [99] due to small contrast in the refractive indexes. Therefore we assume here that $\Delta_{PC} \ll \Delta_\Gamma$. In this approximation the resonant frequency is $\omega_R = \omega_d - \Omega_s$, where

$$\Omega_s = \frac{\Delta_\omega}{2M+1} + 16\frac{M^2\Delta_\omega^2\Delta_{PC}}{\Delta_\Gamma^2(2M+1)^3}. \tag{3.67}$$

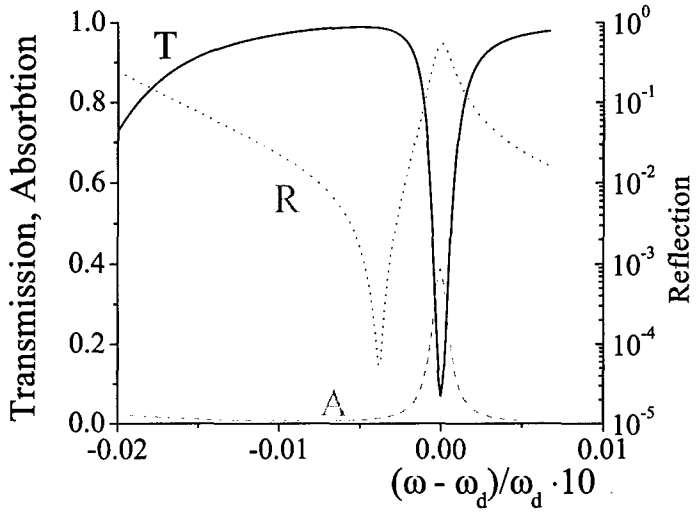

Figure 3.8: The reflection (dotted line, right scale), transmission and absorbtion (solid and dashed lines respectively, left scale) are shown in a vicinity of ω_R for a Bragg $5-1-5$ structure. The parameters of the quantum wells are the same as those used in Fig. 3.3 except: $\gamma = 25$ μeV, $\omega_h = 1.491$ eV, $\omega_d = 1.495$ eV. To emphasize the resonant character of the change of the reflection it is plotted in the log-scale. It should be noted that due to large (in comparison with γ) separation between ω_R and ω_d the drop of the reflection is *not* accompanied with a resonant absorbtion.

Setting the mismatch of the indices of refraction in this expression to zero we reproduce the expression for ω_R obtained in Ref. [99]. The fact that the contrast does not preclude the reflection coefficient from going to zero at a certain point is not at all obvious because it might have been expected that the interface reflection would set a limit on the decrease of the reflection. However, as seen from Eq. (3.67), the mismatch leads only to an additional shift of the zero point away from the defect exciton frequency. We would also like to comment on the dependence of the resonance frequency on the angle of incidence and the polarization of the electromagnetic wave. These characteristics enter Eq. (3.67) through the Fresnel coefficients, Eq. (3.4), that determine the photonic band gap, $\Delta_{PC} \propto \rho/(1-\rho^2)$. Therefore angular and polarization dependencies of the zero point of reflection follow the behavior of Δ_{PC}.

There is a certain analogy between this effect of the resonant drop of reflection and turning the reflection to zero considered in Section 3.1. In the case of a defect MQW structure, the Fano-like profile of the reflection, in a narrow vicinity of ω_d, can be understood as an interference of the scattering of light by the host structure and by the defect. Comparing Eq. (3.66) with Eq. (3.10) one can see that the second term in Eq. (3.66) plays the role of a background on which the exciton susceptibility of the defect quantum well appears. This is exactly the role played by the second term in Eq. (3.10). Expanding $\tilde{\tilde{S}}$ near ω_R the reflection can be represented in a form similar to Eq. (3.29). There is an essential quantitative difference between these two cases, however. In a defect MQW structure the drop of the reflection occurs not far away from the exciton frequency, therefore this effect becomes more noticeable. A typical form of the reflection, transmission and absorbtion near ω_R is shown in Fig. 3.8.

It should be noted, that if a regular term in the effective susceptibility of the defect layer

is taken into account, then Eq. (3.66) for $\tilde{\tilde{S}}$ becomes valid not only in an immediate vicinity of ω_R but in a much wider region, including for example ω_h. In this region, the reflection can be seen to resemble the Fano profile in the case of two metastable states interacting with continuum [101]. As a result, the reflection has two resonances – near ω_h and ω_d. The first resonance is $2N$ times wider than the second one.

If broadenings are taken into account the reflection do not vanish but rather reaches a minimum at a frequency ω_- and maximum at ω_+.

For sufficiently *short* systems, Ω_s can become larger than Δ. For example, in a structure with parameters typical for GaAs/AlGaAs multilayers, the condition $\Omega_s \gg \sigma$ is fulfilled when $M \lesssim M_0 = 5$. In this case, an approximate analytical description of the spectrum is possible. However, since the maximum and the minimum of the spectra lie at significantly different distances from ω_d, the description of these two spectral regions would require different approximations. The maximum of the reflectivity takes place close to the defect frequency, and therefore the inhomogeneous broadening near the maximum has to be taken into account. At the same time, $\omega_- - \omega_d \gg \sigma$, and the inhomogeneous broadening in this frequency region can be neglected. Thus, we can approximate D_d using Eq. (3.61) in the vicinity of ω_- and using Eq. (3.63) near ω_+. Using these approximations we find that the minimum and the maximum of the reflection coefficient are at the frequencies

$$\omega_- = \omega_d - \Omega_s - \frac{\gamma^2}{\Omega_s} \tag{3.68}$$

and

$$\omega_+ = \omega_d + \frac{1}{\pi}\left(\tilde{\Omega}_s - \Omega_s\right) + \frac{\Gamma_0\tilde{\gamma}}{\tilde{\Omega}_s\Omega_s}\left(\tilde{\Omega}_s + \Omega_s\right) \tag{3.69}$$

respectively, where $\tilde{\Omega}_s = \sqrt{\Omega_s^2 + 4\tilde{\gamma}^2}$ and $\tilde{\gamma}$ is the effective broadening defined by Eq. (3.45). The values of the reflection at these points are

$$R_{min} \approx \frac{|\bar{\Gamma}|^2\gamma^2(2M)^4}{\Delta_\omega^4 2M^2}, \qquad R_{max} \approx \frac{|\bar{\Gamma}|^2(\tilde{\Omega}_s + \Omega_s)^2}{(\omega_+ - \omega_h)^2(2\Gamma_0 + \pi\tilde{\gamma})^2}. \tag{3.70}$$

The exact and approximate forms of the reflectivity are compared in Fig. 3.9. One can see that these approximations give a satisfactory description of the reflectivity in the vicinities of the extrema for short systems.

The minimal value of the reflection is determined only by the small parameter of the homogeneous broadening, γ, and can therefore become very small. This fact reflects the suppression of the inhomogeneous broadening in this situation. When the length of the system increases, R_{min} grows as $16M^4$, however, when $M > M_0$, the inhomogeneous broadening starts coming into play: γ must be replaced with a larger effective broadening containing a contribution from σ. This also leads to a significant increase in R_{min}. This behavior is illustrated in Fig. 3.10, where a comparison of the reflection coefficients for two MQW structures with different lengths is provided.

Thus, the highest values of the contrast, defined as the ratio of the maximum and minimum reflections $\eta = R_{max}/R_{min}$

$$\eta \approx \left(\frac{\Delta_\omega}{2M\sqrt{\gamma\tilde{\gamma}}}\right)^4 \tag{3.71}$$

are obtained when the number of periods in the structure is small. For low temperature values of γ the contrast can be as large as 10^4. However, these large values of the contrast are accompanied by rather small values of R_{max}. For possible applications it would be useful to have the large contrast, and the large maximum reflection. The latter can be improved by considering structures with multiple defect wells composed of several blocks ABA considered above. This leads, of course,

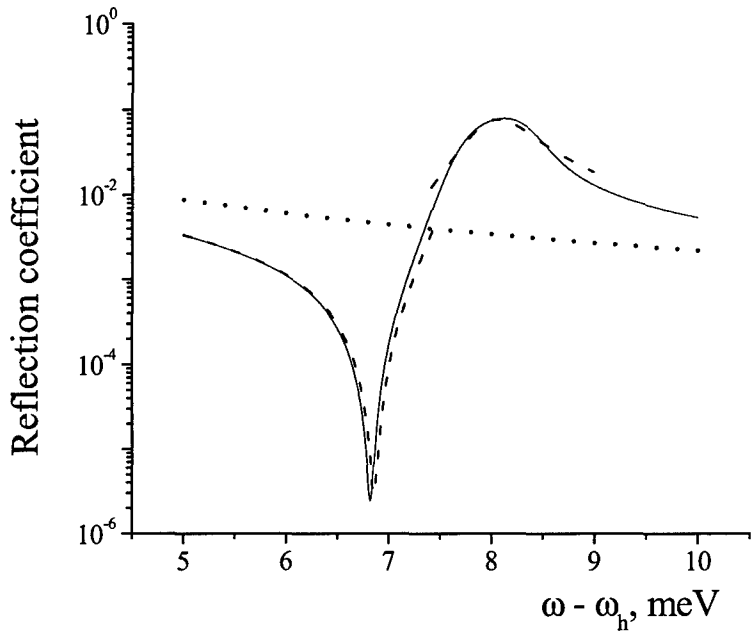

Figure 3.9: Reflection coefficient near the exciton frequency of the shallow defect (solid line) for $M = 3$. The dashed lines depict approximation using different expressions for the defect quantum well susceptibility at the vicinities of the extrema: near the minimum the inhomogeneous broadening is neglected, while in the vicinity of the maximum it is accounted for as a renormalization of homogeneous broadening [Eq. (3.45)]. For reference, the reflection coefficient of a pure MQW structure without a defect is shown (dotted line).

to the increase in the total number of wells, but as we show, one can achieve a significant increase in R_{max} for quite reasonable total length of the structure without compromising the contrast too much. The reflection of such structures can be qualitatively described by Eq. (3.27) where N is understood as the number of such blocks. This expression shows that increasing N can be interpreted as increasing an effective radiative decay rate. This qualitatively explains the results of numerical calculations shown in Fig. 3.11. The structures were constructed of several blocks, each of which is a 9-period long BMQW with a single defect well in the middle. One can see that, indeed, the spectrum of such multi-defect structures exhibits large R_{max} (up to 0.8 for structures no longer than 80 periods), while preserving high values of the contrast (of the order of 10^4).

3.4.3 Tunability of the reflection spectrum

Applications of MQW structures with a defect for switching or modulating devices is based upon a possibility to change the value of the reflection coefficient at a working frequency ω_w by switching between $\omega_w = \omega_{max}$ and $\omega_w = \omega_{min}$ using for instance the quantum confined Stark effect in order to change the value of ω_d. The structures under consideration, however, allow also for

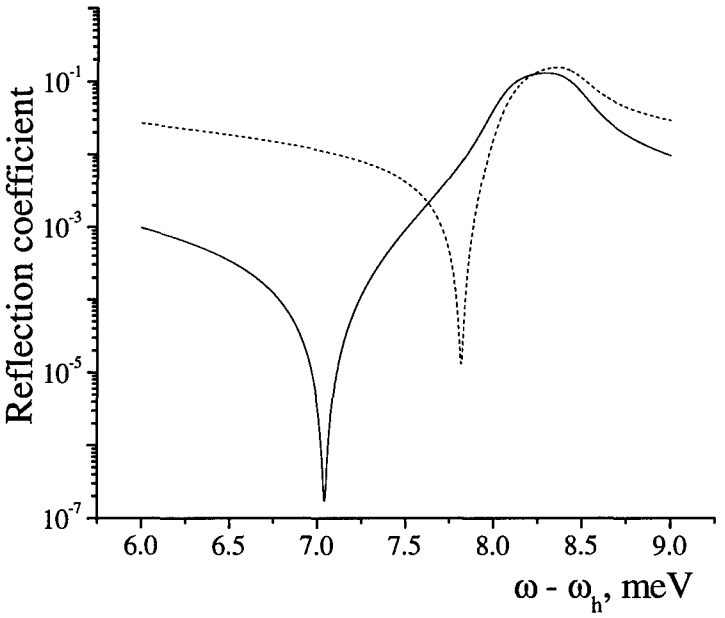

Figure 3.10: Dependence of the reflection coefficient on the frequency in the neighborhood of the exciton frequency of the defect well for different lengths of the MQW structure (solid line $M = 1$, dashed line $N = 2$). The great difference of minimal reflections results from the shift of the resonance frequency Ω_s, Eq. (3.67).

tuning of the working frequency of the device by shifting the entire spectrum of the structure using the Stark effect in host wells. There are several differen ways to implement this idea, but here we only want to demonstrate its principal feasibility. The main possible difficulty results from the fact that shifting ω_h will detune the whole system from the Bragg resonance and, may destroy the nice spectral features discussed above. In order to see how the detuning affects the spectrum, we assume that for simplicity that ω_h and ω_d change uniformly, and study the reflection spectrum of an off-Bragg structure.

As has been shown in Chapter 2 and Section 3.2 (see also Ref. [55]) a small detuning from the Bragg resonance results in opening up a propagating band at the center of the forbidden gap significantly complicating the spectrum. It turns out, however, that as long as ω_{min} and ω_{max} are well separated from ω_h, the detuning does not affect the part of the spectrum associated with the defect. Indeed, we show that the reflection spectrum of an off-Bragg structure is described by the same expressions as in the case of the Bragg structure. The only modification is the change of the definition of $\bar{\Gamma}$, which becomes now

$$\bar{\Gamma} = \frac{\Gamma_0(2M+1)}{1 - i(2M+1)\sin\pi(\omega - \omega_B)/\omega_B}. \tag{3.72}$$

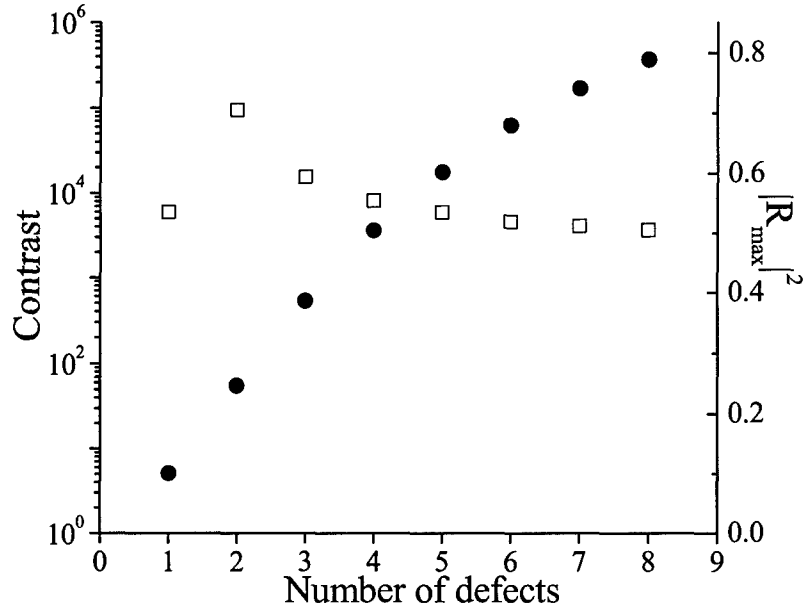

Figure 3.11: Dependencies of the maximal reflection (filled circles, left scale) and the contrast (empty squares, right scale) upon the number of the defects in BMQW structures.

Thus, for such shifts of the exciton frequencies, ω_s, that satisfy the condition

$$2M \sin\left(\pi \frac{\omega_s}{\omega_B}\right) \ll 1 \tag{3.73}$$

the destructive effect of the detuning of the structure away from the Bragg resonance is negligible in the vicinity of ω_d. It is important to note that the smallness of the shift is required in comparison with the relatively big exciton frequency rather than, for example, with the width of the reflection band. Because of this circumstance, our structures can tolerate as large changes of the exciton frequencies as are possible with the quantum confined Stark effect. The result of such a change is simply a uniform shift of the part of the spectrum.

3.4.4 Characterization of the reflection spectra in the case of intermediate lengths

In the previous subsections we examined special situations when the defect can be considered as either deep or shallow. In both cases, we were able to derive approximate analytical expressions describing defect-induced modification of the spectra and to obtain a qualitative understanding of how the defect affects the reflection spectrum. In particular, it was demonstrated that the characteristic frequencies related to the modification of the spectrum are shifted from the resonant defect frequency of a single well. This shift is the result of radiative coupling between the

excitons in the defect well and the collective excitations of the host system. One of the important consequences of this shift is the possibility for almost complete suppression of the effects due to inhomogeneous broadening in some spectral intervals. In this subsection we consider systems with intermediate lengths, when M is larger than M_0, but is still smaller or of the order of magnitude of the penetration length. From the practical point of view, this case is of the greatest interest, since this interval of lengths is still easily accessible experimentally, and at the same time, it is expected that for such structures the defect-induced modifications of the spectrum become most prominent. Unfortunately, none of the approximations used in the previous subsections can be applied here, and we have to resort to a numerical treatment. Nevertheless, the qualitative understanding gained as a result of the previous analytical considerations, serves as a useful guide in analyzing and interpreting the numerical data.

As it was pointed out in the previous section, when M becomes larger than M_0, the position of the minimum of the reflection, ω_- moves closer to ω_d, and the inhomogeneous broadening starts contributing to R_{min}. This effect can phenomenologically be described as the emergence of an effective broadening parameter $\gamma_{eff}(\gamma, \sigma, M)$, which is not a simple combination of γ and σ, but depends upon M. This parameter is limited from below by γ, when the inhomogeneous broadening is suppressed, and from above by $\tilde{\gamma}$, when the contribution from σ is largest. Because the minimum value of the reflection is always achieved at a point shifted with respect to ω_d, generally γ_{eff} is always smaller than $\tilde{\gamma}$, and the homogeneous broadening makes a contribution to it comparable to that of the inhomogeneous broadening *despite the fact that* $\gamma \ll \sigma$. At the same time, the position of ω_+, which determines the width of the spectral interval affected by the defect, depends upon $\tilde{\gamma} \approx \sigma$.

Thus the effect of the broadenings on the spectrum can in general be summarized in the following way: while the width of the resonance is determined equally by both homogeneous and inhomogeneous broadenings, its strength depends mostly upon the homogeneous broadening.

We illustrate this conclusion quantitatively by defining the width of the resonance as the distance between the extrema of the reflection spectrum, $W(\gamma, \sigma, M) = \omega_+ - \omega_-$, and its depth as the difference between the values of the reflection at these points, $H(\gamma, \sigma, M) = R_{max} - R_{min}$. In order to see how these quantities depend upon parameters γ and σ, we chose several different values of W and H, and plot constant level lines, $W(\gamma, \sigma, M) = W_i$, $H(\gamma, \sigma, M) = H_i$. These lines represent values of γ and σ for which W and H remain constant (Fig. 3.12).

The locus of constant widths is the set of nearly straight lines running almost parallel to the axis representing the homogeneous broadening. Slight deviation from the straight-line behavior is seen only for non-realistically high values of γ. Such a behavior confirms our assertion that the width of the resonance is determined by an effective parameter, in which γ and σ enter additively. As we see, this is true even for systems which cannot, strictly speaking, be described by approximations leading to Eq. (3.69). Since usually $\gamma \ll \sigma$, the latter makes the largest contribution to this effective parameter, and determines the value of W. The shape of the lines of constant height demonstrates almost equal contributions from γ and σ, which means that the effect due to the inhomogeneous broadening is significantly reduced as far as this feature of the spectrum is concerned. This is also consistent with an approximate analysis presented in the previous section of the paper.

The remarkable feature of Fig. 3.12 is that the lines of the constant width and the constant high cross each other at a rather acute angle and at a single value of γ and σ for each of the values of W and H. This means that one can extract both γ and σ from a single reflection spectrum of the MQW structure. This is a rather intriguing opportunity from the experimental point of view, since presently, the only way to independently measure parameters of homogeneous and inhomogeneous broadenings is to use complicated time-resolved techniques.

It is clear, however, that the shape of the lines of constant W and H depends upon the choice of the distribution function used for calculation of the average susceptibility of the defect well. It is important, therefore, to check how the results depend upon the choice of the distribution

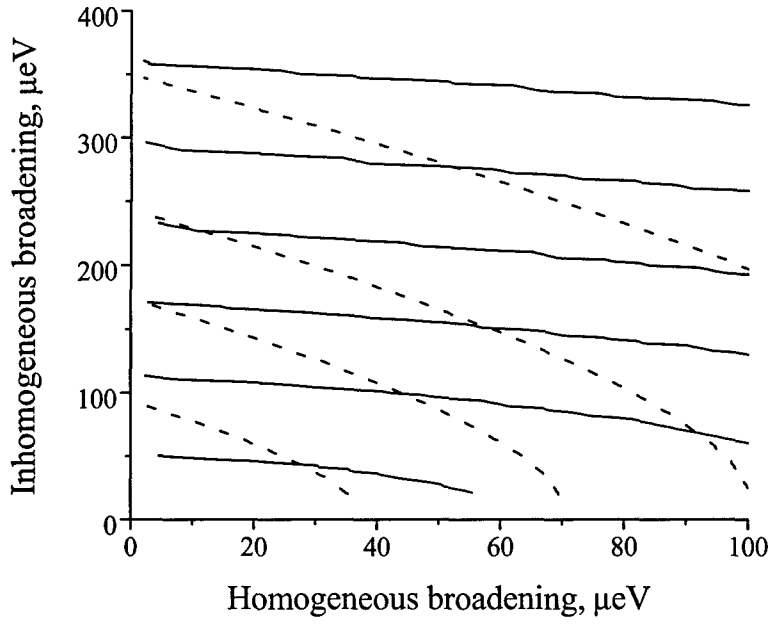

Figure 3.12: Intersections of lines of constant height (dashed lines) and width (solid lines) of the resonance allow determination of the values of the homogeneous and inhomogeneous broadenings.

function of the exciton frequencies. As an extreme example, one can consider the Cauchy distribution

$$f(\omega_0) = \frac{\sigma}{(\omega_0 - \bar{\omega})^2 + \sigma^2}. \tag{3.74}$$

In this case, all the effects due to the inhomogeneous broadening can be described by a simple renormalization, $\gamma \to \gamma + \sigma$, and the level lines in Fig. 3.12 would have the form of parallel lines. This distribution though, hardly has any experimental significance, while the Gaussian function has a certain theoretical justification [102]. However, the symmetrical character of the normal distribution is in obvious contradiction with a natural asymmetry of the exciton binding energies, which can be arbitrarily small but are bounded from above. It was suggested in Ref. [103] to take this asymmetry into account by introducing two different variances in the Gaussian distribution: σ_- for frequencies below some (most probable) frequency ω_c, and σ_+ for the frequencies above it. Accordingly, the distribution function can be written as

$$f(\omega_0) = \frac{2}{\sqrt{\pi}(\sigma_+ + \sigma_-)} \begin{cases} e^{-\frac{(\omega_0 - \omega_c)^2}{\Delta_-}}, & \omega_0 < \omega_c, \\ e^{-\frac{(\omega_0 - \omega_c)^2}{\Delta_+}}, & \omega_0 > \omega_c. \end{cases} \tag{3.75}$$

It was shown that this choice gives a satisfactory description of time-resolved spectra of MQW's [103]. The distribution function Eq. (3.75) can be parameterized either by $\sigma_\pm$ and ω_c or, more

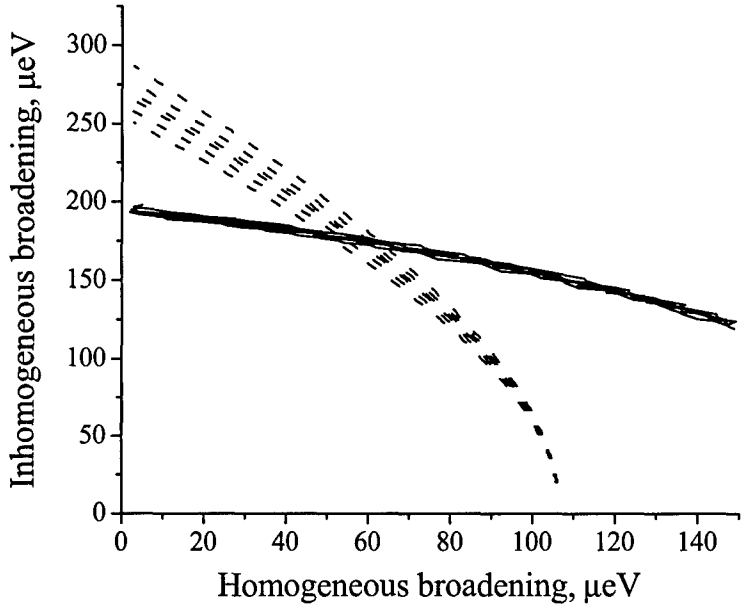

Figure 3.13: Intersections for different values of the parameter of asymmetry. Dashed and solids lines are lines of constant height and width respectively.

traditionally, by the mean value, $\bar{\omega}$, the second moment, σ, and the parameter of asymmetry, n, defined as

$$\bar{\omega} = \omega_c + \frac{\sigma_+ - \sigma_-}{\sqrt{\pi}}, \quad n = \frac{\sigma_+}{\sigma_-}, \quad \sigma^2 = \frac{\sigma_+^3 + \sigma_-^3}{\sigma_+ + \sigma_-} - \frac{2}{\pi}(\sigma_+ - \sigma_-)^2. \tag{3.76}$$

We use the corrected distribution function, Eq. (3.75), with the fixed mean frequency and the variance, but different values of the asymmetry parameter, in order to see how sensitive the defect induced features of the reflection spectrum are to the shape of the distribution function. To this end, we plot the lines of constant height and width for different values of the asymmetry parameter n ($1 \leq n \leq 2$). The results are presented in Fig. 3.13.

An interesting result revealed by these graphs is that with the change of the asymmetry, the points at which W and H level lines cross move parallel to the axis of γ, while the respective values of σ remain quite stable. This shift can be explained by noticing that with change of the parameter of asymmetry the total width of the distribution remains the same while the effective value of the inhomogeneous broadening at the point of the reflection changes. This indicates that the value of σ, which can be obtained by comparing experimental reflection spectra with the theory presented in this paper, is not sensitive to the choice of the distribution function of the exciton frequencies. The value of the parameter of the homogeneous broadening is more sensitive to the asymmetry of the distribution function: it varies by approximately ten percent when the parameter of the asymmetry changes by a factor of two. However, the estimate for γ can be improved by studying the temperature dependence of the reflection spectra.

3.5 Discussion

The effects of the refractive index contrast on the optical properties of MQW structures have not been, of course, overlooked in previous studies. In particular, modifications of the Bragg condition and reflection spectra at normal incidence of Bragg MQWs in the presence of the contrast have been discussed in Refs. [32, 33]. The effects of the dielectric mismatch on optical properties of single quantum wells [37, 51] or an MQW structure embedded in a dielectric environment [53] was also taken into account. However, this problem suffers a lack of an analytical approach. While optical spectra of any given MQW based structure can be easily obtained numerically, this is not sufficient when one needs to design a structure with predetermined optical properties, which is a key element in utilizing these structures for optoelectronic applications. The main difficulty of this task is the presence of a large number of experimental parameters such as an angle of incidence, a polarization state, indices of refraction, widths of the barriers and the quantum wells, etc, which are in a complicated way related to spectral characteristics of a structure. In order to resolve this difficulty, one needs a general effective analytical approach that would facilitate establishing relationships between material parameters and spectral properties of MQW based structures for an arbitrary angle of incidence and polarization state of incoming light.

In the present chapter such a method is developed. It is based on a transfer matrix approach and consists of two steps. In the first step it is shown that a quantum well embedded in a dielectric environment can be described in exactly the same way as a quantum well in vacuum by introducing an effective excitonic susceptibility and an effective optical width of the quantum well layer. In the second step relations between these effective quantum well characteristics and parameters of a total transfer matrix are established. The method is rather general and can be applied to a great variety of different MQW structures with light of an arbitrary polarization, incident at an arbitrary angle.

Chapter 4

Luminescence of quantum wells

A general approach developed in the previous chapters allows its applications not only for an analysis of optical properties of the heterostructures but also for an investigation of more complicated problems. One of such problems is the exciton luminescence in quantum heterostructures. Let an external pump field with the frequency higher than the semiconductor fundamental edge create the the electrons in the conduction zone and the holes in the valence zone. These excitations lose their energy in both radiative and non-radiative ways until they reach the exciton states where the final radiative recombination occurs. To obtain microscopical equations describing the relaxation processes it is necessary to extend the consideration provided in Section 1.2.1 by taking into account the intersubband terms, $\propto w_b^* w_{b'} \hat{\mathbf{A}} \psi_b^+ \nabla \psi_{b'}$, where the field $\hat{\mathbf{A}}$ has its maximum magnitude at small frequencies comparing with the exciton resonance frequency. This describes the radiative relaxation of the electrons and the holes. The non-radiative relaxation is accounted by consideration of the interaction with phonons. This adds two more terms in the equation governing the population of the exciton level. The structure of these new terms is similar to that of the terms describing the radiative relaxation. It is clear that the introduction of all these terms yields a Shrödinger equation with a source in its r.h.s. similar to Eq. (1.24).

The difference between the case considered in the previous chapters and the problem of the exciton luminescence is that now the sources in the Shrödinger equation are of different nature. One of the sources describes a contribution of the external electric field to the population of the exciton level. This corresponds to the situation considered in the previous chapters. The sources of the second kind are responsible for the change of the exciton polarization due to transitions (photon or phonon assisted) to the exciton level from other states.

The recombination of an exciton produces light which has to propagate through the structure and therefore is strongly affected by its optical properties. This is where the results obtained in the previous chapters will be extensively used.

4.1 Macroscopic Maxwell equations

A qualitative consideration of the recombination processes provided above allows to write down macroscopic Maxwell equations governing the spatial distribution of the electric field

$$\nabla \times \nabla \times \mathbf{E} = \frac{\omega^2}{c^2} \left[n^2(z)\mathbf{E} + 4\pi \mathbf{P}_{\text{exc}} \right] - \mathbf{F}. \tag{4.1}$$

Here $n(z)$ is the background index of refraction which is assumed to be periodically modulated $n(z+d) = n(z)$, $\mathbf{F}(z)$ is an electric field source function describing a "background" excitation and

P_{exc} is the exciton contribution to the polarization given by

$$P_{\text{exc}} = -\chi(\omega)\sum_m \Phi_m(z)\left[\int dz'\,\Phi_m(z')\mathbf{E}_\perp(z',\boldsymbol{\rho}) + \boldsymbol{\Sigma}_m(\boldsymbol{\rho})\right]. \tag{4.2}$$

The sum in this expression is taken over all quantum wells which are enumerated by the index m. The wavefunction, $\Phi_m(z)$, of the exciton localized in an m-th well is taken in the form $\Phi_m(z) = \Phi(z-z_m)$, where z_m is the position of the center of the m-th well. As well as in the previous chapters, we assume that the period of the spatial arrangement of the quantum wells coincides with the period of the modulation of the dielectric function $z_{m+1} - z_m = d$. The term $\boldsymbol{\Sigma}_m(\boldsymbol{\rho})$ is the exciton polarization source function in the m-th quantum well, $\boldsymbol{\rho}$ is the coordinate in the plane perpendicular to the growth direction. In Eq. (4.2) we explicitly have taken into account that only the projection of the electric field perpendicular to growth direction $\mathbf{E}_\perp$ is optically active. The intensity of the exciton-light interaction is characterized by the exciton susceptibility $\chi(\omega)$ which we take in the form assuming an absence of the exciton dispersion in the plane of the quantum well.

$$\chi(\omega) = \frac{\alpha}{\omega - \omega_0 + i\gamma}. \tag{4.3}$$

Here $\alpha \sim |\langle c|\, p\,|v\rangle|^2$ is the exciton-light coupling parameter, ω_0 is the exciton resonance frequency and γ is the homogeneous broadening of the exciton line.

Our final objective is to establish a general approach for a consideration of the exciton luminescence in the resonant photonic crystals. We apply this approach to an analysis of the luminescence spectrum in the direction normal to the plane of the layers. Therefore, to avoid unnecessary technical complications, we will consider only s-polarized electric field emitted by the structure. The Maxwell equation (4.1) allows the separation of variables that can be performed in the following way. Let the electromagnetic wave propagate with the wave vector $\mathbf{k}$ along the plane of quantum wells, i.e.

$$\mathbf{E}(z,\boldsymbol{\rho}) = e^{i\mathbf{k}\boldsymbol{\rho}}\mathbf{E}(z,\mathbf{k}). \tag{4.4}$$

For a s-polarized field the direction of $\mathbf{k}$ fixes the direction of $\mathbf{E}(z,\mathbf{k})$

$$\mathbf{E}(z,\mathbf{k}) = E(z,\mathbf{k})\hat{\mathbf{e}}_s(\mathbf{k}), \tag{4.5}$$

where $\hat{\mathbf{e}}_s(\mathbf{k}) \equiv \hat{\mathbf{e}}_z \times \hat{\mathbf{e}}_\mathbf{k}$ is the unit polarization vector. In what follows we will omit the argument $\mathbf{k}$ when it is clear that the value of the scalar amplitude is taken at a fixed value of the in-plane wave vector.

Since we are interested in s-polarized field only we can assume that both source fields $\mathbf{F}$ and $\boldsymbol{\Sigma}_m$ have a corresponding distribution in the plane of the layers. Formally this requirement is formulated in the form of a possibility to represent the sources as

$$\boldsymbol{\Sigma}_m(\boldsymbol{\rho}) = \int d^2k\,\hat{\mathbf{e}}_s(\mathbf{k})\Sigma_m(\mathbf{k})e^{i\mathbf{k}\boldsymbol{\rho}}, \qquad F(\boldsymbol{\rho},z) = \int d^2k\,\hat{\mathbf{e}}_s(\mathbf{k})F(\mathbf{k},z)e^{i\mathbf{k}\boldsymbol{\rho}}, \tag{4.6}$$

where the integrals are taken over vectors lying in the plane of quantum wells and the coefficients $\Sigma_m(\mathbf{k})$ and $F(\mathbf{k},z)$ can be found using the Fourier transformation

$$\Sigma_m(\mathbf{k}) = \hat{\mathbf{e}}_s(\mathbf{k})\cdot\int d^2\rho\,\boldsymbol{\Sigma}_m(\boldsymbol{\rho})e^{-i\mathbf{k}\boldsymbol{\rho}}, \qquad F(\mathbf{k},z) = \hat{\mathbf{e}}_s(\mathbf{k})\cdot\int d^2\rho\mathbf{F}(\boldsymbol{\rho},z)e^{-i\mathbf{k}\boldsymbol{\rho}}. \tag{4.7}$$

In what follows we will drop the wave vector $\mathbf{k}$ as the argument of the amplitudes $\Sigma_m(\mathbf{k})$ and $F(\mathbf{k},z)$.

Substitution of Eqs. (4.4), (4.5) and (4.6) into Eq. (4.1) gives the equation with respect to the scalar amplitude of the electromagnetic wave

$$\frac{d^2E(z)}{dz^2} + \kappa^2(z)E(z) = F(z) - \frac{4\pi\omega^2}{c^2}\chi(\omega)\sum_m \Phi_m(z)\left[\int dz'\,\Phi_m^*(z')E(z') + \Sigma_m\right], \tag{4.8}$$

where $\kappa^2(z) = \omega^2 n^2(z)/c^2 - k^2$. The solution of the initial vector equation is obtained from the solution of Eq. (4.8) as the inverse Fourier transform of the electric field similar to Eq. (4.6).

4.2 Transfer matrix

The initial problem being reduced to a one-dimensional ordinary differential equation can be effectively studied using transfer matrices. We will use the approach developed in Chapter 2. To apply it for the luminescence problem it is necessary to take into account the circumstance that now the transformation of the electric field from one boundary to another is not linear because of the sources. Fortunately, it requires only a slight modification.

Without loss of generality we consider a layer with the quantum well situated at $z = 0$ with the left and right boundaries at z_- and z_+ respectively. Inside a single layer the summation over quantum wells in Eq. (4.8) can be dropped and so can the number of the quantum well. The r.h.s. of the equation obtained can be considered as an inhomogeneity in a second order differential equation

$$\frac{d^2E(z)}{dz^2} + \kappa^2(z)E = \mathcal{F}(z). \tag{4.9}$$

A general solution of such an equation is written in the form

$$E(z) = c_1h_1(z) + c_2h_2(z) + (G \star \mathcal{F})(z), \tag{4.10}$$

where

$$(G \star \mathcal{F})(z) = \frac{1}{W_h}\int_{z_-}^{z} dz'\,\mathcal{F}(z')\left[h_1(z')h_2(z) - h_1(z)h_2(z')\right]. \tag{4.11}$$

Here $h_{1,2}(z)$ are linearly independent solutions of the homogeneous equation

$$\frac{d^2E(z)}{dz^2} + \kappa^2(z)E = 0, \tag{4.12}$$

and $W_h = h_1h_2' - h_2h_1'$ is the Wronskian of these solutions. To avoid unnecessary complications of the following formulas we assume that $h_{1,2}$ are real functions, e.g. they solve the Cauchy problem (4.12) with real initial conditions at $z = 0$. In Eq. (4.11) we explicitly have taken into account that for Eq. (4.12) the Wronskian does not depend on z.

Substitution the r.h.s. of Eq. (4.8) into Eq. (4.10) yields for the field at the right boundary of the elementary cell

$$\begin{aligned} E(z_+) =& h_1\left[c_1 - \frac{F_2}{\sqrt{W_h}} + \tilde{\chi}\frac{4\pi\omega^2\varphi_2}{c^2}\left(c_1\varphi_1 + c_2\varphi_2 + \frac{\tilde{\Sigma}}{\sqrt{W_h}}\right)\right] \\ &+h_2\left[c_2 + \frac{F_1}{\sqrt{W_h}} - \tilde{\chi}\frac{4\pi\omega^2\varphi_1}{c^2}\left(c_1\varphi_1 + c_2\varphi_2 + \frac{\tilde{\Sigma}}{\sqrt{W_h}}\right)\right], \end{aligned} \tag{4.13}$$

where $\varphi_{1,2}$ and $F_{1,2}$ are the "projections" of the exciton state and the non-resonant field source onto the solutions of the solutions $h_{1,2}$

$$\varphi_{1,2} = \frac{1}{\sqrt{W_h}} \int\limits_{QW} dz' \Phi^*(z') h_{1,2}(z'), \qquad F_{1,2} = \frac{1}{\sqrt{W_h}} \int\limits_{z_-}^{z_+} dz\, F(z) h_{1,2}(z). \tag{4.14}$$

In Eqs. (4.14) the integrals are taken over the period of the structure (or over the elementary cell of the photonic crystal). The effective polarization source function $\tilde{\Sigma}$ is the initial Σ modified by the field source function

$$\tilde{\Sigma} = \Sigma + \int\limits_{QW} dz\, \Phi(z)(G \star F)(z). \tag{4.15}$$

Using the solution (4.13) the relation between the values of the field at different boundaries of the elementary cell can be found. If the field is specified by the amplitudes $c_{1,2}$ one has

$$\begin{pmatrix} c_1 \\ c_2 \end{pmatrix}(z_+) = \widehat{T}_f \begin{pmatrix} c_1 \\ c_2 \end{pmatrix}(z_-) + \begin{pmatrix} \Delta c_1 \\ \Delta c_2 \end{pmatrix}, \tag{4.16}$$

where $\widehat{T}_f$ is the transfer matrix through the elementary cell written in the basis of the linearly independent solutions

$$\widehat{T}_f = \hat{1} + \frac{4\pi\omega^2\tilde{\chi}}{c^2} \begin{pmatrix} \varphi_2\varphi_1 & \varphi_2^2 \\ -\varphi_1^2 & -\varphi_2\varphi_1 \end{pmatrix}, \tag{4.17}$$

where $\hat{1}$ is the unit matrix. The contribution of the sources is described by the second term in r.h.s. of Eq. (4.16)

$$\begin{pmatrix} \Delta c_1 \\ \Delta c_2 \end{pmatrix} = \frac{1}{\sqrt{W_h}} \begin{pmatrix} -F_2 \\ F_1 \end{pmatrix} + \tilde{\Sigma} \frac{4\pi\omega^2\tilde{\chi}}{c^2\sqrt{W_h}} \begin{pmatrix} \varphi_2 \\ -\varphi_1 \end{pmatrix}. \tag{4.18}$$

This is one of the main results of this Section. The important feature of this addition is that it does not depend upon the state of the "incoming" field. In other words, the field at the right boundary of the elementary cell is obtained as a superposition of a regular transfer of the field at the left boundary (as if there were no sources at all) and the field generated by sources. It might seem that there is on symmetry between the left and right boundaries of the elementary cell, however, it must be noted that such symmetry must appear as a solution of an appropriate boundary value problem. In particular, results similar to Eq. (4.16) can be obtained for a general case of absent mirror symmetry of the elementary cell, multilevel structure of the exciton susceptibility χ, including both even and odd exciton states and so on. In these cases the symmetry between the fields at the left and right boundaries can barely be expected. At this stage the solution given by Eq. (4.16) must be considered as a general solution of a Cauchy problem (general solution of homogeneous equation plus a particular solution of inhomogeneous). The application of this solution to a problem with boundary conditions will be shown in the next section.

So far we considered a general situation. The expressions obtained greatly simplify when the symmetries of the profile of the quantum well and the modulation of the dielectric function are consistent, i.e. $n(z_m + z) = n(z_m - z)$, where z_m is the position of the center of m-th quantum well. In this case the elementary cell of the structure can be chosen such a way that it explicitly has the mirror symmetry with respect to its center (see Fig. 4.1). In what follows the elementary cell will be meant having such symmetry.

Because of invariance of Eq. (4.12) with respect to mirror reflection its solutions have definite parity. Therefore as the pair of linearly independent solutions $h_{1,2}$ can be chosen functions which are even and odd with respect to the center of the quantum well. Let h_2 be the odd solution

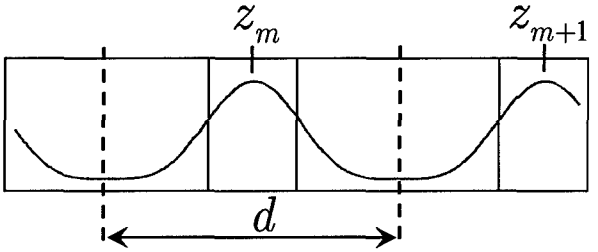

Figure 4.1: The periodic structure built of quantum wells (the shadowed rectangulars) and the barriers between them. Vertical dashed lines show the boundary of the elementary cell having the property of the mirror symmetry. The smooth line illustrates the modulation of the dielectric function in the structure.

then $\varphi_2 = 0$ what essentially simplifies Eqs. (4.17) and (4.18). The generalization of the results obtained below for a non-symmetrical case can be obtained but it requires more cumbersome analysis (see e.g. Section 2.4). Therefore, to avoid blurring the main ideas by technical complications we will consider the symmetric situation.

The basis of a pair of linearly independent functions is convenient to derive the transfer matrix through a single elementary cell staying inside the cell. However, for consideration of optical properties (e.g. a field emitted by the structure) the conventional basis of planar waves is more convenient. In this basis the field is naturally represented in the form

$$E = E_+ e^{iqz} + E_- e^{-iqz}, \tag{4.19}$$

where $q = \kappa(z_+)$ is determined by boundary conditions at the interface between elementary cells. The transfer matrix written in this basis relates the amplitudes of the waves propagating to the left and to the right $E_\pm$ at the different boundaries of the elementary cell. Using the transformation rule (A.9) the transfer matrix in the basis of plane waves can be obtained in the form [see Eq. (2.22)]

$$T = \begin{pmatrix} af & (\bar{a}f - a\bar{f})/2 \\ (a\bar{f} - f\bar{a})/2 & \bar{a}\bar{f} \end{pmatrix}, \tag{4.20}$$

where

$$\begin{aligned} a &= g_2, & f &= g_1 - iSg_2, \\ \bar{a} &= g_2^*, & \bar{f} &= g_1^* + iSg_2^*, \end{aligned} \tag{4.21}$$

and

$$g_1 = \frac{1}{\sqrt{W_h}}\left[h_1(z_+) + \frac{h_1'(z_+)}{iq}\right], \quad g_2 = \frac{1}{\sqrt{W_h}}\left[iqh_2(z_+) + h_2'(z_+)\right]. \tag{4.22}$$

The function $S(\omega)$ in the one-level approximation for $\chi(\omega)$ has the form

$$S(\omega) = \frac{\Gamma_0}{\omega - \omega_0 - \Delta\omega + i\gamma}, \tag{4.23}$$

where $\Gamma_0 = 2\pi\alpha\omega^2\varphi_1^2/qc^2$ is the radiative decay rate. As well as in previous chapters, since χ and $S(\omega)$ differ only by a factor slowly changing with frequency we will refer to function $S(\omega)$ as the exciton susceptibility.

The source term (4.18) in the basis of plane waves has the form

$$|v_m\rangle = -F_2\,|a\rangle + \frac{F_1}{iq}\,|s\rangle + \frac{2\tilde{\Sigma}S}{i\varphi_1}\,|s\rangle\,, \tag{4.24}$$

where $|a\rangle = g_1\,|+\rangle + g_1^*\,|-\rangle$ and $|s\rangle = g_2\,|+\rangle - g_2^*\,|-\rangle$. The index m in the notation $|v_m\rangle$ reminds that relevant quantities (e.g. sources) depend on the number of the well and should be taken for the particular m-th well. The first two terms in Eq. (4.24) can also be represented as a vector with components $[1 \pm (iq)^{-1}d/dz](G\star F)(z_+)$ relating it more directly to the external sources of the field. However, for the following analysis it is more important to establish the relation between the source terms in the basis of plane waves and the solutions of Eq. (4.12) with the definite parity. Let us look, for example, at the term $\propto F_1$ in Eq. (4.24). Its magnitude is determined by the projection of the non-resonant source to the even solution of Eq. (4.12). In particular this term vanishes if the external excitation is antisymmetric with respect to the center of the elementary cell of the structure. A comparison of this term and the term $\propto \tilde{\Sigma}$ allows to identify the symmetry of the excitation of the electric field induced by the exciton recombination as symmetric with respect to the center of the elementary cell. Of course, such identification is supported by assumed above the same symmetry of the exciton wave function and the spatial modulation of the dielectric functions and is formally established by the choice $\varphi_2 \equiv 0$ used above.

4.3 Radiative boundary conditions and the field emitted by an m-th well

In this Section we consider a structure containing N layers and find the field outside the structure subject to the radiative boundary conditions. For example, if the structure is embedded into vacuum it is necessary to take into account additional scattering of light by the interface. It is done by introducing the interface transfer matrices so that the field outside the structure (behind its right end) is

$$\begin{pmatrix} E'_+ \\ E'_- \end{pmatrix} = T_\rho \begin{pmatrix} E_+ \\ E_- \end{pmatrix} \equiv \frac{1}{1+\rho}\begin{pmatrix} 1 & \rho \\ \rho & 1 \end{pmatrix}\begin{pmatrix} E_+ \\ E_- \end{pmatrix}, \tag{4.25}$$

where

$$\rho = \frac{n_{out}\cos\theta_{out} - n_b\cos\theta_b}{n_{out}\cos\theta_{out} + n_b\cos\theta_b} \tag{4.26}$$

is the Fresnel coefficient for the s-polarized field. The angle of incidence is determined by $\tan\theta_b = k/q$. The outgoing wave propagates at the angle following from Snell's law $n_{out}\sin\theta_{out} = n_b\sin\theta_b$.

First, we consider the case when only m-th quantum well emits light. There are waves propagating away from the structure in the surrounding medium. In other words, in the half-space $z < z_L$, one has the wave propagating to the left, that is $E_-^{(m)}\,|-\rangle$ and in the half-space $z > z_R$ there is the wave propagating to the right $E_+^{(m)}\,|+\rangle$. Here $z_{L,R}$ are the coordinates of the left and the right ends of the structure, respectively, and

$$|-\rangle = \begin{pmatrix} 0 \\ 1 \end{pmatrix}, \qquad |+\rangle = \begin{pmatrix} 1 \\ 0 \end{pmatrix}. \tag{4.27}$$

Using the results obtained above we can find the relation between the field outside the structure

$$E_+^{(m)}\,|+\rangle = T_\rho T^{N-m}\,|v_m\rangle + E_-^{(m)} T_\rho T^N T_\rho^{-1}\,|-\rangle\,. \tag{4.28}$$

This equation is written using essentially the results obtained above in Eq. (4.16). The field state given at the left boundary of the layer is transferred through the luminescent layer in a usual way

by a simple multiplication by the transfer matrix. This gives the term proportional to T^N. The sources of the electric field lead to the appearance of one more term. Because of the linearity, the transfer of this summand can be considered independently. This results in the term proportional to T^{N-m} in Eq. (4.28). Multiplication of Eq. (4.28) from the left by $\langle +|$ and $\langle -|$ gives the system of two inhomogeneous equations with respect to $E_{\pm}^{(m)}$. The solution of this system is

$$\begin{aligned} E_{-}^{(m)} &= -\frac{\langle -|\, T_\rho T^{N-m} \,|v_m\rangle}{\langle -|\, T_{PC} \,|-\rangle}, \\ E_{+}^{(m)} &= \left(\langle +| - \frac{\langle +|\, T_{PC} \,|-\rangle}{\langle -|\, T_{PC} \,|-\rangle} \langle -| \right) T_\rho T^{N-m} \,|v_m\rangle\,, \end{aligned} \tag{4.29}$$

where $T_{PC} = T_\rho T^N T_\rho^{-1}$ is the transfer matrix through the whole structure including the interfaces between the terminating layers and the surrounding medium. Let us note, that this is not essential for the derivation of these expressions that all transfer matrices in the structure are the same or that the elementary cell possess the mirror symmetry. For example, if the the transfer matrices are different then instead of the powers of T in Eq. (4.29) products of the corresponding transfer matrices would appear. What is crucial is the possibility to separate different contributions in the field at the right boundary of the elementary cell as is emphasized by Eq. (4.18). However, as has been discussed above, such a separability is the general result.

The apparent asymmetry of these expressions for $E_{\pm}^{(m)}$ is a consequence of the definition of $|v_m\rangle$ and, actually, reflects a possible difference between the fields emitted in positive and negative directions in an asymmetrical case. Since we are interested in the case where both the dielectric function and the exciton wave function have the mirror symmetry with respect to the center of the elementary cell, it is convenient to have such a form of Eqs. (4.29) which is similar for both $E_{-}^{(m)}$ and $E_{+}^{(m)}$. It can be done using the general property of the transfer matrix through a structure with the mirror symmetry, $\sigma_x T^{-1} \sigma_x = T$. Using this property, the second equation of Eqs. (4.29) can be shown to be

$$E_{+}^{(m)} = \frac{\langle +|\, T_\rho T^{-m} \,|v_m\rangle}{\langle -|\, T_{PC} \,|-\rangle}. \tag{4.30}$$

Of course, to prove the actual symmetry it is necessary to show that Eqs. (4.29) imply the equality

$$E_{-}^{(N-m+1)} = E_{+}^{(m)}. \tag{4.31}$$

It should be noted, however, that such an equality is a consequence of the symmetry not only of the structure itself but also of the sources. For example, as is seen from Eq. (4.24), generally the non-resonant source term $F(z)$ in the r.h.s. of Eq. (4.8) can provide such excitations which do not have a definite symmetry with respect to the center of the elementary cell of the structure. It occurs when both $F_{1,2} \neq 0$. In this case a relation similar to Eq. (4.31) generally does not take place. However, when the sources have a definite symmetry, one can prove that Eq. (4.31) holds. The most interest case for us is when $F_2 \equiv 0$. Then, in order to prove Eq. (4.31) one should use the relation $T^{-1}\,|s\rangle = -\sigma_x\,|s\rangle$, which validity can be shown either by direct calculations or by an analysis of the derivation of Eq. (4.24).

It is convenient to rewrite the expressions for the external field in terms of Green functions defined as the field radiated by a source with a unit intensity. As follows from Eqs. (4.29) one has

$$E_{\pm}^{(m)} = \zeta_m \mathcal{G}_{\pm}^{(s)}(m) + \bar{\zeta}_m \mathcal{G}_{\pm}^{(a)}(m), \tag{4.32}$$

where

$$\zeta_m = \frac{F_1}{iq} + \frac{2\tilde{\Sigma}_m S}{i\varphi_1}, \qquad \bar{\zeta}_m = -F_2 \tag{4.33}$$

are the amplitudes of the sources. The Green functions $\mathcal{G}_{\pm}(m)^{(s,a)}$ describe the response on the excitations with the different symmetries and can be written in the form

$$\mathcal{G}_{\pm}^{(s,a)}(m) = \pm t_N \langle \pm | T_{\mp}^{(m)} T_\rho | s, a \rangle . \tag{4.34}$$

Here we have taken into account the definition of the transmission coefficient through the whole structure t_N in terms of the transfer matrix $t_N = \langle - | T_{PC} | - \rangle^{-1}$. Also, in Eq. (4.34) we introduced partial transfer matrices $T_{-}^{(m)} = T_\rho T^{-m} T_\rho^{-1}$ and $T_{+}^{(m)} = T_\rho T^{N-m} T_\rho^{-1}$. These matrices have the property $T_{PC} T_{-}^{(m)} = T_{+}^{(m)}$ which illustrates their physical sense and makes the structure of the Green functions $\mathcal{G}_{\pm}^{(s,a)}$ clear.

It should be noted that Eqs. (4.32) and (4.34) are direct consequences of Eqs. (4.29) and up to the definition of $T_{\pm}^{(m)}$ do not depend on a specific form of the transfer matrices through the individual layers.

Eq. (4.32) solve the general problem of the field created outside a resonant photonic crystal by the sources of different nature localized inside the structure. It follows immediately from Eqs. (4.33) that the specific feature of the contribution to the radiated field due to the exciton recombination is its resonant character. This is the main contribution at frequencies close to ω_0 while the non-resonant sources specified by $F(z)$ create the background component which is characterized by a relatively smooth frequency dependence and becomes important far away from the exciton resonant frequency. These non-resonant sources are not important for the problem of the exciton luminescence in the resonant photonic crystals. Therefore, below we assume that the only source of the electric field in the structure is the exciton recombination and neglect the non-resonant sources. As the result the amplitudes of the sources in Eq. (4.32) become $\zeta_m = 2\Sigma_m S/i\varphi_1$ (note that $\tilde{\Sigma}_m = \Sigma_m$ as $F \equiv 0$) and $\bar{\zeta}_m \equiv 0$. Since the only relevant Green function in this case is $\mathcal{G}_{\pm}^{(s)}(m)$ we will drop the superscript (s) hereafter.

4.4 The intensity of the field outside the structure

The full field created by a luminescent structure is obtained by the summation of $E^{(m)}$ with respect to all quantum wells. To analyze the intensity spectrum, one should, however, take into account the fact that the spatial correlations of Σ_m are shorter than the characteristic length of the structure (the period of the structure). This leads to non-coherent contributions to the emitted electric field from different quantum wells and different points of the wells. This circumstance is taken into account by averaging the total intensity over the realizations of Σ_m. We assume the function Σ_m to be a random function of the frequency, ω, and the in-plane wave number, k. The statistical properties of this function are characterized by a correlation function of the following form: $\langle \Sigma_m(\mathbf{k},\omega)\Sigma_l(\mathbf{k}',\omega')\rangle = \Xi(\omega,k)\delta(\omega-\omega')\delta(\mathbf{k}-\mathbf{k}')\delta_{ml}$, where $\Xi(\omega,k)$ is a spectral function, which we do not expect to depend strongly on ω and k at the frequency scale involved in our discussion.

Using these properties of Σ_m, one obtains $\langle E(\mathbf{k}_1)E(\mathbf{k}_2) = \mathcal{I}(\mathbf{k}_1)\delta(\mathbf{k}_1-\mathbf{k}_2)$. Here $\mathcal{I}(\mathbf{k}_1)$ is the spectral density of the electric field which has the form

$$\mathcal{I}(\omega,k) = 4\,\Xi(\omega,k)\left|\frac{S(\omega,k)}{\varphi_1}\right|^2 \sum_m |\mathcal{G}(m;\omega,k)|^2. \tag{4.35}$$

This is the general expression which allows analyzing both the frequency and the directional dependence of the luminescence spectrum. In what follows we restrict ourselves to the consideration of the intensity of the electromagnetic waves emitted along the growth direction of the structure (i.e. $k = 0$). The directional distribution of the radiation will be studied elsewhere. When one considers

a wave propagating along the growth direction, generally, it is necessary to take into account that there are two s-polarized waves in this case. The relation between the intensities of these waves is determined by the stochastic properties of $\mathbf{\Sigma}(\boldsymbol{\rho})$. Generally they are specified by the average $\langle \mathbf{\Sigma}(\boldsymbol{\rho}) \otimes \mathbf{\Sigma}(\boldsymbol{\rho}') \rangle = \widehat{\Xi}(\boldsymbol{\rho} - \boldsymbol{\rho}')$, where $\widehat{\Xi}(\boldsymbol{\rho})$ is a symmetric correlation second-rank tensor. For each wave polarized along the principal axes of the tensor one restores Eq. (4.35). Thus, the relation between the intensities of the waves with these polarizations is determined by the relation between the eigenvalues of the tensor $\widehat{\Xi}$. Moreover, it is clear that the correlation tensor gives all Stocks parameters [44]. In the structures under consideration, however, it is natural to assume the isotropic distribution of $\mathbf{\Sigma}(\boldsymbol{\rho})$ what leads to unpolarized emitted wave and the general validity of Eq. (4.35). The spectral function $\Xi(\omega)$ is an important parameter determining the form of the luminescence spectrum and should be determined from a microscopical consideration of the electron relaxation processes. However, it barely changes essentially on the frequency scales under the interest. Because of this circumstance we assume $\Xi(\omega) = 1$ in our numerical calculations while formally keep it in the expressions.

Eq. (4.35) shows that the form of the luminescence spectrum is determined by several factors with different frequency dependencies. The exciton susceptibility, $S(\omega)$ for instance, strongly reduces the luminescence far away from the exciton frequency ω_0. The spectral density, $\Xi(\omega)$ can be considered as a slowly changing function of frequencies at the scale of the width of the polariton stop-band. The last term in Eq. (4.35) has two contributions. One is the transmission coefficient t_N, which has singularities at the eigenfrequencies of the quasi-modes of the structure. These singularities determine the fine structure of the luminescence. The second term is responsible for the variations in the luminescence intensity at a much larger scale. In the presence of homogeneous and inhomogeneous broadenings only these variations survive.

The summation over the quantum wells can be performed using an assumption that all transfer matrices T entering the definition of $T_-^{(m)}$ in Eq. (4.34) are the same. Also we assume that the structure is made of an integer number of the elementary cells. This means, in particular, that the terminating layers are half-barriers. These assumptions imply that all partial transfer matrices possess the mirror symmetry and can be represented in the form actively used in Chapter 3

$$T(\theta, \beta) = \begin{pmatrix} \cos\theta - i \sin\theta \cosh\beta & -i \sin\theta \sinh\beta \\ i \sin\theta \sinh\beta & \cos\theta + i \sin\theta \cosh\beta \end{pmatrix}. \tag{4.36}$$

Comparison of Eqs. (4.36) and (4.20) gives the relation between the parameters of these representations

$$\cos\theta = \frac{1}{2}(af + \bar{a}\bar{f}), \qquad \tanh\beta = \frac{\bar{a}f - a\bar{f}}{af - \bar{a}\bar{f}}. \tag{4.37}$$

The parameter θ determines the polariton spectrum and has a sense of $\theta = Kd$, where K is the polariton Bloch wave-number.

The representation (4.36) is convenient for performing the summation in Eq. (4.35) because all $T_-^{(m)}$ are characterized by the same β (including the scattering at the interface between the structure and the surrounding medium which does not change the spectral parameter), while the spectral parameter of $T_-^{(m)}$ is merely $-m\theta$. Thus, $T_-^{(m)}$ can be written as

$$\begin{aligned} T_-^{(m)} = {} & e^{im\theta} T_H(\beta/2) \left|+\right\rangle \left\langle+\right| T_H^{-1}(\beta/2) \\ & + e^{-im\theta} T_H(\beta/2) \left|-\right\rangle \left\langle-\right| T_H^{-1}(\beta/2), \end{aligned} \tag{4.38}$$

where T_H is a matrix describing a hyperbolic rotation with a dilation

$$T_H(\beta) = e^{\beta} \begin{pmatrix} \cosh\beta & -\sinh\beta \\ -\sinh\beta & \cosh\beta \end{pmatrix}. \tag{4.39}$$

Using Eq. (4.38) one can find

$$\frac{1}{|t_N|^2}\sum_m |\mathcal{G}(m)|^2 = \frac{\sinh N\theta''}{\sinh\theta''}\left[|A|^2 e^{-(N+1)\theta''} + |B|^2 e^{(N+1)\theta''}\right] + \frac{\sin N\theta'}{\sin\theta'}\left[AB^* e^{i\theta'(N+1)} + A^* B e^{-i\theta'(N+1)}\right], \tag{4.40}$$

where we have represented $\theta = \theta' + i\theta''$ and have introduced

$$\begin{aligned} A &= \frac{1}{1+\rho}\left[(g_2 - \rho g_2^*)\cosh^2(\beta/2) - \frac{1}{2}(g_2^* - \rho g_2)\sinh\beta\right] \\ B &= -\frac{1}{1+\rho}\left[(g_2 - \rho g_2^*)\sinh^2(\beta/2) - \frac{1}{2}(g_2^* - \rho g_2)\sinh\beta\right]. \end{aligned} \tag{4.41}$$

For the purposes of numerical calculations instead of direct calculations of the parameter β it is more convenient to multiply both parts of Eqs. (4.41) by $\sin\theta$ and, then, use Eq. (4.36) to establish direct relation of corresponding terms with the elements of the transfer matrix through the period of the structure.

It is immediately seen from Eq. (4.40) that the luminescence is reduced at frequencies corresponding to the interior of the forbidden gap. At these frequencies the main contribution to the r.h.s. of Eq. (4.40) is due to the exponentially large terms $\propto \exp(N\theta'')$. However, these terms are cancelled by the exponentially small transmission at these frequencies. As the result $\mathcal{I}(\omega)$ tends to values which are independent on the length of the structure. Thus, for sufficiently long structures where the polariton band structure essentially affects their optical properties the luminescence at the forbidden frequencies is relatively small.

Before we turn to a more detailed analysis of the luminescence spectrum it should be noted that the optical properties of the resonant photonic crystals strongly depend on the relation between the resonant frequency and the position of the photonic band gap. The strongest exciton effect on the light propagation takes place in Bragg structures (see Chapter 2). The condition for the Bragg resonance is the coincidence of the exciton frequency, ω_0, and a special frequency ω_B. In MQW structures with the homogeneous dielectric function the frequency ω_B corresponds to the boundary of a Brillouin zone. In resonant photonic crystal ω_B is a boundary of the photonic band gap existing in a passive photonic crystal characterized by the same spatial modulation of the dielectric function. More specifically the condition of the Bragg resonance is determined by the details of the modulation of the dielectric function. For concreteness we will assume that the dielectric function reaches its maximum value at the quantum well and monotonously decreases towards the boundaries of the elementary cell. In this case the Bragg resonance takes place when the exciton frequency coincides with the high-frequency boundary of the photonic band gap, Ω_+. The structures where ω_0 is close to ω_B are characterized by a relatively wide forbidden gap with a transparency window between ω_0 and ω_B. We will call such structures quasi-Bragg in order to separate them from those where ω_0 lies far away from the photonic band gap. The polariton spectrum in the latter case consists of two gaps — narrow exciton related gap near ω_0 with the width $\sim \Gamma_0$ and almost unperturbed photonic band gap. We will refer to these structures as off-Bragg.

The exciton luminescence is not an exception and also depends on the relation between ω_0 and ω_B. Therefore, one should make a distinction between the luminescence of the quasi- and off-Bragg structures. Eq. (4.40) allows a constructive analysis in both these cases. We consider in details the case of quasi-Bragg structures and shortly discuss main features of the off-Bragg case.

It can be noted that the luminescence spectrum is mainly concentrated near the edges of the bands of the exciton polaritons when ω_0 is close to ω_B. Indeed, at frequencies inside the forbidden gap the contribution to $\mathcal{I}(\omega)$ of the exponentially big terms in the r.h.s. of Eq. (4.40) is cancelled by

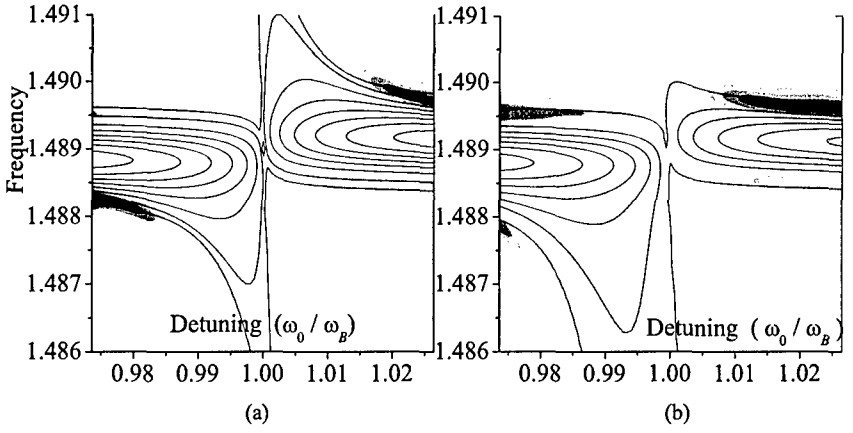

Figure 4.2: The luminescence spectrum and the polariton band structure are shown for quasi-Bragg structures near the boundary of the first Brillouin zone. Smooth filling corresponds to the term $|S|^2 \sum_m |\mathcal{G}(m)|^2$. The lines are the level curves of θ''. Frequency changes along the vertical axis and the horizontal axis presents the detuning from the Bragg resonance measured as a ratio ω_0/ω_B. (a) Pure MQW structure with parameters typical for $Al_xGa_{1-x}As/GaAs$ structures: $\Gamma_0 = 15$ μeV, $\omega_0 = 1.489$ eV, $\gamma = 50$ μeV, also inhomogeneous broadening has been taken into account $\sigma = 200$ μeV. (b) An example of MQW based photonic crystal. The exciton related parameters are the same as in (a). The modulation of the index of refraction is taken to be $n(z) = 3.4 + 0.1\cos^{20}(\pi z/2d)$.

the exponentially small transmission at these frequencies. Besides, at frequencies far away from the ω_0 the luminescence is subsided by the smallness of the exciton susceptibility. In a neighborhood of the band edges Eq. (4.40) drastically simplifies. At such frequencies we can represent the spectral parameter as $\theta = \pi + i\epsilon$ and assume that ϵ is sufficiently small resulting in $N|\epsilon| \ll 1$. Obviously, this approximation fails when ϵ is large which happens when the exciton frequency is essentially detuned away from the Bragg resonance. However, it suffices for a semi-qualitative analysis.

At a vicinity of the band edges Eq. (4.35) takes a simple form

$$\mathcal{I}(\omega) = 4N\Xi(\omega)|t_N|^2 \left|\frac{S(\omega)}{\varphi_1}\right|^2 \left|\frac{g_2 - \rho g_2^*}{1+\rho}\right|^2. \tag{4.42}$$

As follows from this expression the intensity of the emitted field increases linearly with the number of quantum wells as one should expect. This is the consequence of the transparency of the structure at these frequencies and of the independence of the contributions of different wells to the radiated field.

We would like to note that Eq. (4.42) can be simplified even more using the fact that the last term changes very slowly in the region of frequencies under the interest. Indeed, near the photonic band gap one has $h_2(z_+)' \approx 0$, thus the last term reduces to $|h_2 q/\sqrt{W_h}|^2$.

It is seen from Eq. (4.42) that the luminescence of the Bragg structures is relatively small. The reason is that in this case there is a solid gap with the width $\Delta \gg \max(\Gamma_0, \gamma)$. As the result, the edges of the gap are situated so far away from the exciton frequency that the intensity of the field is essentially reduced by the exciton susceptibility. When the structure does not satisfy the Bragg condition a transparency window appears which splits the gap into two parts. One part

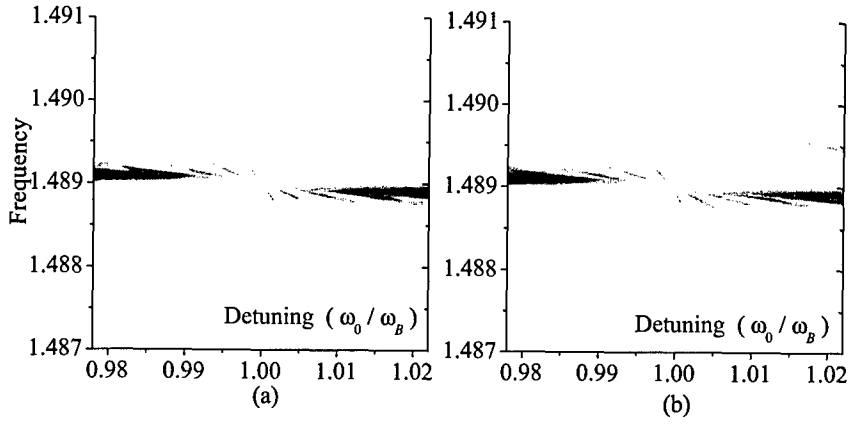

Figure 4.3: The fine structure of the luminescence spectrum. Smooth filling corresponds to the term $|S|^2 \sum_m |\mathcal{G}(m)|^2$. The parameters of the structures are the same as in Fig. 4.2 except $\gamma = 10$ μeV and $\sigma = 0$. (a) The MQW structure with a homogeneous dielectric function. (b) The MQW based photonic crystal.

is detached from the exciton frequency and another is adjacent to it. Using the same reasoning as above one can show that the luminescence spectrum is concentrated near the edges of the gap adjacent to ω_0. The relatively smooth dependence of the luminescence spectrum on the frequency and the period of the structure is modulated by strong frequency and period oscillations of the transmission $|t_N|^2$. These oscillations constitute a fine structure of the luminescence spectrum and become visible when the exciton broadening is sufficiently small. Numerical calculations using the exact form of $\mathcal{I}(\omega)$ shown in Figs. 4.2 and 4.3 qualitatively confirm these results. Fig. 4.2 shows the luminescence spectrum together with the polariton stop band. Because of the exciton broadening, the notion of the gap becomes ill-defined and, in particular, the edges of the gap can not be determined unambiguously. However, at the frequency corresponding to the band edge in a system without broadening the imaginary part of the polariton Bloch wave-number drastically increases what can be traced on the level curves of θ'' in Fig. 4.2. The outer curves correspond to the smallest value of θ''. It is seen that the maxima of the luminescence spectrum approximately follow these lines with the change of the relation between the exciton frequency and the period of the structure. The exact positions of the maxima are determined by an interplay between a smaller value of θ'' (and, hence, a higher transmission) and a smaller distance from the exciton frequency (a higher value of $S(\omega)$). It is interesting to note that a clear difference exists between the luminescence spectra in a MQW structure with a homogeneous dielectric function and in a MQW based photonic crystal. The latter is clearly asymmetric with respect to the point of the Bragg resonance. It is related to the asymmetrical structure of the polariton band gap in such structures. In a structure tuned to the Bragg resonance the exciton frequency is not situated at the center of the forbidden gap as it is in the case of the optical lattice but is rather shifted toward the high-frequency boundary of the gap.

Fig. 4.3 shows the luminescence spectrum for a sufficiently smaller value of the exciton broadening so that the fine structure is clearly visible. It is constituted by maxima of the luminescence following the period dependence of the resonances on transmission [104, 105]. These maxima appear as the characteristic scars on the spectrum.

The approximation used above is suitable while the structure is slightly detuned from the Bragg resonance. A detailed analysis shows that when the detuning becomes essential $|\omega_0 - \omega_B| \gg \Delta$ the relevant approximation is to keep only the term $\propto |B|^2$ in Eq. (4.40). It shows that the luminescence spectrum is concentrated only near the exciton frequency ω_0 with a characteristic width determined by the parameters of the exciton susceptibility — radiative decay rate Γ_0 and the exciton broadening γ.

Appendix A

Transfer matrix formalism

The transfer matrix technique has been reviewed in a lot of publications. Here, however, we use this technique in a bit unusual aspect and, therefore, find it relevant to recall important results.

There are transfer matrices of different kind. As the basic one serves the matrix built for values of the electric field and its derivative. The formal reason for it is that Eq. (2.5) can be considered as a Cauchy problem whose solution is specified by initial condition at some point with coordinate z, i.e. by $E(z)$ and $E'(z)$. This approach has proved its power in problems with piecewise constant dielectric function, ϵ. The Maxwell equation can be easily solved in each region of constancy of ϵ and the solution is determined by the initial conditions at the boundary of this region. This solution supplemented by the Maxwell boundary conditions at the point of jump of the dielectric function gives the values of E and E' that are considered as initial conditions for the next region of the constancy and so on. The matrix relating these values is called transfer matrix

$$\begin{pmatrix} E(z+d) \\ E'(z+d) \end{pmatrix} = T_\psi(z+d,z) \begin{pmatrix} E(z) \\ E'(z) \end{pmatrix}. \tag{A.1}$$

However, this basis is rather formal and masks some features that are specific for *propagation* of light along the structure. This inconvenience can be improved by choosing a special way of constructing the transfer matrix. For example, the problem of scattering of light is naturally set by giving the amplitude of incident, say on the left boundary, wave and obtaining the amplitudes of transmitted and reflected waves. That is the field is sought in the form $e^{i\kappa z} + re^{-i\kappa z}$ at the left side and in the form $te^{i\kappa z}$ at the right side. More generally, the field is represented in the form

$$\begin{aligned} E(z) &= a_+ e^{i\kappa z} + a_- e^{-i\kappa z}, \\ E(z+d) &= a'_+ e^{i\kappa z} + a'_- e^{-i\kappa z} \end{aligned} \tag{A.2}$$

and the transfer matrix (sometimes it is called a scattering matrix [106]) relates the amplitudes at the left and the right boundaries

$$\begin{pmatrix} a'_+ \\ a'_- \end{pmatrix} = T \begin{pmatrix} a_+ \\ a_- \end{pmatrix}. \tag{A.3}$$

As follows from Eqs. (A.2), the transfer matrices written in these two bases are related by a similarity transformation, $T = \widehat{W}_e^{-1}(z) T_\psi(z+d,z) \widehat{W}_e(z)$, where

$$\widehat{W}_e(z) = \begin{pmatrix} e^{i\kappa z} & e^{-i\kappa z} \\ i\kappa e^{i\kappa z} & -i\kappa e^{-i\kappa z} \end{pmatrix}. \tag{A.4}$$

Another important way to introduce a transfer matrix (see e.g. Ref. [107]) is based on a possibility of a representation of the solution of the Maxwell equation as a sum of two linearly independent functions, $f_{1,2}(z)$, with modulated amplitudes

$$\begin{aligned} E(z) &= c_1(z)h_1(z) + c_2(z)h_2(z), \\ E'(z) &= c_1(z)h_1'(z) + c_2(z)h_2'(z). \end{aligned} \tag{A.5}$$

Now, the transfer matrix gives the relation between the amplitudes at different points, usually a period of structure apart,

$$\begin{pmatrix} c_1(z+d) \\ c_2(z+d) \end{pmatrix} = T_h(d) \begin{pmatrix} c_1(z) \\ c_2(z) \end{pmatrix}. \tag{A.6}$$

From Eq. (A.5) follows that

$$T_h(d) = \widehat{W}_h^{-1}(z+d) T_\psi(z+d, z) \widehat{W}_h(z), \tag{A.7}$$

where $\widehat{W}_h(z)$ is the Wronsky matrix

$$\widehat{W}_h(z) = \begin{pmatrix} h_1(z) & h_2(z) \\ h_1'(z) & h_2'(z) \end{pmatrix}. \tag{A.8}$$

Eq. (A.8) allows to derive a relation between transfer matrices obtained for a different choice of the basis functions $h_{1,2}$.

The relation between the transfer matrices written in the bases of plane waves and a pair of linearly independent functions is written as

$$T = M(d/2) T_h(d) M^{-1}(-d/2), \tag{A.9}$$

where $M(z) = \widehat{W}_e^{-1}(0)\widehat{W}_h(z)$. Substitution of Eqs. (A.4) and (A.8) gives

$$M(z) = \frac{1}{2} \begin{pmatrix} h_1(z) + \dfrac{h_1'(z)}{i\kappa} & h_2(z) + \dfrac{h_2'(z)}{i\kappa} \\ h_1(z) - \dfrac{h_1'(z)}{i\kappa} & h_2(z) - \dfrac{h_2'(z)}{i\kappa} \end{pmatrix}. \tag{A.10}$$

All different bases to write the transfer matrix have their advantages and disadvantages. For example, the basis of a pair of linearly independent functions is naturally related to solutions of the differential equation, is easy to find but is inconvenient for solution of scattering problems. The fact that, generally, it is not related to T_ψ by a similarity transformation [see Eq. (A.7)] makes it difficult to consider the spectrum problem in the frameworks of this basis. Indeed, divergence or vanishing the amplitudes $c_{1,2}$ themselves says nothing about the behavior of the field. It is necessary to consider additionally details of the dependence of the basis functions. Therefore, to solve the spectrum problem it is not enough to look at the transfer matrix itself but it is necessary to solve an appropriate boundary value problems for amplitudes $c_{1,2}$. The basis of plane waves, on the contrary, is the most suitable for solution of such problem since the transfer matrix itself contains all the information one needs. However, finding of the transfer matrix in this basis calls extra efforts because it requires a solution of a differential equation with boundary conditions. Therefore, conversion rule from one basis to another similar to Eq. (A.9) is very useful.

Concluding, a solution of a particular problem using the transfer matrix technique can be quite straightforward provided by using different bases for representation of transfer matrix — the most convenient for particular sub-problems.

Summary

The thesis is devoted to an analysis of optical properties of quantum heterostructures — the structures characterized by a periodic spatial arrangement of elements with optically active excitations (e.g. excitons). These structures are the merging point of two active trends — conventional photonic crystals and optical lattices. In the present thesis the one-dimensional situation (photonic crystals based on multiple-quantum-well structures) is considered and the following most important results have been obtained.

1. An effective approach for the description of propagation of the electromagnetic waves in the structures under consideration has been developed. This approach takes into account an arbitrary spatial modulation of the dielectric function, an arbitrary form of the exciton states, an arbitrary angle of propagation of the electromagnetic wave and its polarization state. This approach is naturally free from the problem of the eigenstates in media with dispersion and absorption.

2. The exciton polariton dispersion law has been studied in details for a special case when the modulation of the dielectric function possesses the mirror symmetry. It is shown that the interaction of light with excitons can lead to an essential modification of the spectrum of electromagnetic waves when a special condition of an optimal coupling between the quantum wells is met (the Bragg resonance). In the simplest case of consistent symmetry of the dielectric function and the exciton wavefunction this condition is the coincidence of the exciton resonance frequency and the high-frequency boundary of the photonic band gap existing in a passive structure with the same modulation of the dielectric function. The polariton spectrum is characterized by a solid gap with the width equal to the Pythagorean sum of the photonic and the excitonic gap widths.

3. The effect of a complex structure of the exciton states on the polariton spectrum has been analyzed. This effect can be significant in special structures with sufficiently close quantum wells in the elementary cell. In this case the hybridization of the exciton states localized in different wells results in the states with different symmetries and close energies. It is shown that in this case the optical mixing of the exciton states appears. The exciton related optical peculiarities (e.g. on transmission and reflection spectra) appear at such frequencies as if there were an additional interaction between the excitons.

4. The general approach for an analysis of the optical spectra of the finite quantum heterostructures has been developed. One of the key features of this approach is that a single quantum well embedded in a dielectric environment allows description as a quantum well in a vacuum but with modified excitonic susceptibility and the optical width. These modifications allow relatively simple taking into account the angular and the polarization dependencies of the optical spectra. The introduction of these effective quantities establishes a relation between the results obtained in the particular case of a homogeneous multiple-quantum-well structure and in the general case of a resonant photonic crystal.

5. It is shown that one of the specific features of the spectrum of quantum heterostructures is vanishing reflection at *one* of the frequencies, ω_{min}, where the different contributions to the scattering of light (scattering by the inhomogeneities of the dielectric function and by the excitons) become equal. This effect has the same origin as the Fano resonance. The characteristic frequency ω_{min} depends upon the spatial distribution of the dielectric function and plays the role of the Fano parameter.

6. Optical spectra of finite structures with a "defect" layer at the middle have been studied. A special attention has been paid to Ω-defect. It is shown that there exists a resonant drop of the reflection, also with the same origin as the Fano resonance. This is the important feature of this effect that the drop occurs not at the frequency of the defect layer but is rather shifted away from it. The magnitude of the shift is determined, in particular, by the whole structure and can be made essential comparing with the values of the homogeneous and inhomogeneous broadenings. As the result the effect of the broadenings can be made quite small leading to extremely small values of the reflection at the frequency of the drop.

7. General effects of the homogeneous and inhomogeneous broadenings on the optical spectra have been considered. It is shown that the approximation of the inhomogeneous broadening is exact when one considers only the specular component of the scattered wave. It is shown that because of different frequency dependencies of homogeneously and inhomogeneously broadened excitonic susceptibilities these broadenings lead to different modifications of the reflection spectrum. This allows a principal possibility of independent measurements of the broadenings.

8. Using the approaches developed, the problem of the exciton luminescence in the resonant photonic crystals has been solved. It is shown that luminescence spectrum is mostly concentrated near the edges of the forbidden gaps in the polariton spectrum. The spectrum is modulated by the exciton susceptibility and the transmission coefficient. The latter has strong frequency dependence near the edge of the gap. This leads to a strong frequency modulation of the luminescence spectrum which becomes visible when the broadenings in the system become sufficiently small.

Bibliography

[1] S. Glutsch, *Excitons in Low-Dimensional Semiconductors* (Springer-Verlag, Berlin, 2004).

[2] L. Chang and K. Ploog, eds., *Molecular beam epitaxy and heterostructures* (Nijhoff, Dorderecht, 1985).

[3] E. L. Ivchenko and G. E. Pikus, *Superlattices and other heterostructures. Symmetry and optical phenomena* (Springer-Verlag, Berlin, 1997), 2nd ed.

[4] L. D. Landau and E. M. Lifshitz, *Quantum Mechanics (Non-relativistic Theory)* (Butterworth-Heinemann, 1977), 3rd ed.

[5] W. Schäfer and M. Wegener, *Semiconductor Optics and Transport Phenomena* (Springer, Berlin, 2002).

[6] P. Harrison, *Quantum wells, wires and dots: theoretical and computational physics* (Wiley, Chichester, 2000).

[7] H. Haug and S. Schmitt-Rink, Prog. Quant. Electr. **9**, 3 (1984).

[8] A. Stahl and I. Balslev, *Electrodynamics of the semiconductor band edge* (Springer-Verlag, Berlin, Heidelberg, 1987).

[9] M. Kira, F. Jahnke, W. Hoyer, and S. Koch, Prog. Quant. Electr. **23**, 189 (1999).

[10] K. Cho, *Optical response of nanotstructures. Microscopic nonlocal theory* (Springer-Verlag, Berlin, Heidelberg, 2003).

[11] C. Cohen-Tannoudji, J. Dupont-Roc, and G. Grynberg, *Atom-Photon Interactions. Basic processes and applications* (Wiley, New York, 1992).

[12] L. Butov, Sol. St. Commun. **127**, 89 (2003).

[13] S. I. Pekar, Sov. Phys. JETP **6**, 785 (1958), [Zh. Eksp. Teor. Fiz. **33**, 1022 (1957)].

[14] E. I. Rashba and M. Sturge, eds., *Excitons* (North-Holland, Amsterdam, 1982).

[15] P. Halevi, ed., *Spatial Dispersion in Solids and Plasmas* (North-Holland, Amsterdam, 1992).

[16] D. Gershoni, I. Brener, G. A. Baraff, S. N. G. Chu, L. N. Pfeiffer, and K. West, Phys. Rev. B **44**, 1930 (1991).

[17] S. Nojima, Phys. Rev. B **47**, 13535 (1993).

[18] M. V. Belousov, V. L. Berkovits, A. O. Gusev, E. L. Ivchenko, P. S. Kop'ev, N. N. Ledentsov, and A. I. Nesvizhskii, Phys. Solid State **36**, 596 (1994).

[19] G. Armelles, P. Castrillo, P. S. Dominguez, L. González, A. Ruiz, D. A. Contreras-Solorio, V. R. Velasco, and F. García-Moliner, Phys. Rev. B **49**, 14020 (1994).

[20] M. V. Belousov, E. L. Ivchenko, and A. I. Nesvizhskiĭ, Phys. Solid State **37**, 763 (1995).

[21] G. L. Bir and G. E. Pikus, *Symmetry and Strain-induced Effects in Semiconductors* (Wiley, New York, 1970).

[22] J. Davies, *The Physics of low-dimensional semiconductors. An introduction* (Cambridge University Press, New York, 1998).

[23] V. Kuzmiak and A. Maradudin, Phys. Rev. B **55**, 7427 (1997).

[24] L. Deych, D. Livdan, and A. Lisyansky, Phys. Rev. E **57**, 7254 (1998).

[25] S. Nojima, Phys. Rev. B **61**, 9940 (2000).

[26] A. Y. Sivachenko, M. E. Raikh, and Z. V. Vardeny, Phys. Rev. A **64**, 013809 (2001).

[27] A. Christ, S. Tikhodeev, N. Gippius, J. Kuhl, and G. H., Phys. Rev. Lett. **91**, 183901 (2003).

[28] K. Huang, P. Bienstman, J. Joannopoulos, K. Nelson, and S. Fan, Phys. Rev. Lett. **90**, 196402 (2003).

[29] O. Toader and S. John, Phys. Rev. E **70**, 046605 (2004).

[30] L. Pilozzi, A. D'Andrea, and K. Cho, Phys. Rev. B **69**, 205311 (2004).

[31] E. Ivchenko and A. Poddubny (2005), cond-mat/0505510, unpublished.

[32] E. L. Ivchenko, V. P. Kochereshko, A. V. Platonov, D. R. Yakovlev, A. Waag, W. Ossau, and G. Landwehr, Phys. Solid State **39**, 1852 (1997).

[33] E. L. Ivchenko, M. M. Voronov, M. V. Erementchouk, L. I. Deych, and A. A. Lisyansky, Phys. Rev. B **70**, 195106 (2004).

[34] A. Tip, Phys. Rev. E **69**, 016610 (2004).

[35] A. Figotin and J. H. Schenker, J. Stat. Phys. **118**, 199 (2005).

[36] P. M. Morse and H. Feshbach, *Methods of Theoretical Physics*, vol. 1 (McGraw-Hill, Tokyo, 1953).

[37] F. Tassone, F. Bassani, and L. C. Andreani, Phys. Rev. B **45**, 6023 (1992).

[38] L. C. Andreani, G. Panzarini, A. V. Kavokin, and M. R. Vladimirova, Phys. Rev. B **57**, 4670 (1998).

[39] T. Ikawa and K. Cho, Phys. Rev. B **66**, 085338 (2002).

[40] B. Vainberg and S. Molchanov (2005), math.CA/0503075, unpublished.

[41] J. D. Joannopoulos, R. D. Meade, and J. N. Winn, *Photonic crystals: Molding the flow of light* (Princeton University Press, 1995), ISBN 0691037442.

[42] B. A. Dubrovin, S. P. Novikov, and A. T. Fomenko, *Modern geometry: methods and applications* (Springer, New York, 1992), 2nd ed.

[43] J. Bendickson, J. Dowling, and M. Scalora, Phys. Rev. E **53**, 4107 (1996).

[44] M. Born and E. Wolf, *Principles of Optics* (Cambridge University Press, Cambridge, 1999), 7th ed.

[45] A. Yariv and P. Yeh, *Optical waves in crystals* (John Wiley & Sons, New Jersey, 2003).

[46] L. C. Andreani, F. Tassone, and F. Bassani, Solid State Commun. **77**, 641 (1991).

[47] D. S. Citrin, Phys. Rev. B **47**, 3832 (1993).

[48] L. V. Keldysh, Superlatt. Microstruct. **4**, 637 (1988).

[49] E. L. Ivchenko, Sov. Phys. Solid State **33**, 1344 (1991).

[50] D. S. Citrin, Solid State Commun. **89**, 139 (1994).

[51] A. Kavokin and M. Kaliteevski, Solid St. Commun. **95**, 859 (1995).

[52] S. Haas, T. Stroucken, M. Hübner, J. Kuhl, B. Grote, A. Knorr, F. Jahnke, S. W. Koch, R. Hey, and K. Ploog, Phys. Rev. B **57**, 14860 (1998).

[53] D. Ammerlahn, B. Grote, S. W. Koch, J. Kuhl, M. Hübner, R. Hey, and K. Ploog, Phys. Rev. B **61**, 4801 (2000).

[54] M. V. Erementchouk, L. I. Deych, and A. A. Lisyansky, Phys. Rev. B **71**, 235335 (2005).

[55] L. I. Deych and A. A. Lisyansky, Phys. Rev. B **62**, 4242 (2000).

[56] M. Hübner, J. P. Prineas, C. Ell, P. Brick, E. S. Lee, G. Khitrova, H. M. Gibbs, and S. W. Koch, Phys. Rev. Lett. **83**, 2841 (1999).

[57] J. P. Prineas, C. Ell, E. S. Lee, G. Khitrova, H. M. Gibbs, and S. W. Koch, Phys. Rev. B **61**, 13863 (2000).

[58] J. Winn, Y. Fink, S. Fan, and J. Joannopoulos, Optics Letters **23**, 1573 (1998).

[59] D. Chigrin, A. Lavrinenko, D. Yarotsky, and S. Gaponenko, Appl. Phys. A **68**, 25 (1999).

[60] A. Bruyant, G. Lerondel, P. Reece, and M. Gal, Appl. Phys. Lett. **82**, 3227 (2003).

[61] T. Yonte, J. Monzon, A. Felipe, and L. Sanchez-Soto, J. Opt. A: Pure Appl. Opt. **6**, 127 (2004).

[62] R. Courant and D. Hilbert, *Methods of mathematical physics*, vol. 1 (John Wiley & Sons, New York, 1953).

[63] D. Miller, D. Chemla, and T. Damen, Phys. Rev. Lett. **53**, 2173 (1984).

[64] D. Miller, D. Chemla, T. Damen, A. Gossard, W. Wiegmann, T. Wood, and C. Burrus, Phys. Rev. B **32**, 1043 (1985).

[65] S. Schmitt-Rink, D. Chemla, and D. Miller, Adv. Phys. **38**, 89 (1989).

[66] R. Harel, E. Cohen, E. Linder, and A. Ron, Phys. Rev. B **53**, 7868 (1996).

[67] J. Sadowski, H. Mariette, A. Wasiela, R. André, Y. Merle d'Aubigné, and T. Dietl, Phys. Rev. B **56**, R1664 (1997).

[68] P. Kuchment, Waves Random Media **12**, R1 (2002).

[69] P. Kuchment, Waves Random Media **14**, S107 (2004).

[70] D. S. Citrin, Phys. Rev. B **50**, 5497 (1994).

[71] J. J. Monzon and L. L. Sanchez-Soto, Eur. J. Phys. **23**, 1 (2002).

[72] A. Yariv, P. Yeh, and C.-S. Hong, J. Opt. Soc. Am. **67**, 423 (1977).

[73] E. L. Ivchenko, A. I. Nesvizhinskii, and S. Jorda, Phys. Solid State **36**, 1156 (1994).

[74] R. Zimmermann, Phys. Stat. Solidi B **173**, 129 (1997).

[75] R. Zimmermann, F. Grobe, and E. Runge, Pure and Applied Chemistry **69**, 1179 (1997).

[76] D. S. Citrin, Chem. Phys. Lett. **228**, 307 (1994).

[77] V. A. Kosobukin and A. V. Sel'kin, Phys. Solid State **42**, 1914 (2000).

[78] G. V. Astakhov, V. A. Kosobukin, V. P. Kochereshko, D. R. Yakovlev, W. Ossau, G. Landwehr, T. Wojtowicz, G. Karczewski, and J. Kossut, Eur. Phys. J. B **24**, 7 (2001).

[79] V. A. Kosobukin, Phys. Solid State **45**, 1145 (2003).

[80] G. Kocherscheidt, W. Langbein, G. Mannarini, and R. Zimmermann, Phys. Rev. B **66**, 161314 (2002).

[81] E. Runge and R. Zimmermann, Phys. Rev. B **61**, 4786 (2000).

[82] V. Savona, E. Runge, and R. Zimmermann, Phys. Rev. B **62**, R4805 (2000).

[83] W. Langbein, E. Runge, V. Savona, and R. Zimmermann, Phys. Rev. Lett. **89**, 157401 (2002).

[84] G. Malpuech and A. Kavokin, Appl. Phys. Lett. **76**, 3049 (2000).

[85] G. Malpuech, A. V. Kavokin, and G. Panzarini, Phys. Rev. B **60**, 16788 (1999).

[86] V. Savona and C. Weisbuch, Phys. Rev. B **54**, 10835 (1996).

[87] D. S. Citrin, Phys. Rev. B **54**, 14572 (1996).

[88] P. Borri, W. Langbein, U. Woggon, J. Jensen, and J. Hvam, Phys. Rev. B **63**, 035307 (2001).

[89] M. Abramowitz and I. A. Stegun, eds., *Handbook of Mathematical Functions* (Dover, New York, 1970).

[90] R. P. Stanley, R. Houdré, U. Oesterle, M. Ilegems, and C. Weisbuch, Phys. Rev. A **48**, 2246 (1993).

[91] N. Liu, Phys. Rev. B **55**, 4097 (1997).

[92] A. Figotin and V. Gorentsveig, Phys. Rev. B **58**, 180 (1998).

[93] D. Felbacq, J. Phys. A: Math. Gen. **33**, 7137 (2000).

[94] R. Ozaki, Y. Matsuhisa, M. Ozaki, and K. Yoshino, Appl. Phys. Lett. **84**, 1844 (2004).

[95] L. I. Deych and A. A. Lisyansky, Phys. Lett. A **243**, 156 (1998).

[96] L. Deych, A. Yamilov, and A. Lisyansky, Phys. Rev. B **64**, 075321 (1987).

[97] L. Deych, A. Yamilov, and A. Lisyansky, Optics letters **25**, 1705 (2000).

[98] L. I. Deych, A. Yamilov, and A. A. Lisyansky, Nanotechnology **13**, 114 (2002).

[99] L. I. Deych, M. V. Erementchouk, and A. A. Lisyansky, Phys. Rev. B **69**, 75308 (2004).

[100] L. I. Deych, M. V. Erementchouk, and A. A. Lisyansky, Appl. Phys. Lett. **83**, 4562 (2003).

[101] P. Durand, I. Paidarová, and Gadá, J. Phys. B: At. Mol. Opt. Phys. **34**, 1953 (2001).

[102] A. Efros and M. Raikh, in *Optical Properties of Mixed Crystals*, edited by R. Elliot and I. Ipatova (North-Holland, Amsterdam, 1988).

[103] A. Kavokin and J. Baumberg, Phys. Rev. B **57**, R12697 (1998).

[104] M. Hubner, J. Prineas, C. Ell, P. Brick, E. Lee, G. Khitrova, H. Gibbs, and S. Koch, Phys. Rev. Lett. **83**, 2841 (1999).

[105] A. Mintsev, L. Butov, C. Ell, S. Mosor, G. Khitrova, and H. Gibbs, JETP Lett. **76**, 637 (2002).

[106] D. Y. K. Ko and J. C. Inkson, Phys. Rev. B **38**, 9945 (1988).

[107] R. Perez-Alvarez, C. Trallero-Herrero, and F. Garcia-Moliner, Eur. J. Phys. **22**, 275 (2001).